SAND2023-04005R
SAND2020-#####X

DECOVALEX-2023 Task F Specification Revision 10

Spent Fuel and Waste Disposition

Prepared for
US Department of Energy
Spent Fuel and Waste Science and Technology

Tara LaForce, Rick Jayne,
Rosie Leone, Paul Mariner, Emily Stein
Sandia National Laboratories

Son Nguyen
Canadian Nuclear Safety Commission
Tanja Frank
GRS

May 17, 2023

SAND2023-XXXXR

Rev. 11.29.16

DISCLAIMER

This information was prepared as an account of work sponsored by an agency of the U.S. Government. Neither the U.S. Government nor any agency thereof, nor any of their employees, makes any warranty, expressed or implied, or assumes any legal liability or responsibility for the accuracy, completeness, or usefulness, of any information, apparatus, product, or process disclosed, or represents that its use would not infringe privately owned rights. References herein to any specific commercial product, process, or service by trade name, trade mark, manufacturer, or otherwise, does not necessarily constitute or imply its endorsement, recommendation, or favoring by the U.S. Government or any agency thereof. The views and opinions of authors expressed herein do not necessarily state or reflect those of the U.S. Government or any agency thereof.

U.S. DEPARTMENT OF ENERGY | National Nuclear Security Administration

Sandia National Laboratories is a multimission laboratory managed and operated by National Technology and Engineering Solutions of Sandia LLC, a wholly owned subsidiary of Honeywell International Inc. for the U.S. Department of Energy's National Nuclear Security Administration under contract DE-NA0003525.

Sandia National Laboratories

APPENDIX E
NFCSC DOCUMENT COVER SHEET[1]

Name/Title: DECOVALEX-2023 Task F Specification – Revision 10

Deliverable/Milestone/Revision No.: M4SF-23SN010304093

Work Package Title and Number: GDSA-Repository Systems Analysis SNL /SF-23SN01030409

Work Package WBS Number: 1.08.01.03.04

Responsible Work Package Manager: Tara LaForce (Name/Signature)

Date Submitted: 5/10/2023

Quality Rigor Level for Deliverable/Milestone[2]	☐ QRL-1 ☐ Nuclear Data	☐ QRL-2	☒ QRL-3	☐ QRL-4 Lab QA Program[3]

This deliverable was prepared in accordance with

_____ *(Participant/National Laboratory Name)*

QA program which meets the requirements of

☒ DOE Order 414.1 ☐ NQA-1 ☒ Other

This Deliverable was subjected to:

☒ Technical Review ☐ Peer Review

Technical Review (TR)
Review Documentation Provided

☐ Signed TR Report or,
☐ Signed TR Concurrence Sheet or,
☐ Signature of TR Reviewer(s) below

Peer Review (PR)
Review Documentation Provided

☐ Signed PR Report or,
☐ Signed PR Concurrence Sheet or,
☐ Signature of PR Reviewer(s) below

Name and Signature of Reviewers

Kris Kuhlman

NOTE 1: *Appendix E should be filled out and submitted with the deliverable. Or, if the PICS:NE system permits, completely enter all applicable information in the PICS:NE Deliverable Form. The requirement is to ensure that all applicable information is entered either in the PICS:NE system or by using the NFCSC Document Cover Sheet.*

- *In some cases there may be a milestone where an item is being fabricated, maintenance is being performed on a facility, or a document is being issued through a formal document control process where it specifically calls out a formal review of the document. In these cases, documentation (e.g., inspection report, maintenance request, work planning package documentation or the documented review of the issued document through the document control process) of the completion of the activity, along with the Document Cover Sheet, is sufficient to demonstrate achieving the milestone.*

NOTE 2: *If QRL 1, 2, or 3 is not assigned, then the QRL 4 box must be checked, and the work is understood to be performed using laboratory QA requirements. This includes any deliverable developed in conformance with the respective National Laboratory / Participant, DOE or NNSA-approved QA Program.*

NOTE 3: *If the lab has an NQA-1 program and the work to be conducted requires an NQA-1 program, then the QRL-1 box must be checked in the work Package and on the Appendix E cover sheet and the work must be performed in accordance with the Lab's NQA-1 program. The QRL-4 box should not be checked.*

This page is intentionally left blank.

SUMMARY

This report is the revised (Revision 10) Task F specification for DECOVALEX-2023. Task F is a comparison of the models and methods used in deep geologic repository performance assessment. The task proposes to develop a reference case for a mined repository in a fractured crystalline host rock (Task F1) and a reference case for a mined repository in a salt formation (Task F2). Teams may choose to participate in the comparison for either or both reference cases. For each reference case, a common set of conceptual models and parameters describing features, events, and processes that impact performance will be given, and teams will be responsible for determining how best to implement and couple the models. The comparison will be conducted in stages, beginning with a comparison of key outputs of individual process models, followed by a comparison of a single deterministic simulation of the full reference case, and moving on to uncertainty propagation and uncertainty and sensitivity analysis. This report provides background information, a summary of the proposed reference cases, and a staged plan for the analysis.

This page is intentionally left blank.

ACKNOWLEDGEMENTS

Thanks to DECOVALEX organizers Jens Birkholzer and Alex Bond for proposing Task F, and for their guidance in defining its boundaries.

Thanks to the members of the participating teams for their many contributions to the reference cases, especially Jeroen Bartol for testing out the salt creep model.

Thanks to Sandia National Laboratories researchers Peter Swift, Paul Mariner, Rick Jayne, Tara LaForce, Michael Nole, and Kris Kuhlman for their input to and reviews of the draft, and to Rick for compiling information for the salt reference case.

Thanks to the leadership team at the U. S. Department of Energy, Office of Nuclear Energy, Spent Fuel and Waste Science and Technology Campaign, Prasad Nair, Jorge Monroe-Rammsy, and Tim Gunter, for their support of this project.

This page is intentionally left blank.

CONTENTS

TABLE OF FIGURES

TABLE OF TABLES

REVISION HISTORY

Report Version Number	Date	
SAND2020-4598 O (rev 0)	April 29, 2020	Version for April 2020 kickoff meeting
SAND2020-8494 O (rev 1)	August 13, 2020	Benchmark 6.3.3 and appendix updated
SAND2020-12645 O (rev 2)	November 11, 2020	Added model domain to benchmark 6.3.3 Added four-fracture benchmark 6.3.4
SAND2021-01910 O (rev 3)	January 7, 2021	Updated pressure, aperture, and permeability of four-fracture benchmark 6.3.4 Added benchmark 6.3.5
SAND2021-3155 O (rev 4)	March 15, 2021	Updated 4 fracture plus stochastic fracture parameters
SAND2021-6658 O (rev 5)	June 2, 2021	Added revised 4 fracture plus stochastic fracture 6.3.6
SAND2021-11892 O (rev 6)	September 24, 2021	Revised schedule (Section 2.1) Defined initial salt reference case (Section 4) Added 2D transport benchmark 6.2.1
SAND2021-13423 O (rev 7)	October 23, 2021	Defined crystalline reference case with tracer source term (Section 3)
SAND2022-6944 R (rev 8)	May 15, 2022	Crystalline: corrected expression for P32, corrected tracer source term text, added output for comparison (Section 3) Salt: Updated reference case shaft properties and tracers for transport (Section 4)
SAND2022-10439R (rev 9)	Dec 16, 2022	Crystalline: Technical editing throughout. Added five radionuclides and their properties to the reference case (Section 3.8.2); Revised and expanded reference case output metrics (Section 3.9); Added two waste package failure scenarios (Section 3.10); Clarified how to introduce tracers for the 4-fracture benchmarks (Section 5.2); Added a point-source benchmark (Section 5.2.7) and a radionuclide source term benchmark (Section 5.3) Salt: Added radionuclide inventory cross-reference to Section 3.8.2 for salt case in Section 4.6.2. Added salt creep model Section 4.3.4.1.
SAND2023-XXXXR (rev 10)	May 17, 2023	Crystalline:

		Salt: clarifications and correction of inconsistencies. Added additional comparison metrics

This page is intentionally left blank.

ACRONYMS

1-D	1-dimensional
2-D	2-dimensional
3-D	3-dimensional
BWR	boiling water reactor
DECOVALEX	DEvelopment of COupled models and their VALidation against Experiments
DFN	Discrete fracture network
DOE	Department of Energy (US)
ECPM	equivalent continuous porous medium
EDZ	excavation damage zone
FEPs	features, events, and processes
HCD	hydraulic conductor domain
HLW	high-level waste
HRD	hydraulic rock mass domain
IRF	instant release fraction
MTIHM	metric tons initial heavy metal
MTU	metric tons uranium
NWMO	Nuclear Waste Management Organization (Canada)
OCRWM	Office of Civilian Radioactive Waste Management (US)
OoR	out of reactor
PA	performance assessment
PWR	pressurized water reactor
SA	sensitivity analysis
SKB	Svensk Kärnbränslehantering AB (Sweden)
SNF	spent nuclear fuel
THM	thermal-hydraulic-mechanical
TPC	Taiwan Power Company (Taiwan)
UQ	uncertainty quantification
U.S.	United States

VARIABLES AND THEIR UNITS

b	half fracture aperture (m)
c	concentration (mol/L)
D	hydrodynamic dispersion coefficient (m^2/s)
D^*	molecular diffusion coefficient in water (m^2/s)
F_r	flow-related transport resistance in the fractured rock (y/m)
J	solute flux ($mol/m^2/s$)
k	permeability (m^2)
K_d	linear distribution coefficient (m^3/kg)
P	pressure (Pa)
P_{32}	fracture intensity as fracture area per unit volume of rock (m^2/m^3)
q	specific discharge (also called Darcy velocity) (m/s or m/y, as appropriate)
R	retardation coefficient (-)
$t_{1/2}$	halflife (s or y, as appropriate)
t_r	travel time to the biosphere in the fractured rock (y)
v	average linear porewater velocity (m/s, m/d, or m/y, as appropriate)
α_L	longitudinal dispersivity (m)
ϕ	porosity (-)
λ	decay constant (1/s)
μ	viscosity (Pa-s)
ρ	density (kg/m^3)
ρ_b	bulk density (kg/m^3)
ρ_s	solid grain density (kg/m^3)
τ	tortuosity (-)

DECOVALEX-2023 TASK F SPECIFICATION

This task specification is intended for the participants in DECOVALEX-2023 Task F (Performance Assessment).

1. INTRODUCTION

The DECOVALEX program, in general, is interested in coupled processes (e.g., thermal, hydrological, mechanical, and chemical) relevant to deep geologic disposal of nuclear waste. Task F of DECOVALEX-2023 involves comparison of the models and methods used in post-closure performance assessment of deep geologic repositories. A generic reference case describing a repository for commercial spent nuclear fuel (SNF) in a fractured crystalline host rock is one system for comparison (Task F1). A second generic reference case involves a repository for commercial SNF in a domal salt formation (Task F2). Although a direct comparison cannot be made between simulations of a crystalline repository and simulations of a salt repository, it is expected that lessons learned regarding, for instance, methods of coupling process models, propagating uncertainty, or conducting sensitivity analysis will be transferable between concepts.

The primary objectives of Task F are to build confidence in the models, methods, and software used for performance assessment (PA) of deep geologic repositories, and/or to bring to the fore additional research and development needed to improve PA methodologies. The objectives will be accomplished through a staged comparison of the models and methods used by participating teams in their PA frameworks, including: (1) coupled-process submodels (e.g., waste package corrosion, spent fuel dissolution, and radionuclide transport) comprising the full PA model; (2) deterministic simulation(s) of the entire PA model for defined reference scenario(s); (3) probabilistic simulations of the entire PA model; and (4) uncertainty quantification (UQ) and sensitivity analysis (SA) methods/results for probabilistic simulations of defined reference scenario(s).

1.1 Performance Assessment

Performance assessment is a tool of decision management that provides information from quantitative evaluations of the behavior of a complex system to the decision makers. PA involves evaluating the possible future consequences from the repository (i.e., dose or pollution) and the associated level of confidence (taking into account identified uncertainties) in the estimated performance of the system and seeks to provide reasonable assurance that the repository system will meet applicable safety standards. Throughout the lifetime of a repository program, PA is used in an iterative fashion to support site selection, site characterization, and repository design, and to inform data collection and model development.

At any iteration, the first steps of the PA process are to establish performance measures and to develop conceptual models of the repository system from knowledge of the natural and engineered system components (Figure 1-1). Development of computational models may go hand-in-hand with development of conceptual models and the scenarios they are derived from. Ultimately one or more computational models appropriate for forward simulation of the problem and calculation of performance measures is developed. Then, performance measures are calculated, uncertainty and sensitivity analysis performed, and results synthesized.

1.2 Task F

The stages of Task F will follow a similar process (Figure 1-2). As a group, participating teams will agree on the characteristics of the natural and engineered systems (i.e., a scenario), performance measures, and conceptual models describing processes affecting radionuclide mobilization and transport in the repository system (indicated in blue). Each team will then develop its own forward model(s), calculate the performance measures, and perform uncertainty and sensitivity analysis. At each of the independent stages (indicated in green), a comparison of results will be made.

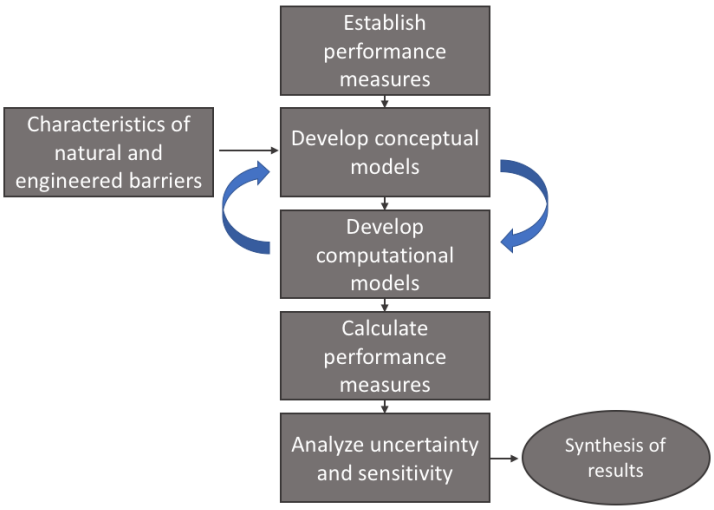

Figure 1-1. The performance assessment process (modified from OCRWM, 1990).

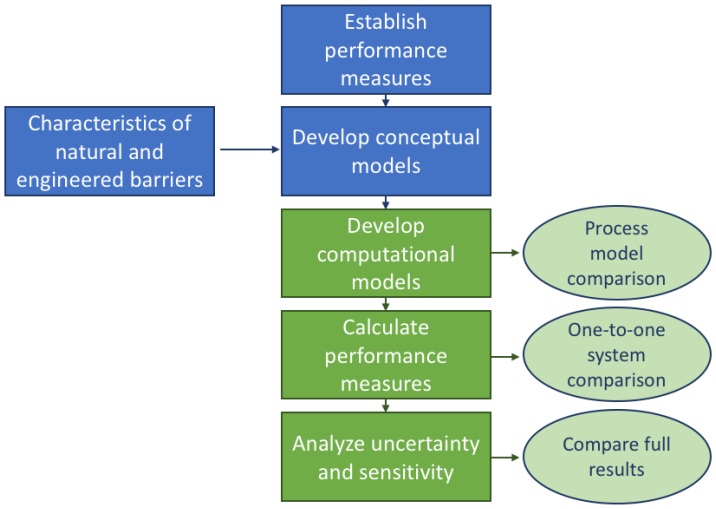

Figure 1-2. Task F workflow: Items in blue rectangles will be given by the task lead or developed as a group. Items in green rectangles will be completed by individual teams. Comparisons to be performed are in ovals.

1.2.1 Characteristics of the Natural and Engineered Barrier Systems

Forward modeling requires information characterizing the repository system and its subsystems. For each of the generic reference cases, we assume all necessary information is available. Key features, events, and processes (FEPs) and associated uncertainties have been identified and adequately characterized.

1.2.2 Performance Measures

Task F will focus on performance measures indicative of the ability of the repository system to isolate radionuclides from the biosphere through containment and retardation. Performance measures will include those related to the overall performance of the repository system, such as radionuclide

concentrations in groundwater some distance from the repository, and those related to the performance of individual components and their safety function in the engineered or natural system, such as canister thickness, radionuclide flux from one component of the system to another, and path length.

1.2.3 Conceptual Models

Conceptual models (i.e., scenarios) describe the key FEPs affecting performance measures. Task F requires that participating teams work from a common understanding of, for instance, regional hydrogeologic conditions, waste canister failure mechanisms, and processes affecting radionuclide transport in the repository and in the host rock.

Conceptual models of interest may also include scenarios for evolution of the repository system that consider the effects of climate cycles or future tectonic events.

1.2.4 Computational Models

Each team will be responsible for choosing specific computational models to simulate the agreed upon scenarios, and the key FEPs included. For example, teams may choose to simulate flow in fractures using a discrete fracture network (DFN) or an equivalent continuous porous medium (ECPM), and to simulate radionuclide transport using the advection/dispersion equation or particle tracking. Generally speaking, a team may choose to include or neglect a particular process or feedback between processes, to use a more or less mechanistic model, and to couple processes more or less tightly.

1.2.5 Quantitative Analysis of Performance Measures

Performance measures resulting from deterministic simulations of the reference case scenario(s) as well as distributions of performance measures resulting from propagation of uncertainty will be compared.

1.2.6 Uncertainty and Sensitivity Analysis

Performance assessment is subject to a variety of uncertainties, which may be categorized in different ways by different programs. Scenario uncertainty relates to uncertainty about FEPs that may affect the future evolution of the repository system. Conceptual or model uncertainty relates to uncertainties regarding understanding and representation (or omission) of processes affecting performance. Uncertainties regarding how well parameter values are known, occurrence of random events, and stochastic distribution of spatially heterogeneous properties may be lumped as data uncertainties or depending on the design of the analysis separated into epistemic (state of knowledge) uncertainties and aleatory (roll of the dice) uncertainties.

Uncertainty and sensitivity analysis in Task F will directly address uncertainties through quantification, sampling, and propagation of uncertain inputs through multiple realizations of the forward model(s).

This page is intentionally left blank.

2. TASK STRUCTURE

DECOVALEX tasks typically involve three model comparison components of increasing complexity, the first two of which are well-constrained by synthetic or experimental data and may involve identifying processes contributing to observed phenomenon, and developing and parameterizing models that explain the data:

- Benchmarks: Relatively simple cases, either synthetic or well-constrained experiments to act as a 'warm-up' for participants and to allow simulators and process models to be compared.
- Test Cases: More complex modelling, often with detailed comparison against experimental data.
- Applications: Forward modelling that applies learning from Benchmarks and Test Cases to situations of direct interest for radioactive waste disposal, at larger spatial and/or temporal scales.

Task F is atypical in that it does not include a comparison to experimental data and does not seek to develop or parameterize models that explain data. Task F assumes that processes have been identified and models have been defined and parameterized. Through comparison of forward models of increasing complexity, Task F seeks to understand the uncertainty introduced by modeling choices (model dimensionality, model fidelity, alternate models, methods of coupling) and uncertain model inputs:

- Benchmarks and Process Models: Comparison of simulators and process model implementations on relatively simple problems that address a subset of the features and/or processes included in the full reference case simulation. These comparisons will develop a common understanding among participants and identify differences in model behavior that may also propagate through the more complex analyses. Uncertainty propagation may be included at this stage to test methods but will be limited by the simplicity of the test problems.
- Deterministic Reference Case: Comparison of a full reference case simulation that addresses coupling between processes and results in multiple performance measures. These comparisons will identify differences in model behavior that appear to arise from methods of coupling, omission of FEPs, or models of differing fidelity.
- Uncertainty Propagation: Comparison of uncertainty in performance measures resulting from propagation of uncertainty through the reference case simulation, and comparison of sensitivity of performance measures to uncertain model inputs.
- Sensitivity Analysis: Interested teams may also compare the utility of different sensitivity analysis methods, such as correlation, regression, or variance-based decomposition; and the use of metamodels and/or data transformations.

2.1 Outline Structure

The task outline structure for the crystalline (C) subtask (Task F1) is as follows:

- Step 0C: Review the DECOVALEX-2023 crystalline reference case proposal. Agree on key FEPs. Finalize details of conceptual model specification and parameterization for one scenario.
- Step 1C: Identify individual process models for benchmark comparisons and make the comparisons. Benchmarks will include simulation of advection, diffusion, and dispersion; fracture flow and transport; radioactive decay and ingrowth; rate-controlled waste form degradation and release of radionuclides. Others will be developed as needed throughout the course of the comparison.

- Step 2C: Crystalline reference case deterministic simulation. (May include multiple realizations of the fracture network.)
- Step 3C: Identify uncertain inputs and appropriate probability distributions for the crystalline reference case. Compare mean, median, and quantitative metrics of uncertainty for performance measures. Calculate prescribed measure of sensitivity such as partial correlation coefficients and standardized regression coefficients and compare them.
- Step 4C (optional): Interested teams may apply sensitivity analysis methods of their choice to the crystalline reference case for a comparison of sensitivity analysis methods.

The task outline structure for the salt (S) subtask (Task F2) is as follows:

- Step 0S: Develop the DECOVALEX-2023 salt reference case proposal. Agree on key FEPs. Finalize details of conceptual model specification and parameterization for one scenario.
- Step 1S: Identify individual process models for benchmark comparisons and make the comparisons. Benchmarks may include simulation of salt creep; crushed salt reconsolidation; advection, diffusion, and dispersion; thermal conduction; radioactive decay and ingrowth; rate-controlled waste form degradation and release of radionuclides; and other processes identified while building the reference case.
- Step 2S: Salt reference case deterministic simulation.
- Step 3S: Identify uncertain inputs and appropriate probability distributions for the salt reference case. Compare mean, median, and quantitative metrics of uncertainty for performance measures. Calculate prescribed measure of sensitivity such as partial correlation coefficients and standardized regression coefficients and compare them.
- Step 4S (optional): Interested teams may apply sensitivity analysis methods of their choice to the salt reference case for a comparison of sensitivity analysis methods.

Steps 4C, 3S and 4S will be proposed as part of a future DECOVALEX task, as will additional uncertainties in Step 3C.

Table 2-1. Revised schedule of Task F steps. Green indicates crystalline. Orange indicates salt.

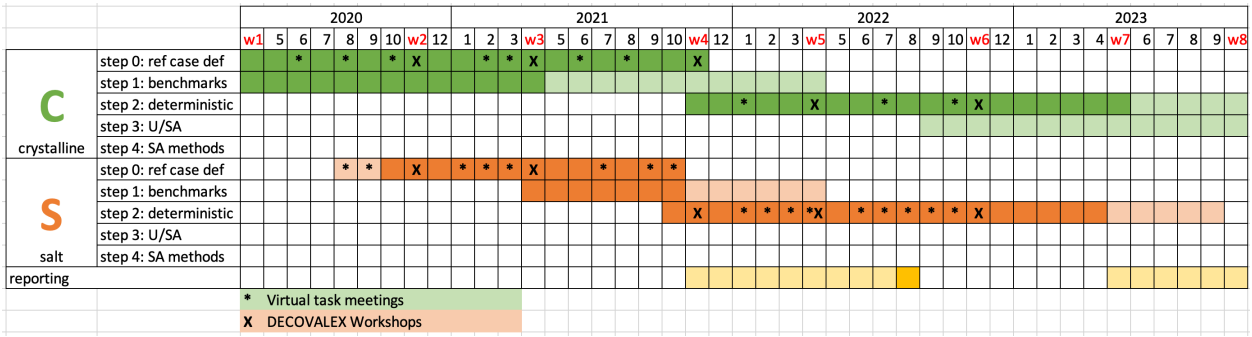

3. STEPS 0C AND 2C FOR THE CRYSTALLINE REFERENCE CASE

This section describes the generic reference case under development in Task F1 for a mined repository in fractured crystalline rock. In Step 0C, participating teams develop a common description of the FEPs to consider in the reference case and quantitatively characterize and parameterize associated materials and models using values from the literature. The result of that ongoing process is the crystalline reference case model presented here.

The final DECOVALEX-2023 description of the crystalline reference case is intended to be documented in this revision of the task specification. The crystalline reference case simulates steady state flow and transient solute transport given generic tracer source terms and a limited radionuclide inventory in the repository. Further decisions regarding key FEPs affecting performance and evolution of the engineered and natural systems and scenarios of interest are potentially forthcoming with additional development of the reference case in future DECOVALEX tasks.

The reference case is described in terms of the geologic setting (Section 3.1), emplacement concept (Section 3.2), radionuclide inventory (Section 3.3), repository layout (Section 3.4), engineered barrier system (Section 3.5), and natural barrier system (Section 3.7). Tracer source terms for the simulations and model outputs for comparison are identified and described in Section 3.7.3 and Section 3.9, respectively. Given a common description of the reference case components, each team is responsible for deciding how to represent the components in its performance assessment model. Such decisions may include, for example, simplifying the geometry of a feature, representing each component of the repository versus lumping components of the repository, or treating the fractured rock as a DFN versus treating it as a continuous porous medium.

In the crystalline reference case, spatial uncertainty is included due to the uncertain distribution of fractures with length less than 1 km. Given the stochastic distributions in Section 3.7.2, teams are tasked with generating 10 realizations of the fractured rock and running 10 realizations of their performance assessment model. Ten realizations of the DFN are provided for teams that lack the capability to generate fractured rock realizations. It is recommended that teams using the provided DFNs make independent choices about upscaling, if they choose to represent the rock as a continuous porous medium.

3.1 Geologic Setting

The reference case repository is located beneath a gently sloping hill in a domain 5 km in length, 2 km in width, and 1 km in depth. The repository is located in the west (left) side of the domain, and the area of lowest elevation is located in the east (right) side of the domain. Conceptually, the area of lowest elevation represents the edge of a large lake or wetland.

Surface elevation decreases 20 m over a distance of 2 km; it is assumed that the hydraulic pressure at the top surface of the domain mimics the topography (Figure 3-1). The surface elevation (z, in meters) is described as a function of distance (x, in meters):

$$[z = 1020]_{0 \le x < 1700}$$

$$[z = 10 * \sin(r) + 1010]_{1700 \le x \le 3700}$$

$$[z = 1000]_{3700 < x \le 5000}$$

where $r(x = 1700) = \pi/2$ and $r(x = 3700) = 3\pi/2$. Hydraulic pressure is calculated from a reference pressure of 101,325 Pa at z = 1000 m, assuming a water density of 1000 kg/m^3 or using the equation of state available in a team's flow simulator. No flow boundary conditions are imposed at all other faces of the domain.

The cross section in Figure 3-1 shows three different depth zones in which fracture intensity and fracture transmissivity decrease with depth; depth zones are described in more detail in Section 3.7.

In such a setting, salinity could be expected to increase with depth, and a layer of sedimentary overburden could be expected. However, for the purposes of simplifying the reference case, variation in salinity and existence of overburden are neglected.

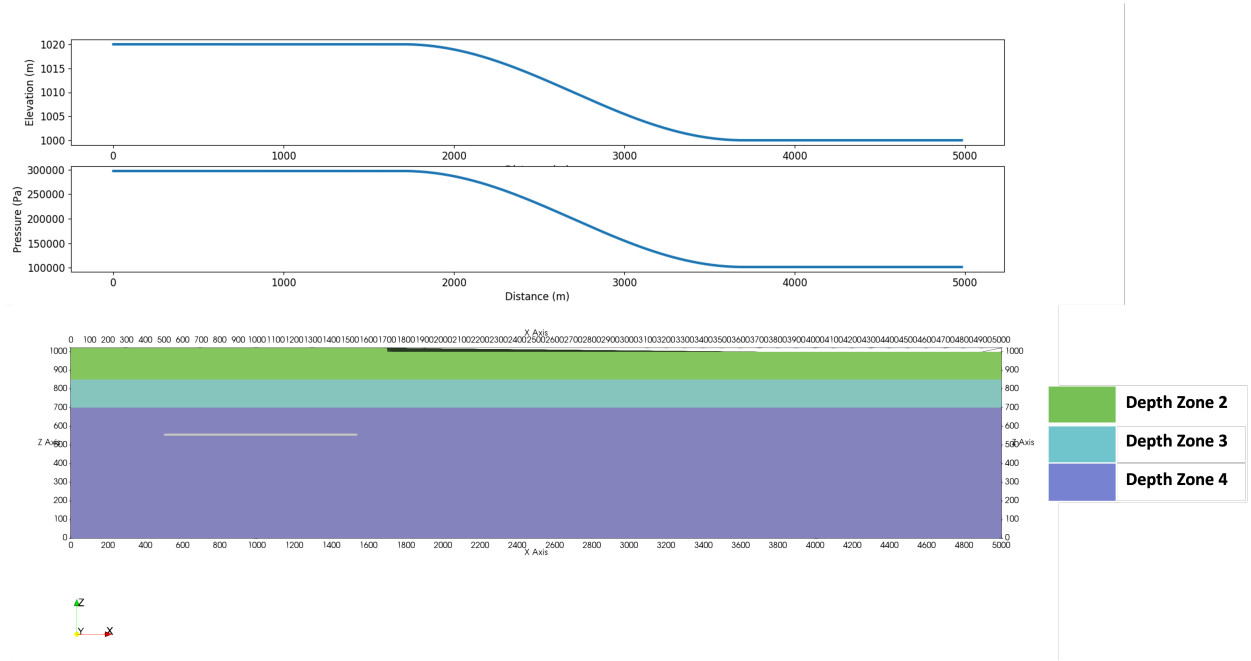

Figure 3-1. Elevation profile and corresponding surface pressure boundary condition (top) and depth zones in the domain (bottom).

3.2 Emplacement Concept

The generic reference case uses the KBS-3V emplacement concept developed for the Swedish and Finnish repository programs (Pettersson and Lönnerberg, 2008) and adopted by several countries as the reference design for a generic reference case or in the preliminary stages of site investigation (TPC, 2017; Choi et al., 2013; NWMO, 2012). The KBS-3V concept is developed for a repository mined at a depth of approximately 500 m in sparsely fractured crystalline rock. Copper canisters each containing a nominal inventory of four pressurized water reactor (PWR) fuel assemblies are emplaced within rings of compacted bentonite in vertical deposition holes beneath the floor of a deposition tunnel, and tunnels are backfilled.

The repository system isolates radionuclides from the biosphere primarily through the safety function of containment, and secondarily through retardation. The depth of burial together with the hydraulic, chemical, and mechanical environment at depth protects the canisters from failure due to corrosion or mechanical loading. The canister itself is designed to withstand mechanical loading and resist corrosion under geochemical conditions at depth. The bentonite buffer additionally protects the canister by slowing transport of corrodents, absorbing shear motion, and preventing direct contact of the canister with the host rock. In the case of canister failure and depending on failure mechanism, the low permeability and high adsorption capacity of the bentonite retards radionuclide transport. Adsorption and matrix diffusion along fracture flow paths also retard radionuclide transport.

3.3 Inventory

The waste inventory is 4350 metric tons initial heavy metal (MTIHM) in the form of PWR SNF. Assuming each PWR assembly contains 0.435 MTIHM, 2500 4-PWR canisters are required to dispose of

the inventory. The waste inventory is deliberately small to reduce the computational burden of simulations.

The initial radionuclide inventory is calculated assuming an initial enrichment of 4.73 wt% ^{235}U, 60 GWd/MTIHM burnup, 100 years out of reactor (OoR) (Carter et al., 2013). The radionuclide mass fractions for this fuel are provided in Table 4-1 along with radionuclide atomic weights and decay constants. Assuming a burnup of 60 GWd/MTIHM provides a conservative upper-bound on heat generation if future iterations of the reference case consider heat.

For the simulations, a subset of radionuclides from this inventory is selected. The radionuclides include ^{129}I and the decay chain of ^{238}U to ^{226}Ra, as described in Section 3.8.2. In addition, two tracers are included in the reference case simulations, as described in Section 3.8.1.

3.4 Repository Layout

The repository, located at a depth of approximately 450 m, comprises 50 deposition drifts branching off two parallel access tunnels (Figure 3-2). The deposition drifts are spaced 40 m center-to-center; 50 deposition holes within each tunnel are spaced 6 m center-to-center. This spacing ensures that peak buffer temperatures do not exceed 100ºC (Pettersson and Lönnerberg, 2008). The deposition drifts are 306 m in length so that the deposition tunnel extends 6 m beyond the center of the last deposition hole at both ends. There are 50 individual deposition drifts which results in a total of 2500 deposition boreholes.

The geometry of the deposition holes is given together with the description of the buffer in Section 3.5.3. The geometry of the access tunnels and deposition drifts is given together with the description of the backfill in Section 3.5.4.

The dimensions of the repository are 1040 m from east to west and 662 m from north to south. With the left, front, bottom corner of the domain defined as (0, 0, 0) in (x, y, z), the reference points locating the repository in the domain are:

- The west face of the short tunnel connecting the two central tunnels is at x = 500 m.
- The midline of the repository in the y direction is at y = 1000.
- The floor of the drifts and tunnels is at z = 550 m (470 m below a surface elevation of 1020 m, or 450 m below a surface elevation of 1000 m).

For simplicity, the shafts and a ramp that would connect the repository to the surface are neglected. For a repository in crystalline rock, primary paths to the biosphere are generally considered to be through fractures in the rock.

The repository is located in the domain such that all parts of the repository are greater than 100 m from the deterministic fracture zones described in Section 3.7.1. A 100-m offset distance of deposition holes from major deformation zones that have the potential to experience large displacements in the case of a seismic event or to provide a highly transmissive transport path to the biosphere will be enforced throughout further development of the reference case.

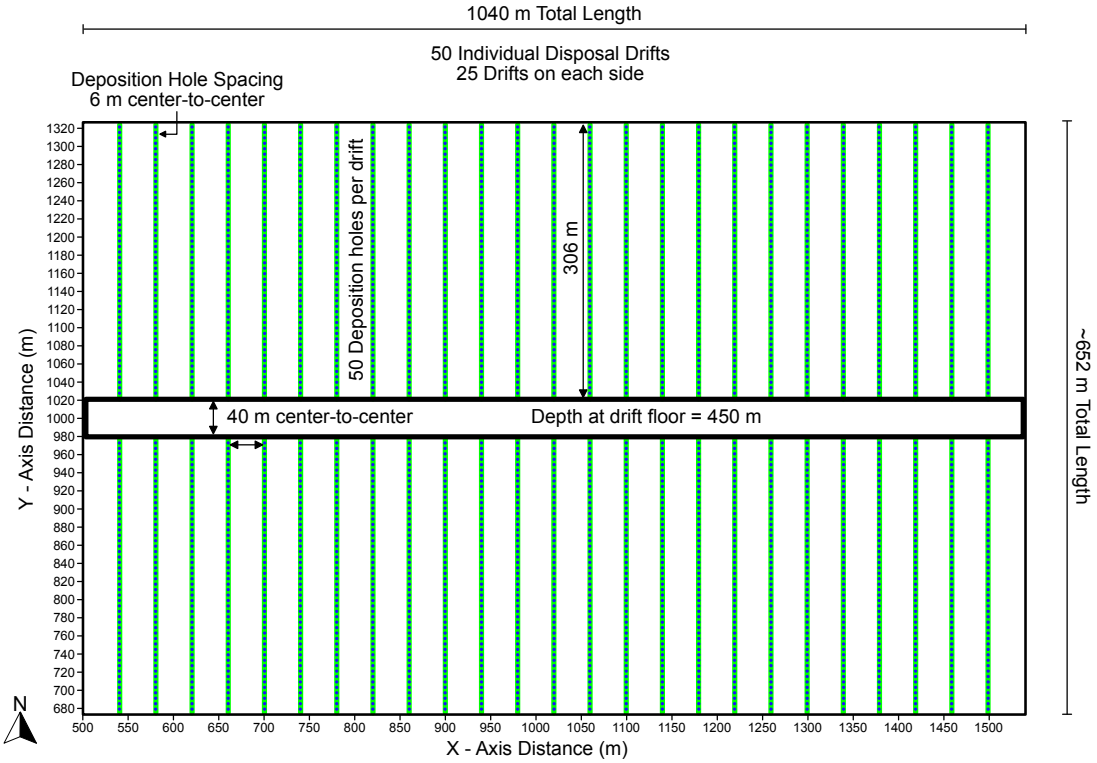

Figure 3-2. Repository layout for the crystalline reference case. (Black outline around the repository is not a tunnel.)

3.5 Engineered Barrier System

3.5.1 Waste Form

Fuel rods are comprised of UO_2 pellets in Zircaloy cladding tubes. No performance credit is taken for the cladding. Upon inundation of a breached canister, radionuclides are released from the UO_2 fuel in two fractions. A fraction of the fission products (accumulated in void spaces within the fuel rods) is released instantly. All other radionuclides are released by rate-controlled congruent dissolution of the UO_2 waste form.

Characterization: UO_2 dissolution is modeled assuming a fractional rate appropriate for the geochemical environment (Werme et al., 2004).

Safety function: Rate-controlled dissolution retards radionuclide release.

Processes to consider in this iteration of the reference case:

- For tracers (Section 3.8.1)
  - Fractional fuel matrix degradation rate for Tracer 2.
- For radionuclides (Section 3.8.2)
  - Radioactive decay and ingrowth within the waste form.
  - Instant release fraction (IRF).
  - Fractional fuel matrix degradation rate.
  - Solubility limitations.

3.5.2 Waste Package

The waste package for the KBS-3V emplacement concept is a copper canister with cast iron insert (Figure 3-3). The copper shell and cast-iron insert are described in the following sections. The canister dimensions are 4905 mm in length and 1050 mm in diameter (Figure 3-4).

Figure 3-3. Exploded view of the canister components (from left: copper base, copper tube, insert, steel lid for insert and copper lid) (from SKB 2011, TR-11-10).

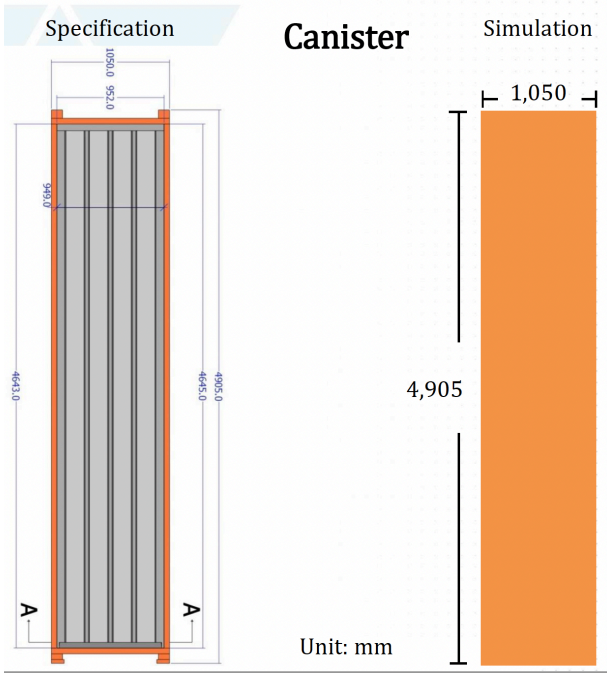

Figure 3-4. Canister dimensions in engineering specification (left) and for use in the reference case (right) (from Chang et al., 2021).

3.5.2.1 Canister Insert

The canister insert for the KBS-3V concept comes in two designs, one for 12 BWR (boiling water reactor) fuel assemblies and one for 4 PWR fuel assemblies (Figure 3-5). The reference case assumes four PWR fuel assemblies. Both insert designs consist of nodular cast iron with a steel tube cassette for each fuel element.

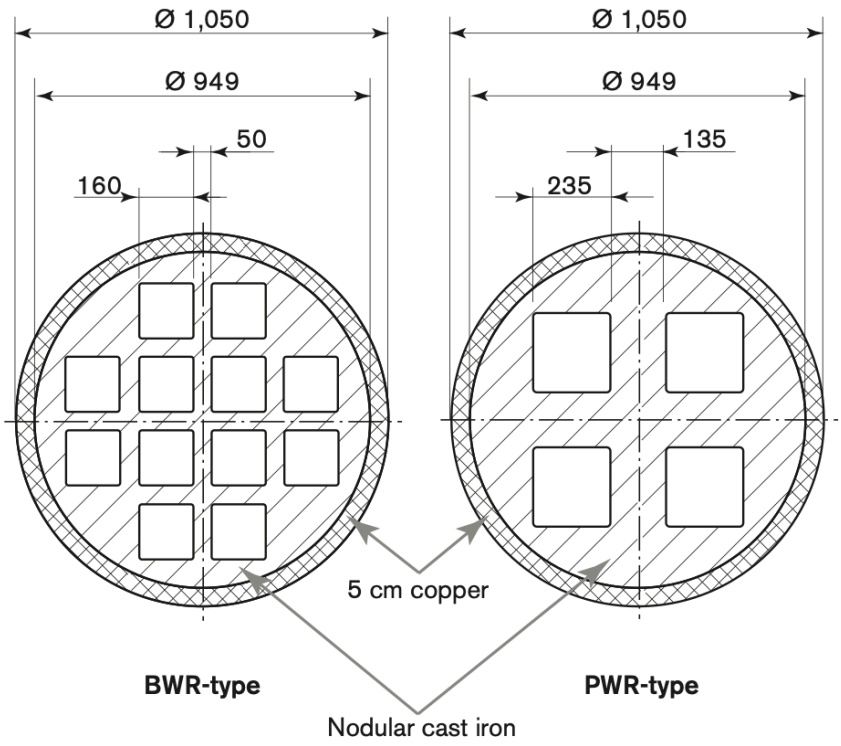

Figure 3-5. Cross section of insert designs of the BWR and PWR type inserts for the KBS-3V concept (from SKB, 2011; dimensions in mm).

Characterization: Teams are responsible for choosing canister properties consistent with their approach to constructing a performance assessment model. For example, if a porous medium flow and transport model is used, it may be necessary to assign permeability and porosity to the canister. If future iterations of the reference case require specific properties to be specified, the properties of the cast iron insert will be taken from SKB (2010a), Section 3.1.

Safety function: Mechanical strength resists isostatic loading and shear stress to contain radionuclides.

Processes to consider in this iteration of the reference case:

- Initial tracer transport simulations assume canisters provide no containment function. Therefore, no processes are considered.

3.5.2.2 Canister Shell

The canister shell goes on the outside of the canister insert and consists of 5-cm thick copper (Figure 3-5).

Characterization: Teams are responsible for choosing canister properties consistent with their approach to constructing a performance assessment model. For example, if a porous medium flow and transport model is used, it may be necessary to assign permeability and porosity to the canister. If future iterations of the reference case require specific properties to be specified, the properties of the copper shell will be taken from SKB (2010a), Section 3.2.

Safety function: The copper canister contains radionuclides by resisting corrosion in repository geochemical conditions. Because it is ductile, it resists shear failure.

Processes to consider in this iteration of the reference case:

- For tracers, no credit is taken for canister shell performance (Section 3.8.1).

- For radionuclides (Section 3.8.2)
  - Early failure (at time zero) is assumed for one canister shell in the center of the repository due to an undetected defect (Section 3.10).
  - All canister shells fail at 50,000 years due to glacial period processes (Section 3.10).

3.5.3 Buffer

Figure 3-6 shows the geometry of the canister and bentonite buffer in the deposition hole, which is 8155 mm in length and 1750 mm in diameter. Each canister is surrounded by blocks of compacted bentonite. The buffer consists of one solid bottom block, six ring-shaped blocks around the canister and three solid blocks on top of the canister. Gaps between bentonite blocks and the wall of the deposition hole are filled with bentonite pellets. Although Figure 3-6 indicates that the bulk density of the buffer would vary along the length of the deposition hole, the reference case does not take into account this variation.

The main function of the buffer is to restrict water flow around the canister. This is achieved by a low permeability, which makes diffusion the dominant transport mechanism, and its combination of ductility and the development of a swelling pressure in the presence of water, which makes the buffer self-sealing. The buffer should also keep the canister in position in the deposition hole, protect the canister from some rock shear movements and maintain its properties for the timescale of the assessment.

Several processes affecting canister integrity and radionuclide transport occur in the bentonite. Hydraulic, mechanical, and chemical processes including inflow, erosion, and reactive transport of solutes may be considered as the reference case progresses.

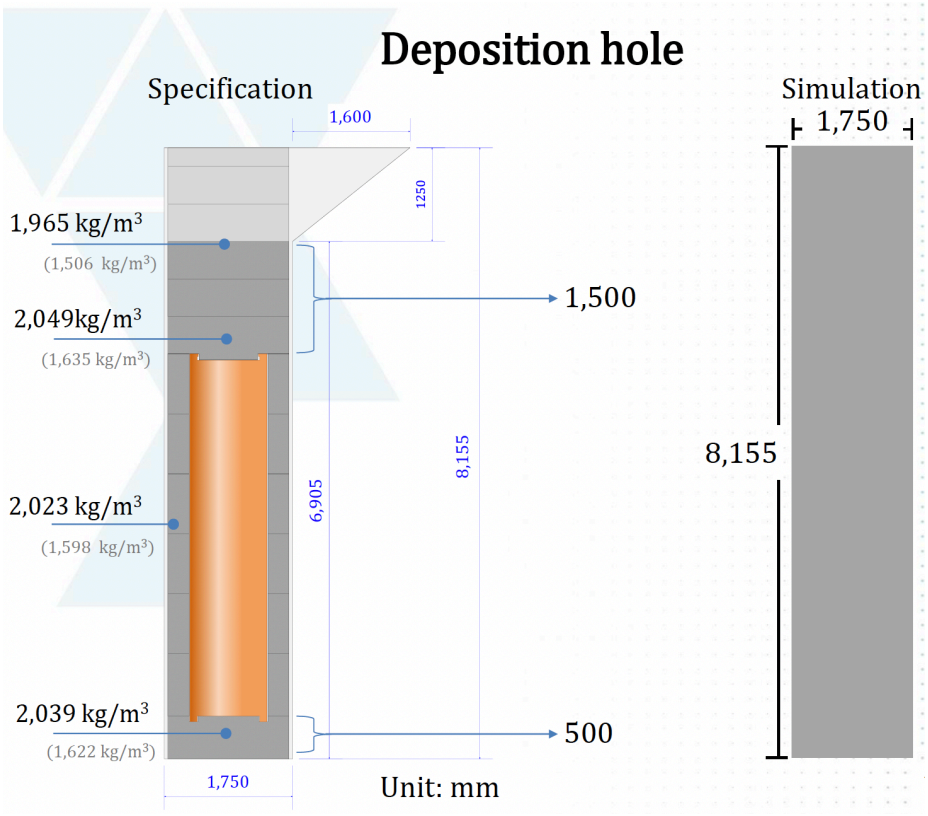

Figure 3-6. Deposition hole dimensions in engineering specification (left) and for use in the reference case (right) (from Chang et al., 2021). The thickness of the buffer around the canister is 35 cm.

Characterization: Hydraulic properties of the bentonite buffer are given in Table 3-1.

Safety function: Bentonite buffer provides the hydraulic, mechanical, and chemical conditions that support canister integrity. The low permeability and high adsorption capacity of bentonite retard radionuclide transport.

Processes to consider in this iteration of the reference case:

- Advection and diffusion. Diffusive transport dominates in intact buffer.
- Retardation of adsorbing radionuclides.

Table 3-1. Material properties of buffer.

Parameter	Value	Reference
Permeability (m^2)	6×10^{-21}	SKB TR-10-44 (Table 12-3)
Porosity (unitless)	0.44	SKB TR-10-15 (Appendix B) SKB TR-10-50 (Table 3-2)
Effective Diffusivity* (m^2/s)	1.4×10^{-10}	SKB TR-10-52 (Equation 5-4)

*Effective diffusivity, $D_e = D_m \phi \tau$, where D_m is molecular diffusion coefficient of solute in free water (1.0E-09 m^2/s), ϕ is porosity, and $\tau < 1$ is tortuosity.

3.5.4 Backfill

Figure 3-7 shows the geometry of the access (main) tunnels and deposition tunnels. The reference case assumes nominal rectangular cross sections. The access tunnels are nominally 10 m in width and 7 m in height. The deposition drifts are nominally 4.2 m in width and 4.8 m in height. Deposition tunnels are backfilled with compacted bentonite blocks and bentonite pellets. For simplicity, the reference case will assume that access tunnels are backfilled with the same.

Although the processes that can occur in the backfill are similar to those that occur in the buffer, they are of less interest in the reference case because the backfill exerts less influence on canister integrity and radionuclide transport. For this reason, the reference case will not consider processes such as erosion or settling that may affect the performance of the backfill.

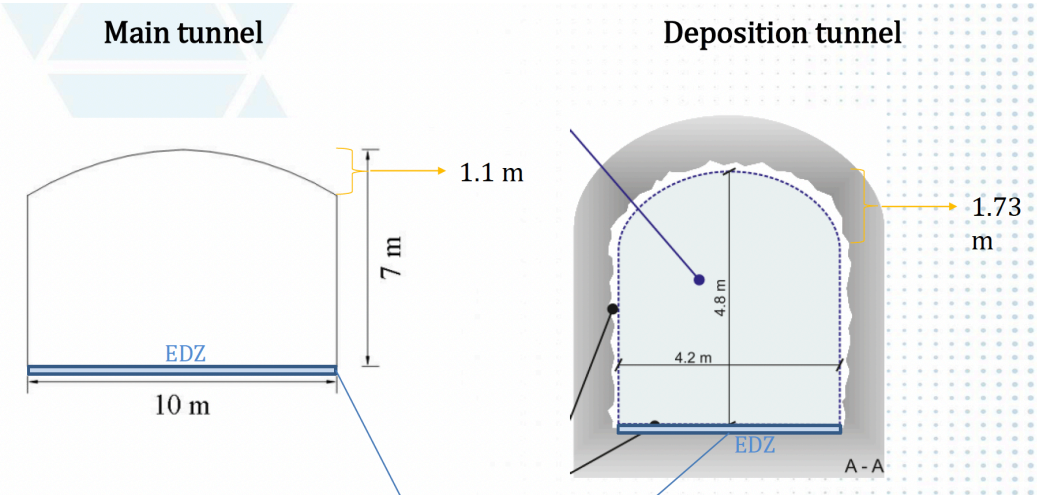

Note: The excavation damage zone is neglected in initial referecne case simulations (Section 3.6.1).

Figure 3-7. Cross section of the access tunnel (right) and deposition tunnel (left) with nominal dimensions indicated (Chang et al., 2021 after SKB TR-10-16 (pg. 28) and SKB R-09-59 (pg. 36)).

Characterization: Hydraulic properties of the bentonite backfill are given in Table 3-2.

Safety function: The backfill provides the hydraulic, mechanical, and chemical, conditions that help maintain canister and buffer emplacement in the deposition holes. The low permeability and high adsorption capacity of bentonite retard radionuclide transport.

Processes to consider in this iteration of the reference case:

- Advection and diffusion of tracer. Diffusive transport dominates in intact backfill.
- Retardation of adsorbing radionuclides.

Table 3-2. Material properties of the backfill.

Parameter	Value	Reference
Permeability (m^2)	1.5×10^{-20}	SKB TR-10-44 (Table 12-3)
Porosity (unitless)	0.46	SKB TR-10-50 (Table 3-2)
Effective Diffusivity (m^2/s)	1.6×10^{-10}	SKB TR-10-52 (Equation 5-4)

3.5.5 Features Not Included

Plugs constructed with low-pH concrete will keep the backfill in the deposition tunnels in place until the main tunnel is backfilled (SKB, 2010b). During excavation, fractures with high inflow rates are grouted with low-pH shotcrete to minimize inflow to the excavation. Grout affects inflow into the repository during excavation, and therefore may be considered in establishing initial conditions for post-closure groundwater flow simulations. Grout and concrete plugs perform no post-closure safety function. Although dissolution of cement will locally affect groundwater chemistry, they are not expected to be durable, are distant from deposition holes, and the reference case neglects them.

3.6 Excavation Damage Zone (EDZ)

3.6.1 Tunnel EDZ

The EDZ is the portion of the tunnel wall whose properties are changed due to excavation or changes in stress field associated with excavation. The EDZ forms a potential path for radionuclide transport because its permeability and, to a lesser extent, porosity are higher than in the intact host rock. Current reference case simulations neglect the EDZ.

3.6.2 Deposition Hole EDZ

Thermal spalling may occur in the deposition holes, increasing the permeability of the host rock and mass transfer rates between the deposition hole and the fractures. Current reference case simulations neglect thermal spalling.

3.7 Natural Barrier System

The crystalline host rock is characterized by occurrence of large-scale, highly-fractured brittle deformation zones and intervening masses of competent rock containing sparse networks of connected fractures. Following the example of SKB (e.g., Joyce et al., 2010), the former are named Hydraulic Conductor Domains (HCD) and the latter are named Hydraulic Rock Mass Domains (HRD).

The fractures within the HRD are subdivided up into three different depth zones, representing vertical variations within the subsurface. Each depth zone contains three different families, representing variations in orientation (strike and dip, or equivalently, trend and plunge) and hydraulic properties.

Conceptually, present day properties such as transmissivity of individual fractures exhibit a dependence on the present-day stress field. As a result, there is a greater density of fractures, larger proportion of subhorizontal fractures, and higher fracture transmissivity at shallower depths, and lower density of fractures, lower proportion of subhorizontal fractures, and lower fracture transmissivity at greater depths.

HCD and HRD are described in more detail below.

Safety function: The crystalline host rock and depth of the repository within it provide hydraulic, mechanical, and chemical conditions that protect the waste canisters. Matrix diffusion and adsorption retard radionuclide transport.

Processes to consider in this iteration of the reference case:

- Steady-state flow in open, connected fractures and fracture zones.
- Advection and diffusion of tracer. Advection dominates in fractures.
- Retardation of adsorbing radionuclides.
- Fracture-matrix diffusion.

3.7.1 Hydraulic Conductor Domains (Deterministic Features)

HCD are defined as local to regional-scale deformation zones with widths of meters and lengths greater than a kilometer that contain a high density of transmissive fractures. HCDs are observable on surface outcrops, as surface lineaments, and as highly fractured intervals in boreholes. Their locations, dimensions, and orientation are constrained by these observations, so that they are included as deterministic features in hydrogeological models and in flow and transport simulations.

Characterization: The reference case employs a representative set of deterministic deformation zones whose spacing and orientations are derived from observations of brittle fracture zones at Olkiluoto (Hartley et al., 2018). In the reference case, the deterministic deformation zones, or HCDs, are represented as singular, planar features – essentially large deterministic fractures. The aperture and transmissivity of the deterministic fractures are defined as outlined in Section 3.7.2 using the cubic law and the correlated relationship between fracture transmissivity and fracture radius, where the dimensionless coefficients *a* and *b* are taken from the EW fractures in Depth Zone 3 (Table 3-4). The deterministic fractures are defined by Table 3-3 and shown in Figure 3-8. These circular subhorizontal and subvertical features are spaced throughout the domain.

Table 3-3. Location and orientation of the deterministic fractures.

ID #	Radius (m)	Translation (x, y, z coordinates of fracture center, m)*	Unit Normal Vector (orientation)
1	3451.39	{-501.41,1823.58,-481.95}	{-0.67342,0.73387,-0.08904}
2	897.266	{-55.38,-452.20,284.20}	{-0.24506,-0.013604,-0.96941}
3	650.303	{2072.39,-676.33,372.32}	{-0.38242,0.09575,-0.91901}
4	2318.13	{-606.04,1176.42,-1042.55}	{-0.50116,-0.63138,-0.59177}
5	1595.92	{1769.15,241.45,124.63}	{-0.55597,0.78048,-0.28590}
6	1625.51	{2275.47,-849.96,-923.85}	{-0.59401,-0.80091,0.07533}

*The (x, y, z) coordinates of the fracture center are given relative to the position (0, 0, 0) at the center of the domain. Add (2500, 1000, 500) to place the fractures relative to the position (0, 0, 0) at the left, front, bottom corner of the domain.

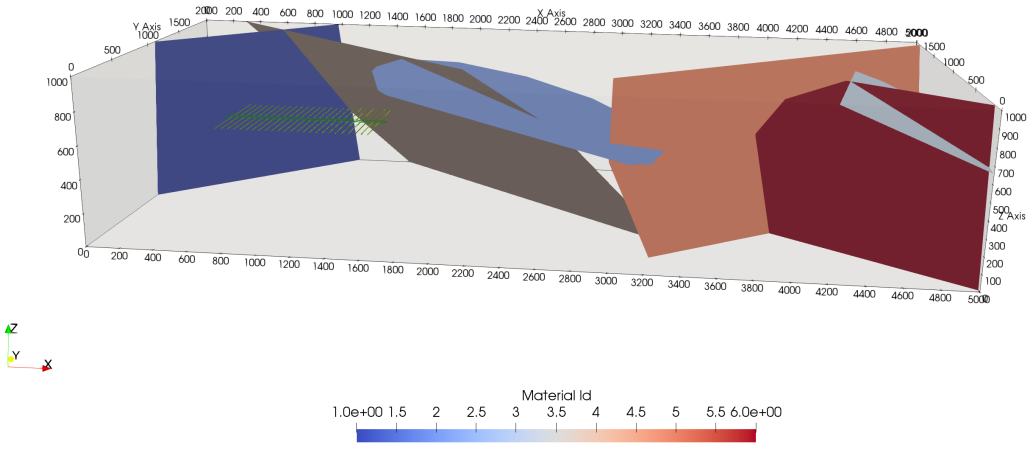

Figure 3-8. Deterministic fractures in the model domain.

3.7.2 Hydraulic Rock Mass Domains (Stochastic Discrete Fracture Networks)

HRD outside the HCDs contain fractures and minor deformation zones with lengths ranging from less than 1 m up to 1 km that are not deterministically mapped. A subset of these features (generalized as discrete fractures) forms a connected network of open fractures through which groundwater can flow. Within each HRD and/or depth interval within an HRD, fractures are grouped into fracture families on the basis of orientation and characterized by fracture intensity and probability distributions for size, orientation, and location. Stochastic realizations of DFNs for use in the hydrogeological model can be generated from these distributions. Alternatively, teams may choose to generate equivalent continuous porous media or other representations of the fractured rock from the stochastic characterization of the fracture network.

Characterization: The intensity of open fractures and probability distributions describing size, orientation, and location of open fractures in three depth zones (Figure 3-1) are taken from the Case A parameterization of the western central hydraulic unit (CHUW) at Olkiluoto, Depth Zones 2-4 (Hartley et al., 2013b). With the bottom of the domain at z = 0, Depth Zone 2 extends from the top surface to z = 850 m; Depth Zone 3 extends from z = 850 m to z = 700 m; and Depth Zone 4 extends from z = 700 m to z = 0 m. The probability distributions characterizing the stochastic fracture network are described in the following sections and corresponding parameters for each fracture family are given in Table 3-4.

This particular Olkiluoto hydraulic unit is proposed for use in the reference case because it provides an opportunity to investigate the hydromechanical coupling between stress field and fracture transmissivity in later iterations of the reference case.

Table 3-4. Parameters for stochastic fractures.

		Pole Orientation (Fisher Distribution)			Fracture Radius [m] (Power-law Distribution)		Intensity of open fractures	Transmissivity [m^2/s]	
		Mean Trend φ [◦]	Mean Plunge θ [◦]	Concentration κ	k	r_0 [m]	P_{32} [m^2/m^3]	a	b
CHUW dz2	E-W	176	4.4	9.4	2.58	0.04	0.21	8.0E-9	0.8
	N-S	270.4	0.2	8.3	2.52	0.04	0.25	1.5E-8	0.8
	SH	300.1	78.9	5.7	2.45	0.04	0.91	1.2E-8	0.8
CHUW dz3	E-W	176	4.4	9.4	2.50	0.04	0.11	2.2E-9	0.7
	N-S	270.4	0.2	8.3	2.65	0.04	0.13	6.0E-9	0.6
	SH	300.1	78.9	5.7	2.35	0.04	0.34	2.0E-9	1.2
CHUW dz4	E-W	176	4.4	9.4	2.40	0.04	0.07	7.0E-11	0.7
	N-S	270.4	0.2	8.3	2.40	0.04	0.08	8.0E-11	0.9
	SH	300.1	78.9	5.7	2.40	0.04	0.17	6.0E-11	1.0

3.7.2.1 Fracture Orientation and Location

Three fracture families, two subvertical and one subhorizontal are defined for each depth zone. The orientation of a fracture can be described by providing the orientation of a pole normal to the plane of the fracture (as in Hartley et al., 2013b). For each fracture family, the probability distribution describing the orientation of poles is a Fisher distribution, an isotropic, directional distribution equivalent to a Gaussian distribution on a sphere (von Mises-Fisher distribution). The Fisher distribution is parameterized by a mean direction (defined by mean trend (φ) and mean plunge(θ)) and a concentration parameter (κ). The larger κ, the more concentrated the poles on the surface of the sphere.

Although Hartley et al. (2013b) gives a bivariate Bingham distribution for the subhorizontal (SH) families, the simpler Fisher distribution is used as a substitution in the reference case.

Fracture locations are uniformly distributed in 3-dimensional space, limited by the fracture intensity of each fracture family.

3.7.2.2 Fracture Radius and Intensity

The probability distribution of fracture radii (r, [m]) is a truncated power law distribution, with the form of (Follin et al., 2007):

$$p(r) = \frac{k r_0^k}{r^{k+1}} \qquad \textbf{Eq. (3-1)}$$

where r_0 is the minimum radius and k is a dimensionless constant, respectively.

Fracture intensity is expressed as fracture area per unit volume of rock (P_{32} [m^2/m^3]). The P_{32} values in Table 3-4 represent the intensity of open, flowing fractures, and were calibrated to borehole flow data assuming r_0 = 0.04 m and maximum radius (r_{max}) of 564 m (Hartley et al., 2013b). P_{32} is related to the average number of fractures per unit volume of rock (n_0) by (Swiler et al., 2020):

$$P_{32} = n_0 \int_{r_0}^{r_{upper}} p(r)\pi r^2 dr = n_0 \int_{r_0}^{r_{upper}} \frac{k r_0^k}{r^{k+1}} \pi r^2 dr = \frac{n_0 \pi k r_0^k}{2-k} [r^{2-k}]_{r=r_0}^{r=r_{upper}}. \quad \textbf{Eq. (3-2)}$$

P_{32} over the range r_0 = 0.04 m to r_{max} = 564 m is equivalent to billions of fractures per km^3, the vast majority of which have radii < 1 m. To determine the P_{32} for a smaller range of radii (e.g., minimum radius, r_{min} = 30 m to r_{max} = 564 m), integrate the above over the range r_{min} to r_{max} (Swiler et al., 2020):

$$P_{32}[r_{min}, r_{max}] = \frac{\pi n_0 k r_0^k}{2-k} [r_{max}^{2-k} - r_{min}^{2-k}]. \quad \textbf{Eq. (3-3)}$$

3.7.2.3 Fracture Transmissivity, Aperture, and Permeability

Fracture transmissivity (T [m^2/s]) is a function of fracture radius. The reference case uses the fully correlated relationship defined in Follin et al. (2007):

$$\log T = \log a r^b$$

Where r is radius [m] and the coefficients a and b are dimensionless constants. Fracture aperture is calculated from the transmissivity using the cubic law (Bear, 1993):

$$aperture = \left(12T \frac{\mu}{\rho g}\right)^{\frac{1}{3}}$$

Where μ is viscosity of water [Pa s], ρ is density of water [kg/m^3], and g is the acceleration due to gravity [m/s^2]. Permeability ([m^2]) is defined as,

$$permeability = \frac{aperture^2}{12}$$

The resulting stochastic fractures are shown in Figure 3-9.

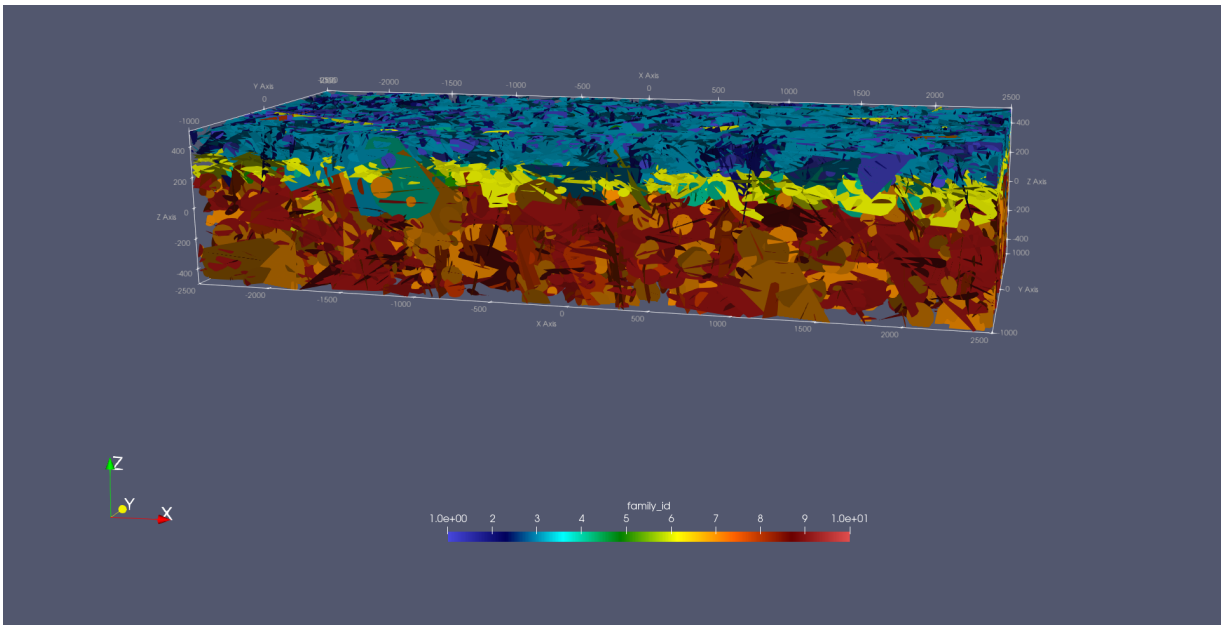

Figure 3-9. Stochastic fractures, colored by fracture family in each depth zone.

3.7.3 Fractured Rock Matrix

The crystalline reference case includes fracture-matrix diffusion. Teams choosing to use a porous medium representation of the crystalline rock need parameters describing the rock matrix. Parameters for matrix diffusion are given in Table 3-5.

Table 3-5. Material properties of the fractured rock matrix.

Parameter	Value	Reference
Permeability (m^2)	10^{-18}	Hartley et al., 2013a (Section 7.1)
Porosity (unitless)	0.0018	SKB TR-10-50 (Section 2.5)
Effective Diffusivity (m^2/s)	$10^{-13.7}$	SKB TR-10-52 (Equation 2-2)
Distance available for diffusion in the matrix (m)	12.5	SKB TR-10-50 (Table 3.2)

3.8 Tracer Transport

3.8.1 Conservative Tracer Transport

Initial simulations of the reference case involve steady state flow and conservative transport of two tracers (Table 3-6). Tracer 1 and Tracer 2 are modeled after ^{129}I. Both have an atomic weight of 128.9 g/mol. The total inventory of the two tracers in each waste package is 5.45 g (0.0423 moles), equivalent to $1/100^{th}$ of the expected inventory of ^{129}I in a waste package containing four PWR assemblies. The inventory of Tracer 1 is 0.545 g (0.00423 moles), or 10% of the total; it is instantly released at the start of the transport simulation. The inventory of Tracer 2 is 4.90 g (0.038 moles), or 90% of the total; it is released at a fractional rate of 10^{-7}/year throughout the transport simulation. (Representative ^{129}I inventory is calculated from values in Table 4-1; IRF and fractional degradation rate of the fuel matrix are taken from Table 4-4 and Table 4-5, respectively.)

Teams are expected to establish a steady state flow solution using a constant pressure (Dirichlet) boundary condition at the top surface of the domain (see Section 3.1) and no flow boundary conditions at all other faces of the domain prior to starting transport simulations. Simulations are run to 100,000 years. Initially the domain is empty of tracer everywhere except in the waste packages. Tracer is allowed to advect out of the domain at the top surface; zero gradient boundary conditions should be applied to prevent diffusion out of the domain.

Table 3-6. Tracer inventories and release mechanisms for initial reference case simulations.

	Atomic weight	Inventory per waste package	Release mechanism
Tracer 1	128.9 g/mole	0.545 g	Instant
Tracer 2	128.9 g/mol	4.9 g	10^{-7}/year

3.8.2 Radionuclide Inventory

In the second iteration of the reference case, teams will look at the decay, ingrowth, sorption, and solubility limits of ^{129}I and the decay chain of ^{238}U (^{238}U → ^{234}U → ^{230}Th → ^{226}Ra) modeled using data from the KURT (KAERI Underground Research Tunnel) site (Cho et al., 2016). The inventory for each isotope is given in Table 3-7. Mass per waste package is calculated from values given in Table 4-1 based on a waste package containing four PWR assemblies. IRFs of the radionuclides and the fractional degradation rate of the fuel matrix are taken from Table 4-4 and Table 4-5, respectively. The solubility of each isotope in reduced conditions is given in Table 3-8 and distribution coefficients in bentonite and rock are given in Table 3-9 and Table 3-10, respectively. The host rock has a density of 2650 kg/m^3 and the buffer has a density of 1600 kg/m^3.

For this iteration, only the nominal (mode) or best estimate values from these tables are to be used. The distributions are retained in this document for potential future application. Triangular and log-triangular distributions are designated in several of these tables. A triangular distribution is a continuous probability distribution shaped like a triangle. The mode, c, of the probability distribution function is the apex of the triangle (the most probable value), and a and b are the minimum and maximum values. If c equals a or b, the triangle is a right triangle (as is the case for radium solubility as shown in Table 3-8). The mean of the distribution is (a+b+c)/3. A log-triangular distribution is similar except that a log scale is used for the x-axis. A triangular distribution can be generated from a log-triangular distribution by log-transforming the parameter values.

Table 3-7. Radionuclide inventory in second iteration of reference case

Isotope	Atomic weight (g/mole)	Inventory per waste package (g)	Decay Constant (1/yr)	Daughter	Instant Release Fraction
^{129}I	128.9	5.45E+02	4.41E-08		10%
^{226}Ra	226.03	6.94E-05	4.33E-04		0%
^{230}Th	230.03	1.81E-01	9.00E-06	^{226}Ra	0%
^{234}U	234.04	8.89E+02	2.83E-06	^{230}Th	0%
^{238}U	238.05	1.58E+06	1.55E-10	^{234}U	0%

Table 3-8. Solubilities of isotopes under reducing conditions

Element	Distribution Type	Maximum Dissolved Concentration (mol/m^3)		
		Min	Best Estimate	Max
I		Unlimited		
Ra	Log-Triangular	1.0E-07	1.0E-03	1.0E-03
Th	Log-Triangular	1.0E-07	5.0E-05	5.0E-03
U	Log-Triangular	1.0E-07	5.0E-05	3.0E-03

Table 3-9. Distribution coefficients of isotopes in bentonite

Element	Distribution Type	K_d in bentonite (m^3/kg)		
		Min	Best Estimate	Max
I	Triangular	0.0	5.1E-04	5.2E-03
Ra	Log-Triangular	1.0E-03	1.0E-02	2.0E-01
Th	Log-Triangular	1.5E-02	8.6E-02	4.9E-01
U	Log-Triangular	1.0E-02	7.6E-01	3.30E+00

Table 3-10. Distribution coefficients of isotopes in rock

Element	Distribution Type	K_d in rock (m^3/kg)*		
		Min	Best Estimate	Max
I		0.0	0.0	0.0
Ra	Log-Triangular	5.0E-02	1.0E-01	5.0E-01
Th	Triangular	4.0E+00	5.0E+00	7.4E+00
U	Triangular	1.7E-02	4.3E-02	6.9E-02

*These values are for crushed crystalline rock. For the purposes of Task F1 reference case simulations, values for intact crystalline rock are assumed to be 10% of these values and are assumed to account for secondary minerals in fractures.

3.9 Output Metrics for Comparison

Teams are asked to generate 10 realizations of the fractured rock for 10 realizations of their performance assessment models. (Ten realizations of the DFN will be provided for teams that lack the capability to generate fractured rock realizations.) All other inputs are deterministic. Teams may elect to generate two sets of 10 realizations because the original simulations with tracers ignore waste package performance, as if all waste packages fail at time zero. Accordingly, all outputs involving tracers, specified below, are

intended for the original simulations with no waste package performance. In contrast, all outputs involving radionuclides, specified below, include waste package performance as defined in Section 3.10.

Conceptually, the reference case will consider two pathways by which a person could ingest radionuclides. The first is by drinking water from a well located at the end of the highest consequence path between the repository and the surface of the hillslope (1700 m < x < 3700 m). The second is by drinking water from the hypothetical body of water resting on the area of lowest elevation (3700 m < x < 5000 m). The following outputs for comparison are designed with these two ingestion pathways in mind. Means and 95% confidence intervals for the 10 realizations will be calculated for each output and shown on plots.

1. Find the cell location on the surface of the hillslope (1700 m < x < 3700 m) where the tracer mass flow is greatest. At this location,
   a. Plot mass flow (moles/year/m^2) of each tracer across the top surface of the cell as a function of time (years). Also, provide the cross-sectional area of the cell surface.
   b. Plot cumulative mass flow (moles/m^2) of each tracer across the top surface of the cell as a function of time (years).
2. Integrate over the area of lowest elevation (3700 m < x < 5000 m) to:
   a. Plot mass flow (moles/year) of each tracer across the top surface of the domain where 3700 < x < 5000 m (into the body of water) as a function of time (years).
   b. Plot cumulative mass flow (moles) of each tracer across the top surface of the domain where 3700 < x < 5000 m (into the body of water) as a function of time (years).
3. Plot the aqueous concentrations (moles per liter) of tracers and radionuclides over time at in the vicinities of two locations (listed below). This output may be the aqueous concentrations in the large grid cells that include the locations specified. For particle tracking models, this may be the average aqueous concentration in a large volume, e.g., 10000 m^3, beneath the locations specified below, or, if there are too few particles in those locations, it may be elsewhere where the concentrations are high.
   a. Hillslope at (3500, 831, 1000) where a deterministic fracture zone (HCD) intersects the bottom of the hill.
   b. Low point at (4337, 609, 1000) where two HCDs intersect at the surface.

The first comparison of tracer transport at a point location, is an attempt at locating and comparing fluxes at the highest consequence location for a well. Likely, this comparison will need to be refined to account for differences in grid discretization and other choices made by modeling teams.

We will also compare outputs that will assist in understanding system behavior and whether teams are achieving similar system behavior:

1. Record the steady state flow of water (kg/year) into and out of the top surface of the domain over the area where 0 m < x < 1700 m (top of hill).
2. Record the steady state flow of water (kg/year) into and out of the top surface of the domain over the area where 1700 m < x < 3700 m (hillslope).
3. Record the steady state flow of water (kg/year) into and out of the top surface of the domain over the area where 3700 m < x < 5000 m (area of lowest elevation).
4. Integrate over the area of the hillslope:
   a. Plot the mass flow (moles/year) of each tracer across the top surface of the domain over the area where 1700 < x < 3700 m (to the hillslope) as a function of time (years).
   b. Plot the cumulative mass flow (moles) of each tracer across the top surface of the domain over the area where 1700 < x < 3700 m (to the hillslope) as a function of time (years).

5. Find the cell location in the area of lowest elevation where the tracer mass flow is greatest. At this location:
   a. Plot mass flow (moles/year/m^2) of each tracer across the top surface of the cell as a function of time (years). Also, provide the cross-sectional area of the cell surface.
   b. Plot cumulative mass flow (moles/m^2) of each tracer across the top surface of the cell as a function of time (years).
6. Plot the inventory (moles) of each tracer and radionuclide in the repository region as a function of time (years). The inventory in the repository will decrease with time. The repository region is defined as the tightest hexahedron encompassing all drifts, access tunnels, and deposition holes; thus, it includes the host rock that falls within the hexahedron. If a model software cannot accommodate this definition, the repository region may be defined instead as the entire excavation volume of the drifts, access tunnels, and deposition holes.

3.10 Waste Package Failure Scenarios

The initial simulations of the reference case involve releasing tracers from all waste package locations at time zero taking no credit for waste package performance. Tracer 1 is instantly released at time zero, and Tracer 2 is released congruently as the fuel matrix degrades.

For the simulations involving radionuclides, two waste package failure scenarios are modeled simultaneously:

1. One waste package fails at time zero due to an undetected defect. For this iteration, the waste package that fails will be the fourth one in the center drift immediately south of the access tunnel. The approximate probability of early failure is assumed based on the estimates in Table 3-11 (taken from Maak et al., 2001). A future iteration could apply this probability distribution to the waste packages.
2. All remaining intact waste packages fail at year 50,000 due to glacial effects.

It is conservatively assumed that the waste packages provide no containment after failure (as if they disappear and there are no internal barriers such as cladding). At this time the specific waste package that fails in scenario 1 is not defined. It is assumed the entire radionuclide inventory defined in Table 3-7 is being used in both scenarios.

Table 3-11. Probability of waste package early failure

Distribution Type	Minimum probability early failure	Best-estimate probability early failure	Maximum probability early failure
Log-Triangular	1.0E-4	2.0E-4	1.0E-3

3.11 Scenarios that may be considered in future rounds of modeling

Three scenarios are proposed. All scenarios involve simulation of processes affecting flow and transport in fractures, and will require teams to make choices regarding, for instance, fracture size range, transmissivity functions, use of DFN and ECPM, use of particle tracking, and treatment of matrix diffusion.

3.11.1 Canister Failure by Corrosion under Temperate Climate Conditions

In this scenario, fracture inflow rates to one or more deposition holes are large enough to cause piping and erosion of bentonite, creating an advective pathway to the copper canister. Resulting transport rate of

sulfide to the canister is sufficient to cause the copper to corrode through. This scenario provides an opportunity to investigate the coupling between fracture flow rates, bentonite erosion, solute transport, and corrosion.

3.11.2 Shear Failure of the Canister Due to Ground Motion

In this scenario, a seismic event occurs that is large enough to cause shear failure of one or more canisters. Bentonite buffer remains essentially intact, so that the dominant transport mechanism between canister and fractured host rock is diffusion. This scenario provides an opportunity to investigate the coupling between stress, slip on fractures, and canister shear failure (for geomechanics enthusiasts) and/or to investigate alternate models for radionuclide retardation in the bentonite including adsorption isotherms, ion exchange, and/or surface complexation (for geochemistry enthusiasts).

3.11.3 Glacial Loading

In this scenario, glacial loading causes pore pressures and the stress field to change. The changes in normal and shear stress on each fracture (and deterministic HCD) cause changes in transmissivity. For the ambitious, this scenario may provide an opportunity to explore coupling between changes in stress field and canister failure mechanisms. For the less ambitious, we could simply assume canister failure and investigate influence on flow and transport modeling.

4. STEP 0S/2S SALT REFERENCE CASE

The salt reference scenario presented here will not focus on an undisturbed scenario for a salt repository. It has been shown through multiple performance assessments RESUS, KOMTESS, ISIBEL and VSG (Bollingerfehr et al., 2008; Beuth et al., 2012; Bollingerfehr et al., 2017; Bollingerfehr et al., 2018; Bertrams et al., 2020a) that there are no radiological consequences within 1,000,000 years for disposal in undisturbed salt formations because of their very low permeability and moisture content. Additionally, the integrity of rock salt is given for at least 1,000,000 years for salt rock barriers greater than 200 m in thickness (which is the scenario presented here), which provides no pathway through permeable anhydrite, boudinage, or isolated salt blocks. As a result, here we present a disturbed scenario in which the shaft seals fail 1000 years after repository closure, allowing an influx of brine down the shafts and into the repository.

For this task a staged development of models is planned, building up to a full PA. This stepwise process is done to ensure the consistency between each team's modeling efforts as complexities are added. The planned staged development is:

1. Flow + radionuclide mobilization and transport (problem description will include variably saturated initial conditions)
2. + drift convergence (salt creep and backfill consolidation will be considered)
3. + heat flow and temperature-dependence of drift convergence
4. + model uncertainty in backfill consolidation model
5. (+ gas generation)

The descriptions of the engineered and natural barrier systems have been updated as the exercise progresses so that necessary information is available at each stage of model development. The final task specification (Revision 9) includes only steps 1 and 2, with steps 3-5 to be proposed as part of a future DECOVALEX task.

4.1 Geologic Setting

The salt reference case considers a mined repository for SNF and vitrified high-level waste (HLW) in a salt dome. The generic geological cross section of a salt dome developed for the RESUS project (Bertrams et al., 2020a) is simplified to six homogeneous geologic units for use in this reference case (Figure 4-1). It is assumed that the salt dome geometry shown in Figure 4-1 extends for 9 km perpendicular to the plane of the cross section. The ground surface is at about 50 m above mean sea level (amsl) and the top of the salt dome is roughly -150 m amsl. The base of the salt diapir is at about -3150 amsl and is underlain by basement rock, which extends to the base of the section at about -5500 amsl. The repository is mined at a depth of 850 m below the ground surface, such that the floor of the repository is at an elevation of -800 amsl.

The geometry of the salt dome cross section was provided to teams. Teams are likely to develop model domains that are considerably shallower than the section shown here. Thus, properties of the basement unit should not be needed.

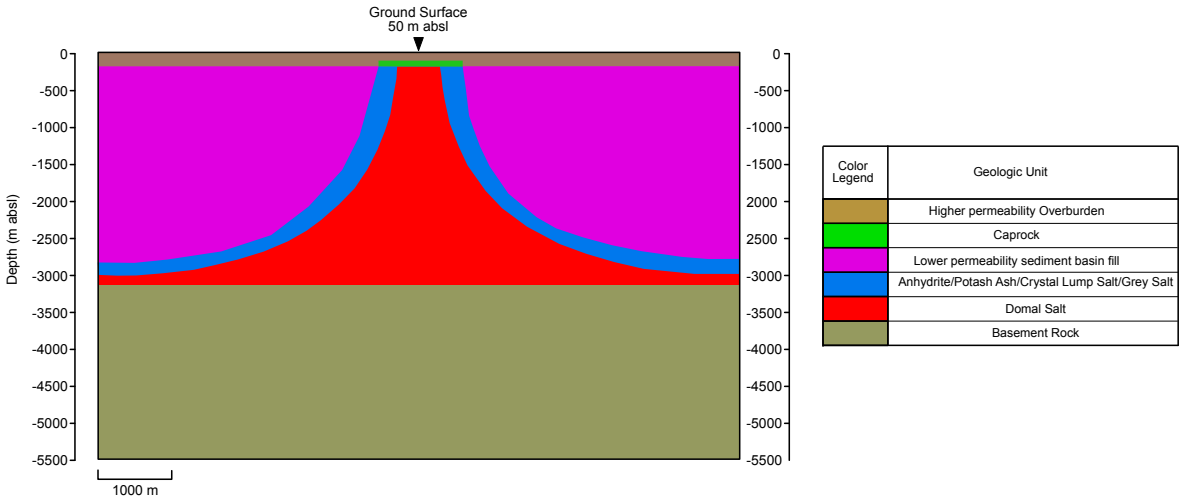

Figure 4-1. Geological cross-section with model units for the generic salt reference case. The model units are simplified from Bertrams et al. (2020a). Hydrological, mechanical, and thermal properties of the upper five units are given in Section 4.4.

4.2 Inventory

To reduce the computational burden of this comparison exercise, the salt reference case assumes small inventories of SNF and HLW. For the same reason, the radionuclides included in transport simulations are limited to single mobile, long-lived fission product, ^{129}I, and a single transuranic decay chain ($^{238}U \rightarrow ^{234}U \rightarrow ^{230}Th \rightarrow ^{226}Ra$).

4.2.1 Spent Nuclear Fuel

The reference case assumes that the inventory of SNF consists entirely of PWR fuel assemblies packaged in 500 POLLUX-10 containers (described in Section 4.3.2), each of which contains (as the name suggests) 10 assemblies. Each assembly contains 0.435 metric tons initial heavy metal (MTIHM) for a total of 2175 MTIHM. To place this value in context, it is 3.1% of the 70,000 MTIHM repository specified by the U.S. Nuclear Waste Policy Act and 20.7% of the total SNF inventory expected in Germany (Bertrams et al., 2020a).

Following the example of previous reference cases developed in the U.S. program (e.g., Mariner et al., 2015; LaForce et al., 2020), the initial radionuclide inventory and heat of decay versus time for SNF is calculated assuming an initial enrichment of 4.73 wt% ^{235}U and 60 GWd/MTIHM burn-up (Appendix C, Carter et al., 2013). A storage time of 100 years OoR prior to emplacement in the repository is assumed. In the U.S., the average burn-up of SNF assuming decommissioning without replacing existing nuclear power plants is predicted to be 54 GWd/MTIHM (Carter et al., 2013). Therefore, the assumption of 60 GWd/MTIHM results in a conservatively high heat load.

Inventories of radionuclides at the time of emplacement (Table 4-1) are expressed as grams radionuclide per MTIHM and grams radionuclide per grams total waste. The former ratio includes only the initial mass of heavy metal (i.e., ^{238}U) in the denominator; the latter ratio includes the total mass of the UO_2 ceramic waste form in the denominator. Table 4-1 also provides the atomic weight and decay constant for each radionuclide (isotope). The heat of decay is not included in the current task and is omitted from this revision of the task specification. See Section 4.3.2 for characterization of the UO_2 waste form and the POLLUX-10 container.

Table 4-1. Inventory of selected radionuclides in PWR SNF at 100 y out of reactor. Abridged from previous iterations of the task specification to include only ^{238}U decay chain and ^{129}I.

Isotope	Inventory (g/MTIHM)[1]	Inventory (g/g waste)[2]	Atomic weight (g/mol)[3]	Approximate Decay Constant (1/s)[4]	Inventory per POLLUX-10 container (g)
^{234}U	5.11E+02	3.55E-04	234.04	8.90E-14	2.22E3
^{238}U	9.10E+05	6.32E-01	238.05	4.87E-18	3.96E6
^{230}Th	1.04E-01	7.22E-08	230.03	2.75E-13	4.52E-1
^{226}Ra	3.99E-05	2.77E-11	226.03	1.37E-11	1.74E-4
^{129}I	3.13E+02	2.17E-04	128.9	1.29E-15	1.36E3
^{99}Tc	1.28E+03	8.89E-04	98.91	1.04E-13	0[5]

[1] from Carter et al. (2013, Table C-2)
[2](g isotope/g waste) is (g isotope/MTIHM)/(g waste/MTIHM), where g waste is g all isotopes (1.44x10^6 g per MTIHM)
[3]Weast and Astle (1981)
[4]Decay constants from ORIGEN (Croff, 1983)
[5] Tc is deliberately excluded from the SNF inventory.

4.2.2 High Level Waste

The salt reference case includes vitrified HLW resulting from the reprocessing of SNF. The characteristics of the vitrified waste form are based on the COGEMA vitrified waste from the Dutch fuel cycle (GRS, 2012). In total, the operation of two nuclear power plants in the Netherlands is expected to result in 478 canisters of vitrified HLW. The reference case assumes a nominal inventory of 500 HLW canisters, each containing 400 kg of waste. The waste, which is 11.3% fission products and 2.2% actinides by mass, is aged 130 years before emplacement into the repository.

Selected radionuclide inventories at the time of emplacement (waste aged 130 y) expressed in Bq per canister, grams per canister, and grams per gram vitrified waste (glass) are given in Table 4-2. The same radionuclide decay chain is included as for the SNF, but there is no ^{129}I in the HLW. The heat of decay is not included in the current task and is omitted from this revision of the task specification. See Section 4.3.3 for characteristics of the glass waste form and the stainless-steel canister.

Table 4-2. Inventory of selected radionuclides in per HLW canister aged 130y. Abridged from previous iterations of the task specification to include only ^{238}U decay chain and ^{99}Tc.

Isotope	Inventory (Bq/canister)[a]	Inventory (g/canister)	Inventory (g/g glass)[b,c]
^{234}U	4.77E+08	2.06E+00	5.16E-06
^{238}U	5.53E+07	4.45E+03	1.11E-02
^{230}Th	1.68E+05	2.25E-04	5.62E-10
^{226}Ra	1.03E+02	2.82E-09	7.04E-15
^{99}Tc	1.25E+12	1.99E+03	4.98E-03

[a] Radionuclide inventory in COGEMA glass from GRS (2012).
[b] assuming 400 kg vitrified waste per canister
[c] Refer to Table 4-1 for atomic weights and decay constants.

4.3 Engineered Barrier System

4.3.1 Repository Layout

The floor of the repository is located at a depth of 850 m below the ground surface (-800 amsl). The repository is oriented so that the emplacement drifts are perpendicular to the orientation of the salt dome in Figure 4-1. With the repository oriented this way and positioned in the center of the salt dome it results in a line of symmetry through the repository and salt dome that modelers can choose to utilize to reduce the computational resources required for simulation. The repository is accessed by two shafts that extend vertically out of the salt dome formation through the cap rock and to the surface. The access shafts are designed this way based on the design of the shaft seal as it is specifically engineered to be an effective seal within a salt formation (see Section 4.3.7).

Within the repository there are three sets of 25 emplacement drifts with a drift spacing of 35 m center-to-center. The waste package spacing for SNF is 3 m end-to-end in an emplacement drift 90 m long with a total of 10 waste packages per drift for a total of 500 POLLUX-10 waste packages. The vitrified waste emplacement area consists of 25 emplacement drifts with 35-m center-to-center drift spacing. Each 45-m-long drift contains 10 vertical boreholes with a center-to-center spacing of 4.5 m; two waste packages per borehole gives a total of 500 vitrified waste packages (Figure 4-2). The spacing of the drifts and waste packages (Table 4-3) should be sufficient to ensure that peak temperatures do not exceed 100°C (GRS, 2012).

The dimensions of all emplacement drifts and access tunnels within the repository are the same, at 7 m width and 4 m height. The infrastructure has a total volume of 240,000 m^3, with dimensions of 240 m × 250 m × 4 m. The infrastructure is utilized during the construction and emplacement phases of disposal. During the post-closure phase this area is filled with gravel to allow for accumulation of excess fluid or gas.

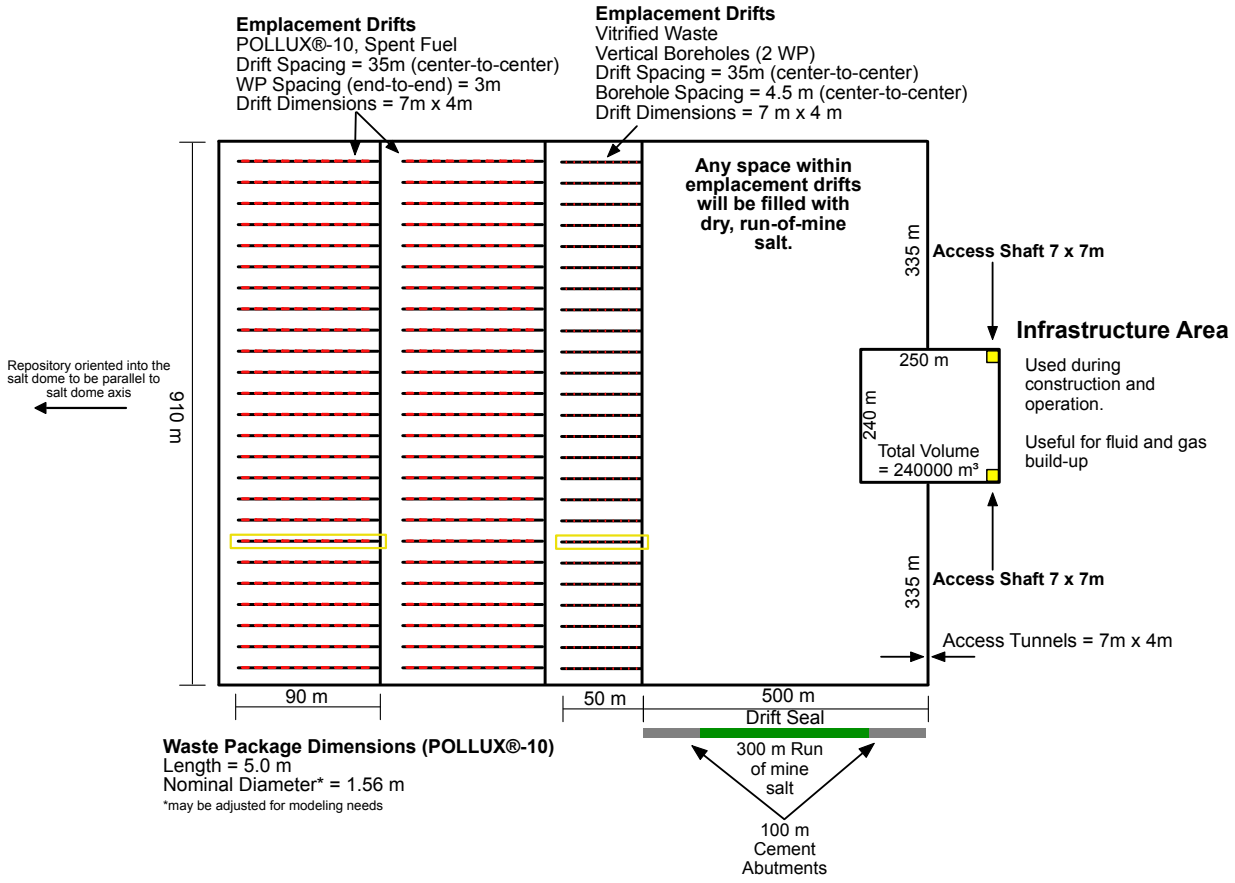

Figure 4-2. Map view schematic of the waste repository in a generic salt dome. The drifts, outlined in yellow, will be used for comparison between each teams' results.

Table 4-3. Dimensions for components of repository layout.

	Number	Width (m)	Height (m)	Length (m)	Spacing (m)
SNF Drifts	50	7	4	90	35 (center-to-center)
HLW Drifts	25	7	4	50	35 (center-to-center)
Access Shafts	2	7	850	7	240 – (7*2) (edge-to-edge)
Infrastructure Area	1	240	4	250	-
POLLUX-10	500	-	1.56*	5.0	3 (end-to-end)
Boreholes	250	1.5†	-	1.5	4.5 (center-to-center)
Drift Seals	2	7	4	500	-

*Diameter of POLLUX-10 container; may be adjusted for modeling needs

†Diameter of borehole

4.3.2 Spent Nuclear Fuel Waste Form and Waste Container

Layout of the SNF waste packages in the repository was described in Section 4.3.1. The reference case neglects any protection that the SNF waste form may provide. An IRF of 10% is assumed for ^{129}I, and the IRF is zero for all radionuclides in the ^{238}U decay chain. The POLLUX-10 container is assumed to contain the waste for 500 years while the repository begins to resaturate and to provide no containment after 500 years (BMU 2010), which represents an early waste package failure scenario. Details of the SNF waste form and container are provided in the following sections for completeness.

4.3.2.1 SNF Waste Form

The SNF waste form is spent uranium oxide (UO_2) fuel pellets encased in tubes of Zircaloy cladding. UO_2 is a polycrystalline ceramic material that is stable to high temperatures and has the potential for slow degradation in the disposal environment (Freeze et al., 2013).

In the reactor, fuel undergoes physical changes due to heating, radiation damage, and the build-up of fission products. Concentration of lighter elements along margins of the UO_2 matrix and in gaps in the waste form results in radionuclide release in two fractions: instant-release (upon failure of the waste canister) and slow-release (as the UO_2 matrix degrades). Each waste container holds 4.35 MTIHM of spent UO_2. Given a ratio of 1.44×10^6 g waste per initial MTIHM, this quantity is equivalently expressed as 6264 kg of waste or (assuming the density of UO_2, 10,970 kg/m^3) 0.571 m^3 of waste.

Radioisotopes such as ^{60}Ni accumulate in the metal components of a fuel assembly due to irradiation. These are neglected in this simplified comparison exercise.

4.3.2.2 Instant Release Fraction

The final salt reference case considers one radionuclide, ^{129}I, having an IRF. The best estimate and pessimistic values for IRF of iodine from 60 GWd/MTIHM-burnup SNF are 10% and 16% (Johnson et al., 2005 cited in Sassani et al., 2016) and are shown in Table 4-4.

Table 4-4. Instant release fractions from Johnson et al. (2005) cited in Sassani et al. (2016). Abridged from previous iterations of the task specification to include only ^{129}I.

Element	Best Estimate IRF (%)	Pessimistic IRF (%)
I	10	16

4.3.2.3 UO_2 Degradation Model

Fuel matrix (UO_2) dissolution begins when the POLLUX-10 containers fail at 500 years. The new reference case assumes mobile initial saturation in the drifts, so that the containers are in contact with water from the beginning of the simulation. Dissolution proceeds at a fractional rate of 10^{-7}/yr, the mode of a log triangular distribution (Table 4-5) appropriate for fuel 3,000-10,000 years OoR and strongly reducing conditions (Werme et al., 2004; Ollila, 2008). For a complete discussion refer to Sassani et al., (2016). Congruent release of radionuclides is assumed, and radionuclide inventories in the waste form are updated as a function of time to account for decay and ingrowth.

Table 4-5. SNF dissolution rates; log triangular distribution from Werme et al. (2004) cited in Sassani et al. (2016, Section 3.2.1).

Parameter	Rate (1/yr)	Time to 50% dissolution (yr)	Time to 99% dissolution (yr)
Min	10^{-8}	6.93E+07	4.61E+08
Mode	10^{-7}	6.93E+06	4.61E+07
Max	10^{-6}	6.93E+05	4.61E+06

4.3.2.4 POLLUX-10 Container

A POLLUX type container is utilized as the reference container. The POLLUX container was conceived and designed for final disposal in salt (Figure 4-3). It consists of an inner and an outer container. The inner container is made of fine-grained structural steel and is tightly sealed by a bolted primary cover and a welded secondary cover. The interior is divided into several chambers, into each of which fuel rods of two PWR or six BWR assemblies can be inserted. Figure 4-3 shows an example of a POLLUX container with the drawn fuel rods from ten PWR fuel assemblies (POLLUX-10). The outer shielding vessel, like the primary and secondary covers, is made of nodular cast iron (German grade 0.7040, also called ductile iron). This shielding vessel has no sealing function to perform and is closed with a bolted cover. In the shell, rods made of polyethylene are inserted in radially distributed holes to reduce the neutron dose rate. The structural container design and the choice of materials ensure the basic requirements for retrievability in the operational phase.

The container shown below has a length of 5.517 m and a diameter of 1.56 m. For the reference case, a nominal length of 5.0 m is assumed. The diameter of 1.56 m is retained, although it is recognized that individual teams may need to adjust the cross-sectional area of the container to simplify modeling.

Each team is responsible for choosing whether to explicitly represent the POLLUX-10 containers in a porous media flow and transport model. If containers are explicitly represented, teams may need to assign porosity and permeability to the volumes occupied by steel containers. This is left up to individual teams, but representative mechanical properties could be based on the properties of nodular cast iron.

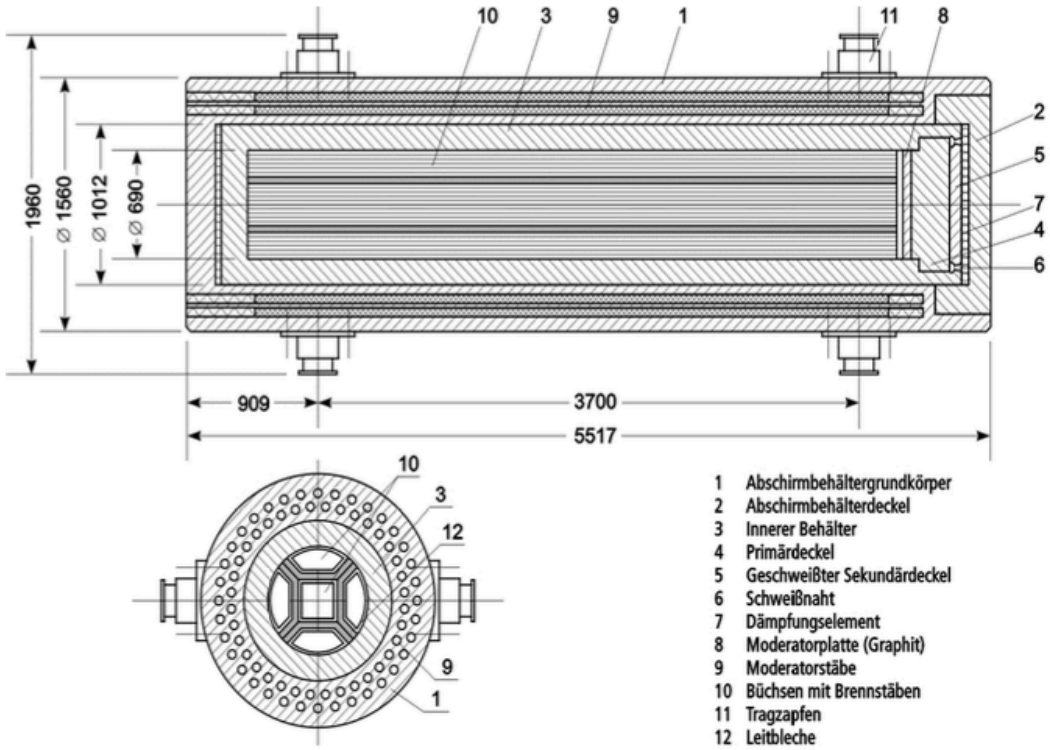

Figure 4-3. Schematic of the POLLUX-10 waste container. 1. Shielding body; 2. Shielding cover; 3. Inner tank; 4. Primary cover; 5. Secondary (welded) cover; 6. Welding seam; 7. Damping element; 8. Moderator plate (graphite); 9. Moderator staff; 10. Bushings with fuel rods; 11. Trunnion; 12. Guide plate (from Bertrams et al., 2020a).

4.3.3 HLW Waste Form and Waste Container

Layout of the HLW waste packages in the repository was described in Section 4.3.1. The reference case neglects any protection that the steel canister waste form containing the vitrified glass may provide. The IRF is zero for all radionuclides in the ^{238}U decay chain, and ^{129}I is not present in the glass waste. Vitrified glass is assumed to dissolve at a constant rate of 3.8727×10^{-7} 1/yr starting at the beginning of the simulation, as calculated according to the glass dissolution model presented below. Details of the glass waste form and container are provided in the following sections for completeness.

4.3.3.1 Vitrified Glass in Stainless Steel Canister (Waste Form)

The vitrified (glass) waste is formed in stainless steel canisters with a height of 1.335 m and an outer diameter of 0.430 m (Figure 4-4). The canisters have a mass of 100 kg when empty. Each canister contains a nominal inventory of 400 kg of vitrified waste. The reference case assumes that the thin-walled stainless steel canister provides no containment function (i.e., the glass waste form begins to dissolve immediately on emplacement), as there is mobile liquid at the start of the simulation. This represents an early waste package failure scenario.

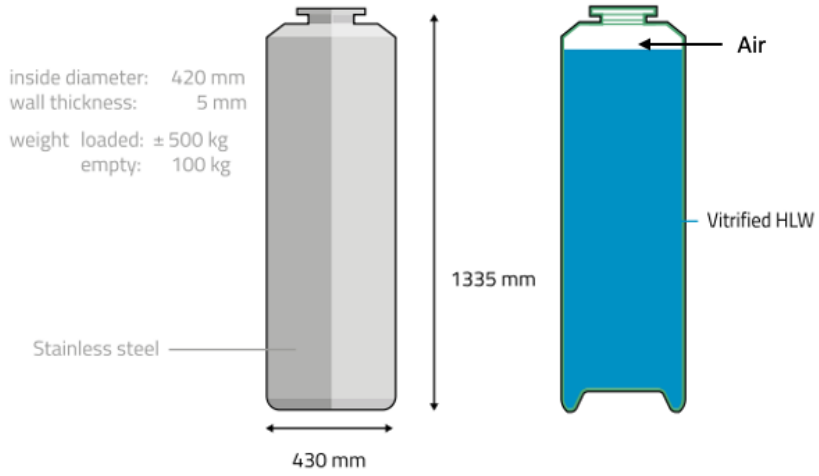

Figure 4-4. Stainless steel canister for vitrified HLW. See Figure 4-5 for overpack dimensions. From Verhoef et al. (2016).

4.3.3.2 Glass dissolution model

Glass dissolution rate depends on many factors, including local pore fluid chemistry, temperature, and glass surface area; and will slow with time as pore fluids become saturated with $SiO_{2(aq)}$ and a surface alteration layer forms (Sassani et al., 2016). This latter stage of dissolution (stage II dissolution, Vienna et al., 2013) is typically assumed to represent long-term dissolution rates for repository modeling (Sassani et al., 2016). The salt reference case uses an empirical rate law fitted to temperature (Kienzler et al., 2012) to model the long-term dissolution of glass:

$$R = 560 \times \exp\left(\frac{-7397}{T}\right) \qquad \textbf{Eq. (4-1)}$$

Where the dissolution rate, R, has the units kg/(m^2-d) and T is temperature in Kelvin. The rate law is appropriate for dilute and saline solutions. Initial flow and transport simulations assume a reference temperature of 38ºC (Sassani et al., 2016; Kienzler et al., 2012).

The surface area of the glass is calculated from the cylindrical geometry of the glass and an exposure factor (f_{exposure}), a number greater than 1 that accounts for additional reactive surface area due to cracking and roughness (Sassani et al., 2016).

$$S = f_{\text{exposure}} \qquad \textbf{Eq. (4-2)}$$

where S is the reactive surface area of the glass. Geometric surface area, A, of the glass decreases with time, and can be calculated as a function of the specific geometric surface area, s_a, [m^2/kg] and the remaining mass of glass, M [kg]:

$$A = s_a M \qquad \textbf{Eq. (4-3)}$$

Given a nominal density of 2754 kg/m^3 for COGEMA glass (Kienzler et al., 2012), a mass of 400 kg, and a diameter of 0.42 m, the glass cylinder has a volume of 0.145 m^3 and a geometric surface area of 1.66 m^2. Kienzler et al. (2012) estimates $f_{\text{exposure}} = 10$. Therefore, the specific geometric surface area is

0.004 m^2/kg and the specific reactive surface area is 10 times larger. A triangular distribution for f_{exposure} is proposed by Strachan (2004) with a minimum and mode of 4 and a maximum of 17. This distribution may be applied to the reference case when we address uncertainty. Congruent release of radionuclides is assumed, and radionuclide inventories in the waste form are updated with time to account for decay and ingrowth.

4.3.3.3 HLW Emplacement

HLW Overpack

Each vitrified HLW canister is placed in an overpack. The overpack has a total length of 1.745 m, with a 0.20-m-long, air-filled crumple zone at the top (Figure 4-5).

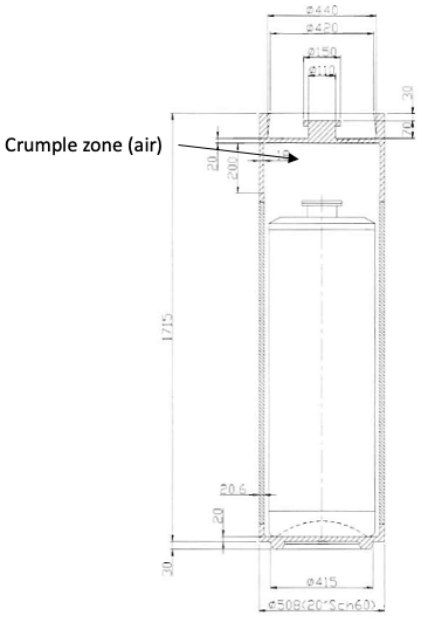

Figure 4-5. Canister dimensions for vitrified HLW (dimensions in mm). From Poley (1999)

Vertical Emplacement Borehole

Two overpacks are emplaced in a vertical borehole, one on top of the other, in the floor of a waste emplacement drift. The emplacement borehole is 14-m in length (Figure 4-6) (Poley, 1999). The two overpacks sit in the lowest 4 m of the borehole, where the borehole is 0.7 m in diameter, lined with steel, and backfilled with sand. A salt plug sits in the upper 10 m of the borehole, which is 1.5 m in diameter.

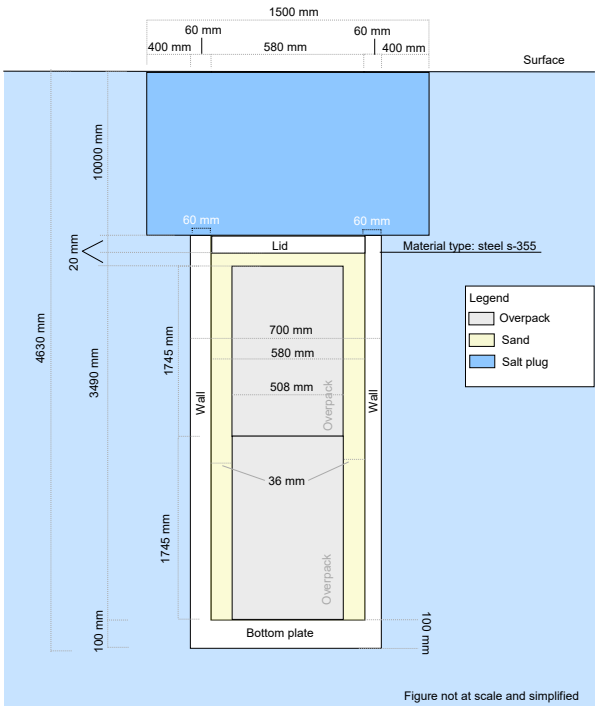

Figure 4-6. Dimensions for vertical borehole emplacement for vitrified HLW canisters. Schematic courtesy of Jeroen Bartol

Each team is responsible for determining whether to explicitly include the HLW waste packages in their model. If the HLW packages are explicitly modeled, the team must determine how to represent the lower borehole (containing vitrified HLW in canisters and overpacks, sand backfill, and steel lining) in the porous media flow and transport model. For instance, teams could calculate bulk porosity from the void space in the HLW canister, overpack, and sand backfill. Permeability is left up to each modeling team to determine. It is proposed that representative mechanical properties be based on the properties of borosilicate glass.

The salt plug is assigned the same properties as the run-of-mine (i.e., granular) salt that backfills the drift as discussed in the next section. This assumption results in conservatively high permeability and porosity, because in practice, the salt plug would likely be pre-compacted at the time of emplacement.

4.3.4 Emplacement and Access Tunnel Backfill

Emplacement drifts and access tunnels (except where drift seals are placed) are backfilled with run-of-mine salt. Due to the compaction of the run-of-mine salt backfill, the backfill will develop a sealing effect over time that is comparable to that of the surrounding, undisturbed geological barrier. The time required to reach the final state ranges from tens to thousands of years, depending on the convergence rate, moisture content and ambient temperature (Bertrams et al., 2020a). Backfill properties have been adopted from Blanco-Martin et al. (2018) and are in Table 4-7.

4.3.4.1 Salt Creep Modelling

The teams chose to model the drift convergence based on Gorleben data (Bertrams et al., 2020b) as computed by LOPOS. Salt creep begins at the start of the simulation. The salt creep model in LOPOS is based on the equations presented in Hirsekorn et al. (1999) and Noseck et al. (2005). These are used for salt creep modelling in LOPOS and were presented by the GRS team at the April 2022 workshop. The

teams agreed to forward-couple the predicted porosity evolution as a function of time to the flow and transport models.

The drift convergence rate and resulting porosity as a function of time was provided to teams as an excel table. An abridged version of the table is given in Table 7-1 to Table 7-3 in Appendix - Crushed salt compaction, and was calculated in LOPOS using the parameters in Table 4-6.

Teams may choose to use the data in Table 7-1 to Table 7-3 or to calculate the porosity from the pore and total compartment volume using the equations for change in salt volume are presented here. In either case, porosity evolution should cut off at the intact salt porosity of 0.001. Change in salt volume (V) can be calculated as a function of time using:

$$\frac{d}{dt}\mathrm{V(t)} = -\mathrm{K(t)} \cdot \mathrm{V(t)} \qquad \textbf{Eq. (4-4)}$$

$$\mathrm{K(t)} = \mathrm{L\,K_{ref}} \cdot f_R \cdot f_P \cdot f_F \cdot f_T \cdot f_Z \qquad \textbf{Eq. (4-5)}$$

where:

- V(t) is volume [m^3] of a compartment at time t
- K(t) is convergence rate [1/s] at time t
- L is the factor for local properties of the surrounding salt
- K_{ref} is reference convergence rate [1/s]
- f_R is dimensionless moisture creep enhancement function
- f_P is dimensionless fluid pressure function
- f_F is dimensionless backfill support function
- f_T is dimensionless temperature function
- f_Z is dimensionless explicit time dependency

The creep rate in a mine can be increased by liquid that intrudes into the surrounding rock and changes its mechanical properties. This increase of the convergence rate is taken into account by the function f_R. As the intrusion of brine into the rock is driven by fluid pressure, f_R is assumed to depend on the pressure, which implicitly accounts for the impact of liquid saturation in Eq. (4-6). For f_R a linear approach is used over the range of pressures $0 \leq p - p_{atm} \leq p_0$:

$$f_R = 1 + x_F \frac{p - p_{atm}}{p_0} \qquad \textbf{Eq. (4-6)}$$

where:

- x_F is the parameter for moisture enhanced creep [-]
- p is the local fluid pressure, which depends on time [MPa]
- p_{atm} is atmospheric pressure [MPa]
- p_0 is local hydrostatic fluid pressure (pressure at fully developed moisture creep) [MPa]

The values of x_F reflect the condition that $K = K_{dry}$ for $p = p_{atm}$ and $K = K_{wet}$ for $p_0 = p - p_{atm}$ and are given for the drifts and the rest of the salt-containing repository regions in Table 4-6.

The fluid pressure function, f_P, is a function of rock and hydrostatic pressure and is given by

$$f_P = \left(\frac{p_G(z) - p}{p_G(z_R)}\right)^n \quad \textbf{Eq. (4-7)}$$

$$p_G(z) = p_G(z_R) - \Delta z\, g\rho_s \quad \textbf{Eq. (4-8)}$$

Where:

- n is the stress exponent of convergence [-]
- $p_G(z) = p_G(z_R)$ is lithostatic rock pressure at repository level [MPa]
- ρ_s is the solid density [kg/m^3]
- z is depth [m]

In the present study $p_G = p_G(z_R)$ because the reference depth is chosen to be the repository depth.

The backfill support function, f_F, is a function of the porosity. It is calculated based on the following boundary conditions:

- The backfill support function is 1 for porosities greater than the reference porosity
  $f_F|_{\Phi>\Phi_r} = 1$
- The backfill support at the reference porosity, Φ_r tends to zero derivative
  $\left.\frac{df_F}{d\Phi}\right|_{\Phi=\Phi_r} = 0$
- For small porosity values the derivative of the backfill support function is 1
  $\left.\frac{df_F}{d\Phi}\right|_{\Phi=0} = 1$
- When approaching the final porosity, the derivative of the backfill support tends towards 0
  $\left.\frac{df_F}{d\Phi}\right|_{\Phi=\Phi_g} = 0$

With these boundary conditions f_F is given by

$$f_F = \left[1 + \frac{h(\Phi, \Phi_r, \Phi_g)}{[(\Phi - \Phi_g)g(\Phi, \Phi_r, \Phi_g)]^{1/m}}\right]^{-m} \quad \textbf{Eq. (4-9)}$$

$$h(\Phi, \Phi_r, \Phi_g) = \mathrm{h}_0 + \mathrm{h}_1\frac{\Phi - \Phi_g}{\Phi_r - \Phi_g} + \mathrm{h}_2\left(\frac{\Phi - \Phi_g}{\Phi_r - \Phi_g}\right)^2 + \mathrm{h}_3\left(\frac{\Phi - \Phi_g}{\Phi_r - \Phi_g}\right)^3 \quad \textbf{Eq. (4-10)}$$

$$g(\Phi, \Phi_r, \Phi_g) = \mathrm{g}_0 + \mathrm{g}_1\frac{\Phi - \Phi_g}{\Phi_r - \Phi_g} + \mathrm{g}_2\left(\frac{\Phi - \Phi_g}{\Phi_r - \Phi_g}\right)^2 \quad \textbf{Eq. (4-11)}$$

Where:

- Φ is porosity of the segment at time t [-]
- Φ_r is reference porosity [-]
- Φ_g is final porosity [-]
- m is the stress exponent for backfill support [-]

- h_0-h_3 and g_0-g_2 are empirical fitting constants calculated internally in LOPOS (Noseck et al., 2005)

where g_2 (dry) is used when there is no liquid in the compartment. When there is liquid in the compartment g_2 (wet) is used.

The temperature function is not used in the current reference case as it is isothermal, so that $f_T = 1$.

Initially the salt rock is disturbed due to excavation, hence the convergence rate of an unfilled mine is faster and approaches a constant value over time. For t → ∞ the convergence rate of an excavation of depth z at constant internal pressure approaches the local stationary reference convergence rate $K_{ref} \cdot L$.

$$\lim_{t\to\infty} K\,(z,t) = K_{ref} \cdot L \qquad \textbf{Eq. (4-12)}$$

The further the convergence has progressed, the closer the current value of K is to the stationary value K_{ref}. This effect is taken into account with f_Z which describes the explicit time dependency of the convergence rate:

$$f_Z = 1 + \frac{A}{\lambda + \int_0^t K(t')dt'} \qquad \textbf{Eq. (4-13)}$$

Where:

- λ is the pre-history of convergence for the time between excavation and t=0 of the model calculation.
- A is how fast f_Z tends toward the value 1.

The further the convergence process has progressed, the larger the integral over the convergence rate and thus the denominator in Eq. (4-13). With $\int_0^t K(t')dt' = ln\frac{V_0}{V(t)}$, where V_0 is the compartment volume at t=0, f_Z simplifies to

$$f_Z = 1 + \frac{A}{\lambda + ln\frac{V_0}{V(t)}} \qquad \textbf{Eq. (4-14)}$$

For t=0 it applies that K=K_0, f_P=1, f_Z=1+$\frac{A}{\lambda}$ and $f_F = f_F(\Phi_0)$ so that

$$K_0 = K_0 \cdot L = K_{ref} \cdot L \cdot f_F(\Phi_0) \cdot \left(1 + \frac{A}{\lambda}\right) \qquad \textbf{Eq. (4-15)}$$

Thus A can be eliminated by

$$A = \lambda \cdot \left(\frac{K_0}{K_{ref} \cdot f_F(\Phi_0)} - 1\right) \qquad \textbf{Eq. (4-16)}$$

Finally, the new compartment volume is calculated as (Storck et al, 1996):

$$V(t+\Delta t) = V(t)(1 - K(t)\Delta t) \qquad \textbf{Eq. (4-17)}$$

$$V_P(t+\Delta t) = V_P(t) - V(t)K(t)\Delta t \qquad \textbf{Eq. (4-18)}$$

and porosity is updated so that

$$\Phi(t+\Delta t) = \frac{V_P(t+\Delta t)}{V(t+\Delta t)} \qquad \textbf{Eq. (4-19)}$$

Where:

- V_P is the pore volume [m^3]
- V is the total compartment volume [m^3]

In the first timestep $V_P(t_o)$ is the initial pore volume calculated based on the initial simulation grid block volume and initial porosity given in Table 4-7. All other parameters for Eq. (4-4) through Eq. (4-16) are shown in Table 4-6.

Table 4-6. LOPOS parameters used in Equations (4.4) - (4.16) to calculate the convergence rate and porosity in Table 7-1.

Parameter	Value
Reference Convergence Rate, K_{ref} [1/y]**	10^{-8}
Reference Porosity, Φ_r [-]**	0.3
Initial Convergence Rate on Reference Level K_o [1/y]	0.1
Parameter for pre-history of convergence in the Emplacement Drifts λ [-]**	1
Parameter for pre-history of convergence in the Salt Compartment between the seals λ [-]**	0.2
Parameter for pre-history of convergence elsewhere λ [-]**	0.008
Stress Exponent for Backfill Support, m [-]**	5
Stress exponent for Convergence, n [-]**	5
Solid density, ρ_s [kg/m^3]	2200
Reference depth, z_R [m]	-850
Backfill Support Function, h_0 [-]*	1
Backfill Support Function, h_1 [-]*	-2
Backfill Support Function, h_2 [-]*	$-(3+2h_1)$
Backfill Support Function, h_3 [-]*	$h_1 + 2$
Backfill Support Function, g_0 [-]*	1
Backfill Support Function, g_1 [-]*	-1
Backfill Support Function, g_2 (dry) [-]*	100
Backfill Support Function, g_2 (wet) [-]*	1000
Final Porosity, Φ_g [-]**	$4 \cdot 10^{-6}$
Hydrostatic Pressure on Reference Level, p_L [MPa]	8.3
Rock Pressure on Reference Level, p_G [MPa]	18.3
Local hydrostatic fluid pressure for Salt Seal at fully developed creep, p_o [MPa]	1.0
Local hydrostatic fluid pressure elsewhere at fully developed creep, p_o [MPa]	0.5
Atmospheric Pressure, p_{atm} [MPa]	0.101
Parameter for moisture enhanced creep in the drifts, x_F [-]**	1
Parameter for moisture enhanced creep elsewhere, x_F [-]**	4

Local Variation of Convergence Rate in the waste-free Drifts L_{drift} [-]**	0.6
Local Variation of Convergence Rate in the Emplacement Drifts L_{ED} [-]**	1
Local Variation of Convergence Rate in the Salt compartment between the seals L_{salt} [-]**	0.2

*Noseck et al, 2005
** Bertrams et al., 2020b

4.3.4.2 Permeability as a function of porosity

In the reference case it is assumed that at the beginning of simulations, backfill has run-of-mine (i.e., crushed) salt properties (porosity of 0.1 and permeability of 8.35×10^{-15} m^2) given in Table 4-7. It is also assumed that the crushed salt will return to intact salt properties (porosity of 0.001 and permeability of 1.0×10^{-22} m^2) given in Table 4-10 once the drifts have fully closed. A Kozeny-Carmen type equation of the form

$$k = A\phi^n \qquad \textbf{Eq. (4-20)}$$

is fit to these two endpoints. A simple regression was conducted and the (nonunique) parameter combination A = 7.36×10^{-11} m^2 and n = 3.961 (-) allow Equation (4.12) to match the two endpoint permeabilities to three significant figures. During the consolidation process, permeability may be modelled as a function of porosity, or teams may wish to implement one or more step changes in permeability as backfill consolidates.

4.3.4.3 Capillary pressure and relative permeability during salt consolidation

At the beginning of simulations, backfill has crushed salt relative permeability and capillary pressure given in Table 4-8. It is logical to assume that these properties will evolve over time to the intact salt properties in Table 4-8 as the salt returns to the intact permeability and porosity. There is no well-established way to model parameter evolution from the crushed to the intact values. It is left up to individual teams to decide if they will include relative permeability and capillary pressure evolution in their models.

4.3.5 Infrastructure Area Gravel Backfill

The shaft landing stations, and the infrastructure area are backfilled with silica or non-salt gravel, which has negligible compaction capabilities, and provides permanent pore storage that will significantly delay an increase in brine pressure at the drift seals. The gravel backfill provides a high porosity reservoir for fluids intruding from the host rock or via the shafts, thus allowing fluids to accumulate in the infrastructure area without causing increased pore fluid pressures in other areas of the repository. Backfill properties are listed in Table 4-7.

4.3.6 Drift Seals

Two drift seals are placed in the 500-m long tunnels connecting the infrastructure area to the emplacement area. These seals provide long-term separation of surface, overburden, and/or formation waters from emplacement drifts, limiting the volume of water that comes in contact with waste and limiting radionuclide transport. Each drift seal comprises two 100-m lengths of Sorel concrete, analogous to the lowest sealing element of the shaft closure (see Section 4.3.7), separated by a 300-m section filled with run-of-mine salt. The Sorel cement provides a seal immediate after closure of the repository, while the run-of-mine salt will consolidate to provide a seal at later times (Bertrams et al., 2020a).

The run-of-mine salt has a non-zero initial liquid saturation to accelerate compaction and has the same properties and initial conditions as the run-of-mine salt backfill in the emplacement drifts and other access tunnels. Properties for sorel cement can be found in Table 4-7.

4.3.7 Shaft Design

Access to the repository is provided by two shafts connecting the infrastructure area to the ground surface. The shafts are 850 m tall with a 7 m by 7 m cross section. The shaft seals limit ingress of water to the repository and limit advective radionuclide transport. In the shaft seal failure scenario considered in the reference case, the shaft seals fail to perform these safety functions after shaft seal failure at 1000 years.

Properties of the engineered barrier system required for simulation of variably saturated flow and advective and diffusive transport are summarized in Table 4-7 and Table 4-8. Table 4-7 defines intrinsic permeability, porosity, tortuosity, and the corresponding effective diffusion coefficient, compressibility.

Table 4-8 defines relative permeability and capillary pressure functions. Grain density assuming no sorption in the engineered barriers is also listed.

The base case option for flow and transport ignores distinct features of the shaft. The bulk hydrologic properties show in Table 4-7 and shall seal relative permeabilities in Table 4-8 are assumed. The bulk permeability of the shaft changes at the time of failure: Prior to shaft seal failure, the bulk permeability is 8.6232×10^{-18} m^2; after shaft seal failure at 1000 years, the bulk permeability is 2.0606×10^{-16} m^2, which is necessary to be consistent with the post-failure average permeability in the heterogenous model. Porosity remains the same before and after shaft seal failure.

The layered shaft seal design shown in Figure 4-7 is a variation of the base case for teams with the capability for complex shaft models. This design contains segments designed to seal and segments designed to act as reservoirs. The uppermost sealing segment is bentonite, which limits advection due to its low permeability and retards radionuclide transport due to adsorption. The porosity and permeability prior to shaft seal failure are given in Table 4-9. After shaft seal failure, the permeability of each layer in the shaft is assumed to increase by two orders of magnitude, while porosity remains the same. Tortuosity, effective diffusion coefficient, compressibility and grain density are the same before and after shaft failure and can be taken from Table 4-7, where the Sealing Elements have the shaft seal properties and Filter/Inlet is assigned gravel properties. Similarly, capillary pressure and relative permeabilities for the layered shaft seal may be taken from Table 4-8.

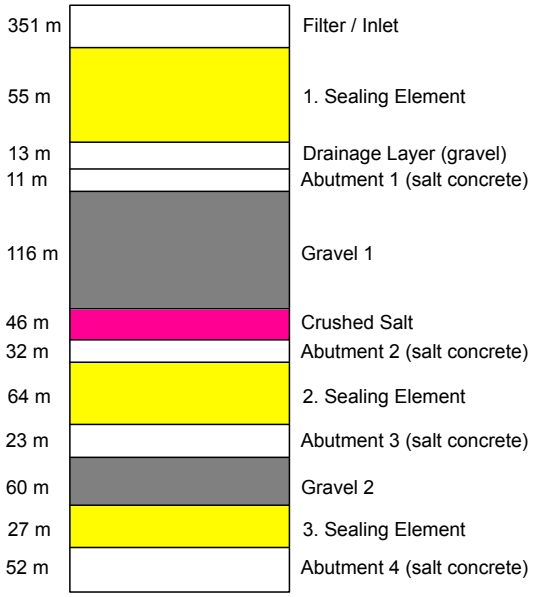

Figure 4-7. Shaft seal for generic salt dome repository (modified from Rübel et al. (2016) by Tanja Frank).

Table 4-7. Engineered barrier system material properties for use in reference case simulations.

	Intrinsic Permeability (m^2)	Porosity (-)	Tortuosity (-)	Effective Diffusion Coefficient (m^2/s) [j]	Compressibility (1/Pa)	Grain Density (kg/m^3)
POLLUX-10 container (bulk) [c]	TBD [a]	TBD [a]	TBD [a]	TBD [a]	TBD [a]	7000
HLW emplacement borehole (bulk) [d]	TBD [a]	0.14	0.14	4.5E-11	TBD [a]	2750
Crushed salt [e]	8.35E-15	0.1	0.1	2.3E-11	1.00E-08	2200
Sorel cement (drift seals) [f]	5.00E-17	0.13	0.13	3.9E-11	1.00E-09	2450
Gravel (infrastructure area) [g]	1.00E-14	0.3	0.3	2.1E-10	1.00E-08	2700
Shaft seals before failure [h]	8.6232E-18	0.24	0.24	1.3E-10	1.00E-08	NA [b]
Shaft seals after failure [h]	2.0606E-16	0.24	0.24	1.3E-10	1.00E-08	NA [b]

[a] To be determined by the individual modeling teams.

[b] These properties are not applicable to the initial flow and transport simulations.

[c] Generic values consistent with ductile cast iron (ASTM A536).

[d] Generic values consistent with properties of borosilicate glass.

[e] Estimated after 1000 years of reconsolidation from results in Blanco-Martin et al. 2018. Permeability (k [m2]) is a function of porosity (ϕ): k= 1.89 × 10^(-10)×ϕ^4.355.

[f] Permeability from Rübel et al. (2016) and generic values consistent with MgO cement with silica sand aggregate (Zaleska et al. 2019).

[g] Permeability from Rübel et al. (2016) and generic values consistent with properties of coarse quartz sand.

[h] Bulk permeability from Rübel et al. (2016). Volume weighted average porosity estimated from shaft seal design in GRS 415.

[j] Effective diffusion coefficient, $D_e = D_m \phi \tau$, where D_m, the molecular diffusion coefficient in free water, = 2.3E-09 m^2/s.

Table 4-8. Relative permeability parameters for salt, crushed salt, and shaft seal.

	Intact Salt[1]	Crushed Salt[1]	Shaft Seal[1]	Concrete[2]	Gravel[3]
Relative Permeability Function	Corey	Corey	Corey	Mualem – VG	VG
Residual Liquid Sat (S_{lr})	0.1	0.03	0.03	0.2	0.19
Residual Gas Sat (S_{gr})	0	0	0	0.1	0
Van Genuchten's λ (-)	0.6	0.6	0.6	0.56	0.675
Van Genuchten's P_0 (MPa)	5.7	1.6	1.6	7.7	1.6
Van Genuchten's S_{lr}	0.01	0.02	0.02	0.0	0.0

[1]Blanco-Martín et al. (2018)
[2]Ecay et al. (2020)
[3]Osselin et al. (2015)

Table 4-9. Material properties for the detailed shaft model prior to seal failure. After shaft failure the permeability of each layer increases by two orders of magnitude.

	Intrinsic Vertical Permeability (m^2)	Porosity (-)
Filter/Inlet	1.00E-12	0.3
Sealing Element 1	1.00E-17	0.27
Drainage Layer 1	1.00E-12	0.25
Abutment 1	1.00E-12	0.1
Gravel 1	1.00E-09	0.23
Crushed Salt	1.30E-15	0.1
Abutment 2	2.00E-15	0.1
Sealing Element 2	7.00E-19	0.1
Abutment 3	2.00E-15	0.1
Gravel 2	1.00E-09	0.38
Sealing Element 3	5.00E-17	0.16
Abutment 4	5.00E-17	0.16

4.4 Natural Barrier System

The natural barrier system is comprised of the 5 simplified geologic units illustrated in Figure 4-1: the salt dome (which is the host rock); a mixed evaporite sequence flanking the salt dome; the caprock; the basin fill; and the overburden. The descriptions below are derived from the geologic units described by Bertrams et al. (2020a) unless otherwise noted. Physical properties are summarized in Table 4-8 and Table 4-10.

4.4.1 Salt Host Rock

In the geological model of the salt dome, the intact host rock consists of homogeneous rock salt (halite), which has no flowable pore space and thus no permeability greater than 10^{-22} m^2. Due to the extremely

low hydraulic permeability of the salt rock, advective mass transport is negligible, so that mass transport is determined solely by, diffusion, which may be included or omitted by teams (Bertrams et al., 2020a).

4.4.2 Mixed Evaporite Sequence

The flank areas of the salt structure consist of a potash (sylvite) seam, an evaporitic sequence of salt and anhydrite, and a clayey strata. These complicated alternating geologic formations are very common within salt dome architecture. As a result of this complexity a simplification is made in Figure 4-1 with this group of formations being represented by a single formation defined by bulk properties.

4.4.3 Caprock

A caprock with a thickness between 55 m to 80 m has formed above the salt structure. The model unit consists largely of gypsum or of the residual formations of the various evaporitic strata following the salt structure. With this formation being dominated by mainly evaporitic strata the permeability is assumed to be low.

4.4.4 Basin Fill

The basin fill, which is present on both sides of the salt structure and absent directly above the salt structure, mainly consists of a limestone to sandstone sequence with conglomerates throughout. Because of this sequence, this formation is assumed to have a higher permeability and effective porosity.

4.4.5 Overburden

Above the salt structure and cap rock, the overburden varies in thickness from 55 – 80 m. The overburden consists largely of unconsolidated sediments with higher pore volume relative to the deeper units. Therefore, this model unit is classified as a freshwater aquifer. Additionally, the permeability specified for this unit of 10^{-15} m^2 may allow for advection to occur (depending on the boundary conditions assigned). As a result, dispersion may need to be considered, which will be left up to the modelers because dispersivity will be dependent on grid discretization.

Table 4-10. Natural barrier system material properties for use in initial flow and transport simulations.

	Intrinsic Permeability (m^2)	Porosity	Tortuosity (-)	Effective Diffusion Coefficient (m^2/s)[b]	Compressibility (1/Pa)	Grain Density (kg/m^3)
Overburden	1.00E-15	0.2	0.2	9.2E-11	1.00E-08	2600
Caprock	1.00E-18	0.4	0.4	3.68E-10	1.00E-09	2200
Basin Fill	1.00E-17	0.25	0.25	1.44E-10	1.00E-08	2500
Anhydrite/Potash	1.00E-19	0.05	0.05	5.75E-12	1.00E-11	2700
Domal Salt	1.00E-22[a]	0.001[a]	0.0001	2.3E-15	1.00E-11	2200
Basement	1.00E-21[a]	0.01	0.01	2.3E-13	1.00E-12	3000

[a] from Bertrams et al., 2020a

[b] Effective diffusion coefficient, $D_e = D_m \phi \tau$ where D_m, the molecular diffusion coefficient in free water, = 2.3E-09 m^2/s.

4.5 Geochemical Environment

In a complex geologic system, solubility limits and adsorption behavior would be controlled by local porewater chemistry and mineral assemblage. For the salt reference case, simplifying assumptions are made.

4.5.1 Solubility

Radioelement solubility limits throughout the model domain are held constant at values calculated for a concentrated, reducing brine as in previous salt reference case simulations conducted in the U.S. (e.g., LaForce et al., 2020; Clayton et al., 2011). The calculated range of maximum dissolved concentration for each element is given as a triangular distribution in Table 4-11. The reference case uses the mode of the distribution as the nominal value.

Table 4-11. Element solubility calculated at 25° C in concentrated brine (Wang and Lee, 2010 as cited in Clayton et al., 2011). Abridged from previous iterations of the task specification to include only ^{238}U decay chain and ^{129}I.

Element	Distribution Type	Maximum Dissolved Concentration (mol kg^{-1})		
		Min	Mode	Max
Ra	Log-Triangular	1.0E-07	1.0E-03	1.0E-03
Th	Triangular	2.00E-03	4.00E-03	7.97E-03
U	Triangular	4.89E-08	1.12E-07	2.57E-07
I	N/A	Unlimited		

[a]Assumed by Clayton et al. (2011)

4.5.2 Adsorption

Adsorption is modeled using linear distribution coefficients (K_d). Distribution coefficients are material specific.

4.5.2.1 Host rock and repository

The reference case assumes that adsorption does not occur within the halite of the salt dome nor within any of the engineered materials in the repository. This assumption is likely conservative, because corrosion products associated with waste package degradation might provide sorption sites.

4.5.2.2 Mixed evaporite sequence and caprock

Clayton et al. (2011) compiled distribution coefficients for anhydrite and expressed them as uniform and log uniform distributions as shown in Table 4-12. Adsorption in the mixed evaporite sequence and the caprock is modeled using a nominal K_d equal to the midpoint of each distribution. The midpoint is equivalent to the average of the minimum and maximum for a uniform distribution, or the value obtained by averaging the logs of the minimum and maximum for a log uniform distribution.

Table 4-12. Anhydrite Kds compiled by Clayton et al. (2011). Abridged from previous iterations of the task specification to include only ^{238}U decay chain and ^{129}I.

Element	Distribution	K_d [m^3/kg]		
		Min	Mid	Max
Ra	Log-Triangular	5.0E-02	1.0E-01	5.0E-01
I	constant	0.0E+00	0.0E+00	0.0E+00
Th	uniform	1.0E-01	5.5E-01	1.0E+00
U	uniform	2.0E-04	6.0E-04	1.0E-03

4.5.2.3 Basin fill and overburden

Adsorption in the basin fill is modeled using K_d values calculated for the Brauner Dogger sandy limestone sequence (a geologic unit overlying the Opalinus clay). Baeyens et al. (2014) calculated values for a reference porewater composition, and three variants including the high salinity case shown in Table 4-13. The salt reference case assumes high salinity porewaters and reducing conditions in the basin fill. Therefore, the high salinity K_d values are adopted, and reduced oxidation state is assumed for uranium, U(IV).

Adsorption in the overburden is also modeled using K_d values calculated for the Brauner Dogger sandy limestone sequence. For the overburden, the reference K_d values and higher oxidation state is assumed for uranium, U(VI).

Table 4-13. Kds for basin fill and overburden (from Baeyens et al., 2014). Abridged from previous iterations of the task specification to include only ^{238}U decay chain and ^{129}I.

Element	K_d [m^3/kg]	
	Reference	High salinity
Ra	5.0E-01	
I(-I)	0.00E+00	0.00E+00
Th(IV)	7.59E+00	2.23E+01
U(IV) [a]	4.20E-02	3.08E-01
U(VI) [b]	7.89E-05	7.95E-04

[a] Use lower oxidation states in the basin fill.

[b] Use higher oxidation states in the overburden.

4.5.2.4 Shaft seal

Adsorption within the shaft seal is neglected in the reference case. The upper shaft seal contains bentonite, which will sorb some radionuclide species, so this represents a conservative assumption.

4.6 Transport

Teams may choose to model tracer transport, radionuclide transport or both in the reference case.

4.6.1 Conservative Tracer Transport

Teams will model conservative transport of three non-sorbing tracers. Tracer 1 and 2 exist only in the SNF waste packages. Tracer 3 is only in the HLW glass. The tracer inventories and release rates are shown in Table 4-14.

In the SNF Tracer 1 and 2 are the same two tracers as the crystalline case, but with inventory updated to be representative of the POLLUX-10 containers. Tracer 1 and Tracer 2 are modeled after ^{129}I and the sum of Tracer 1 plus Tracer 2 is equivalent to the ^{129}I inventory in the next section. Representative ^{129}I inventory is calculated from values in Table 4-1; IRF and fractional rate of release are taken from Table 4-4 and Table 4-5, respectively.

Both SNF tracers have an atomic weight of 128.9 g/mol. The total inventory of the two tracers in each waste package is 1362.0 g (10.6 moles), equivalent to the expected inventory of ^{129}I in a waste package containing 10 PWR assemblies. The inventory of Tracer 1 is 136.2 g (1.06 moles), or 10% of the total; it is instantly released at the time of waste package failure, after 500 years. The inventory of Tracer 2 is 1226.0 g (9.50 moles), or 90% of the total; it is released congruently from the waste form as the waste form degrades at a fractional rate of 10^{-7}/yr throughout the transport simulation.

Tracer 3 is released from the HLW vitrified glass waste. It has properties representative of Technetium (Tc), as Tc has relatively low K_d, half-life in excess of 200,000 yr, and is present in reasonable quantities in the HLW packages (see Table 4-2). There is not expected to be any instant release of radionuclides from glass waste forms, so tracer is released at a fractional rate throughout the transport simulation. The tracer release rate is calculated according to the glass dissolution model given by Equations 4.1-4.3 and reactive surface area of 0.04 m^2/kg given in Section 4.3.3.2, assuming a constant temperature of 38 ºC (311.15 K).

Table 4-14. Tracer inventories and release mechanisms for salt reference case simulations. Tracers 1 and 2 are released from SNF while Tracer 3 is released from HLW canisters.

	Atomic weight	Inventory per waste package or per HLW canister	Release mechanism
Tracer 1	128.9 g/mole	136.2 g	Instant
Tracer 2	128.9 g/mol	1226. g	10^{-7}/yr
Tracer 3	98.91 g/mol	1990. g	3.8727E-07/yr

4.6.2 Radionuclide Transport

For the reference case the radionuclide inventory is limited to a single ^{238}U decay chain (^{238}U→ ^{234}U→^{230Th}→^{226}Ra) and ^{129}I. The radionuclide inventory for these elements in each SNF POLLUX-10 container is given in Table 4-1. Only ^{129}I is instantly released upon container breach. The IRF for ^{129}I is 10%, the best estimate given in Table 4-4. Waste form dissolution is assumed to begin at the time of canister breach at 500 years, with all radionuclides released at a rate of 10^{-7}/yr, which is the mode value given in Table 4-5.

The inventory for each HLW glass canister consists of only the ^{238}U decay chain, as there is no ^{129}I in the glass waste. The inventory is given in Table 4-2. There is no instant release of any radionuclides in the HLW canisters. Dissolution is assumed to take place at a rate of 3.8727/yr, identical to the HLW tracer release rate calculated in the preceding section.

Element solubilities are assumed to be constant throughout the model domain and are given in Table 4-11. The mode solubility is used for the reference case. The linear distribution coefficients (K_d) for each radionuclide depends on the rock type. The reference case makes the conservative assumption that there is no adsorption in the host rock, repository, and shaft. The K_d values in the mixed evaporite sequence and caprock are the midpoint values (Mid) given in Table 4-12. The K_d values in the basin fill are the high salinity values and lower oxidation state value given in Table 4-13, while the overburden values are the reference K_d values and higher oxidation state value for Uranium in Table 4-13.

4.7 Initial Conditions, Etc.

Initial conditions for this salt reference case are shown in Figure 4-8 and are summed up as follows:

1. Fluid pressure will be defined as hydrostatic in the far field. The scenario presented here focuses on the intrusion of water into the mined repository. However, depending on the equation-of-state for the given numerical model, density differences between the fluids may be neglected if the equation-of-state lacks that capability. Fluid flow should be simulated utilizing a single-phase variably-saturated (Richards Equation type) model. No influx into the repository from the geosphere is the base case, and inclusion of influx is an optional variant.
2. Once hydrostatic conditions are calculated, the mined repository and access shafts will be added.
3. The mined repository will be set to 20% initial liquid saturation and atmospheric pressure for all repository regions. This change has been made from previous revisions of the task specification because it has proved extremely numerically challenging for some simulation software to begin simulations with the original initial conditions, which was that the initial liquid saturation was equal to the residual liquid saturation corresponding to the relevant relative permeability models in Table 4-8.
4. The initial average shaft saturation is 35% liquid saturation for both the homogeneous base case and heterogeneous variant. This is the average equilibrium saturation calculated by assuming van Genuchten capillary pressure with Corey relative permeabilities in a single-phase variably saturated model using the homogeneous shaft parameters in Table 4-8. Teams using Richard's-type single-phase variably-saturated flow models cannot change this initial saturation without breaking the earlier assumption of hydrostatic initial conditions.
5. The flow rate (specific discharge or Darcy flux) in the aquifer (overburden) is 10^{-10} m/s (1.31×10^{-4} m/y).
6. Flow and transport simulations should be run to 100,000 years.

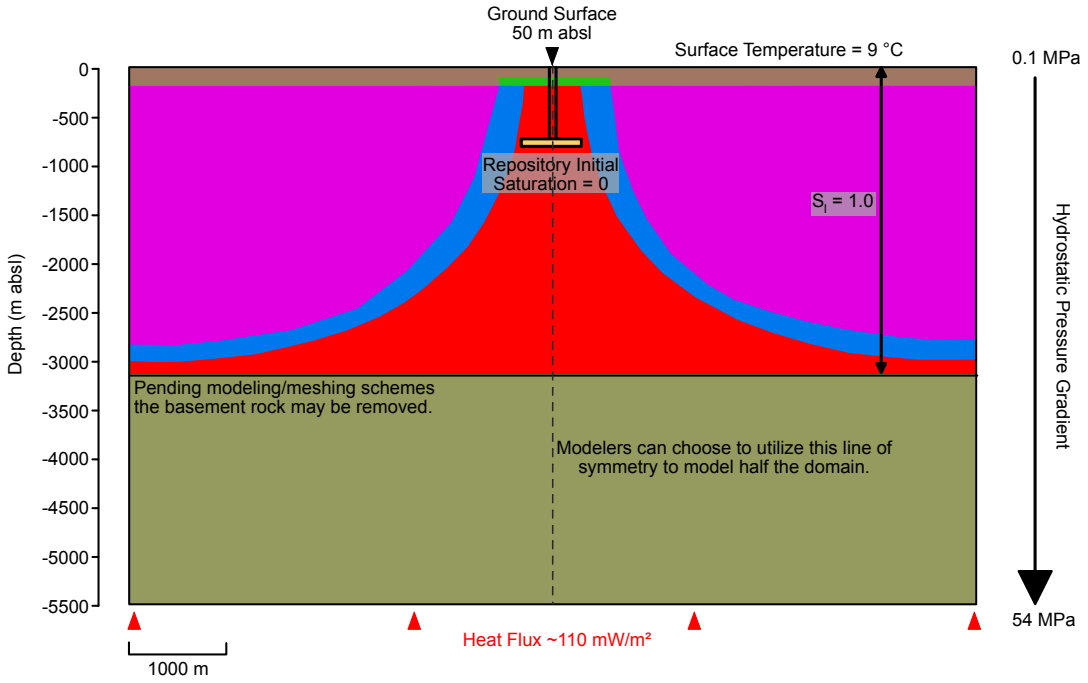

Figure 4-8. Schematic for initial conditions, immediately after waste package emplacement. The orientation and design of the repository and geologic cross section were chosen to provide a symmetry boundary that modelers can choose to leverage to reduce the computational resources required for the presented scenario.

4.8 Outputs for Comparison

This section provides a list of outputs for comparison to compare/contrast modeling schemes, numerical simulators, and assumptions made between the participating teams. Some output comparisons are made at a specific location while others are integrated over an area or averaged over a volume. The sign convention is that flow from the repository towards the shaft (left to right in the schematic shown in Figure 4.2) is positive. For vertical fluxes, flow up towards the surface is defined as the positive direction.

Comparison of team results will be conducted qualitatively. Each team should plot the following quantities of interest as a function of time:

4.8.1 Transport comparisons

4.8.1.1 Radionuclide/Tracer Discharges

1. Lower Shaft(s): Plot as a function of time (years) the mass flow of each radionuclide/tracer (moles/year) across a plane in the shaft 25 m above the ceiling of the infrastructure area, integrated over the 7×7 m^2 cross section of the shaft. Flow from the repository towards the surface will be defined as positive.
2. Upper Shaft(s): Plot as a function of time in years the mass flow of each radionuclide/tracer (moles/year) across a plane in the shaft at the base of the aquifer (overburden), integrated over the 7×7 m^2 cross section of the shaft. Flow from the repository towards the surface will be defined as positive.

3. Drift Seal(s): Plot as a function of time in years the mass flow of each radionuclide (moles/year) across 4 planes in the drift seal, integrated over the 7×4 m^2 cross section. Fluxes should be plotted across
    a. The face of the Sorel cement segment nearest the waste,
    b. The plane where the cement abutment connects to the end of the drift seal nearest the waste,
    c. The plane where the end of the drift seal furthest from the waste connects to the second cement abutment,
    d. The face of the second Sorel cement segment nearest the infrastructure area.

    Flow from the drift towards the shafts will be defined as positive.
4. Emplacement drifts: Plot as a function of time in years the mass flow of each radionuclide/tracer (moles/year)
    a. Out of the 90-m long SNF emplacement drift highlighted in Figure 4-2.
    b. Out of the 50-m long HLW emplacement drift highlighted in Figure 4-2.

4.8.1.2 Radionuclide/Tracer mass

1. Infrastructure Area: Plot as a function of time in years the total moles of each radionuclide in the 240×250 m^2 infrastructure area.
2. Drift Seal(s): Plot as a function of time in years the total moles in
    a. The 100-m Sorel cement segment nearest the waste
    b. The 100-m Sorel cement segment nearest the shaft
    c. The 300-m run-of-mine salt section in the drift seal.
3. Emplacement Drifts: Plot as a function of time in years the total moles of each radionuclide in
    a. The 90-m long SNF emplacement drift highlighted in Figure 4-2.
    b. The 50-m long HLW emplacement drift highlighted in Figure 4-2.
4. Whole system: Plot as function of time in years the total moles of each radionuclide in the entire simulation model.

4.8.1.3 Radionuclide/Tracer concentration

1. Plot concentration of radionuclide/tracer in moles/liter as a function of time in years at the top of the aquifer averaged over the 7×7 m^2 cross section immediately above the shaft.
2. Plot concentration of radionuclide/tracer in moles/liter as a function of time in years 100 m immediately downstream of the shaft in the direction of flow. Teams may choose to calculate concentration at a point in the aquifer or averaged over a small volume in the correct location.
3. Plot concentration of radionuclide/tracer in moles/liter as a function of time in years 1 km immediately downstream of the shaft in the direction of flow. Teams may choose to calculate concentration at a point in the aquifer or averaged over a small volume in the correct location.

4.8.1.4 Radionuclide/Tracer source term

1. Plot as a function of time in years the rate of radionuclide release (moles/year) into the 90-m long SNF emplacement drift highlighted in Figure 4-2.

2. Plot as a function of time in years the rate of radionuclide release (moles/year) into 50-m long HLW emplacement drift highlighted in Figure 4-2.

4.8.2 Flow comparisons

4.8.2.1 Saturation, Pressure and Water Volume

1. Infrastructure Area: Plot as a function of time in years the average liquid pressure (Pa), saturation (unitless) and total water volume (m^3) in the 240 x 250 m^2 infrastructure area. If grid cells vary in volume, calculate the volume-weighted average.
2. Drift Seal(s): Plot as a function of time in years the average liquid pressure, saturation and total water volume (m^3)
    a. The 100-m Sorel cement segment nearest the waste
    b. The 100-m Sorel cement segment nearest the shaft
    c. The 300-m run-of-mine salt section in the drift seal.

    If grid cells vary in volume, calculate the volume-weighted average.
3. Emplacement Drifts: Plot as a function of time in years the average liquid pressure, saturation and total water volume (m^3)
    a. The 90-m long SNF emplacement drift highlighted in Figure 4-2.
    b. The 50-m long HLW emplacement drift highlighted in Figure 4-2.

4.8.2.2 Liquid Discharges

Plot as a function of time in years the volumetric flow of liquid (m^3/year) across all the same planes used to compare radionuclide mass flow:

1. Lower Shaft
2. Upper Shaft
3. Drift Seals
    a. The face of the Sorel cement segment nearest the waste,
    b. The plane where the cement abutment connects to the end of the drift seal nearest the waste,
    c. The plane where the end of the drift seal furthest from the waste connects to the second cement abutment,
    d. The face of the second Sorel cement segment nearest the infrastructure area.
4. Emplacement Drifts:
    a. The 90-m long SNF emplacement drift highlighted in Figure 4-2.
    b. The 50-m long HLW emplacement drift highlighted in Figure 4-2.

5. STEP 1C – TASK F1 PROCESS MODEL BENCHMARKS

5.1 Objectives

The objective of Step 1C is to compare performance measures or other outputs resulting from simple test cases or subsystem process models relevant to a repository in crystalline rock. Test cases related to flow and transport (Section 5.2) and the radionuclide source term (Section 5.3) provide an opportunity to:

1. understand differences in model implementation that affect how a problem can be specified, what results can be obtained, and which unit conversions will be necessary.
2. assess the influence of modeling choices on calculated values of performance measures in relatively simple systems.

5.2 Flow and Transport

Flow and transport test cases will build toward comparison of flow and transport simulations using multiple realizations of a stochastically generated DFN in a 1-km^3 model domain. The objective is to understand how uncertainties due to the stochastic nature of the fracture network compare to differences in solution introduced by modelling choices, which may include, for instance, use of DFN versus ECPM, methods of upscaling to ECPM, use of particle tracking versus the advection/dispersion equation, and implementation of rock matrix diffusion.

5.2.1 Steady-state Flow

Steady-state, single-phase flow in 1-D, 2-D, and 3-D will be compared to analytical solutions. The proposed test problems are adapted from Kolditz et al. (2015) and have been demonstrated using PFLOTRAN (Frederick, 2018). Whereas the OpenGeoSys simulations reported in Kolditz et al. (2015) neglected gravity by using zero liquid density, the PFLOTRAN simulations use constant liquid density and neglect gravity by setting the gravity vector to zero.

5.2.1.1 1-Dimensional (1-D) steady flow with boundary conditions of the first kind

The model domain is a 100 m × 10 m × 10 m beam extending in the positive x direction, discretized into 10 cubic grid cells, each 10 m × 10 m × 10 m. Constant pressure (Dirichlet) boundary conditions are held at either end of the beam (Figure 5-1). Material and fluid properties and boundary conditions are given in Table 5-1. The steady-state pressure solution is provided in Kolditz et al. (2015), Section 2.2.1.

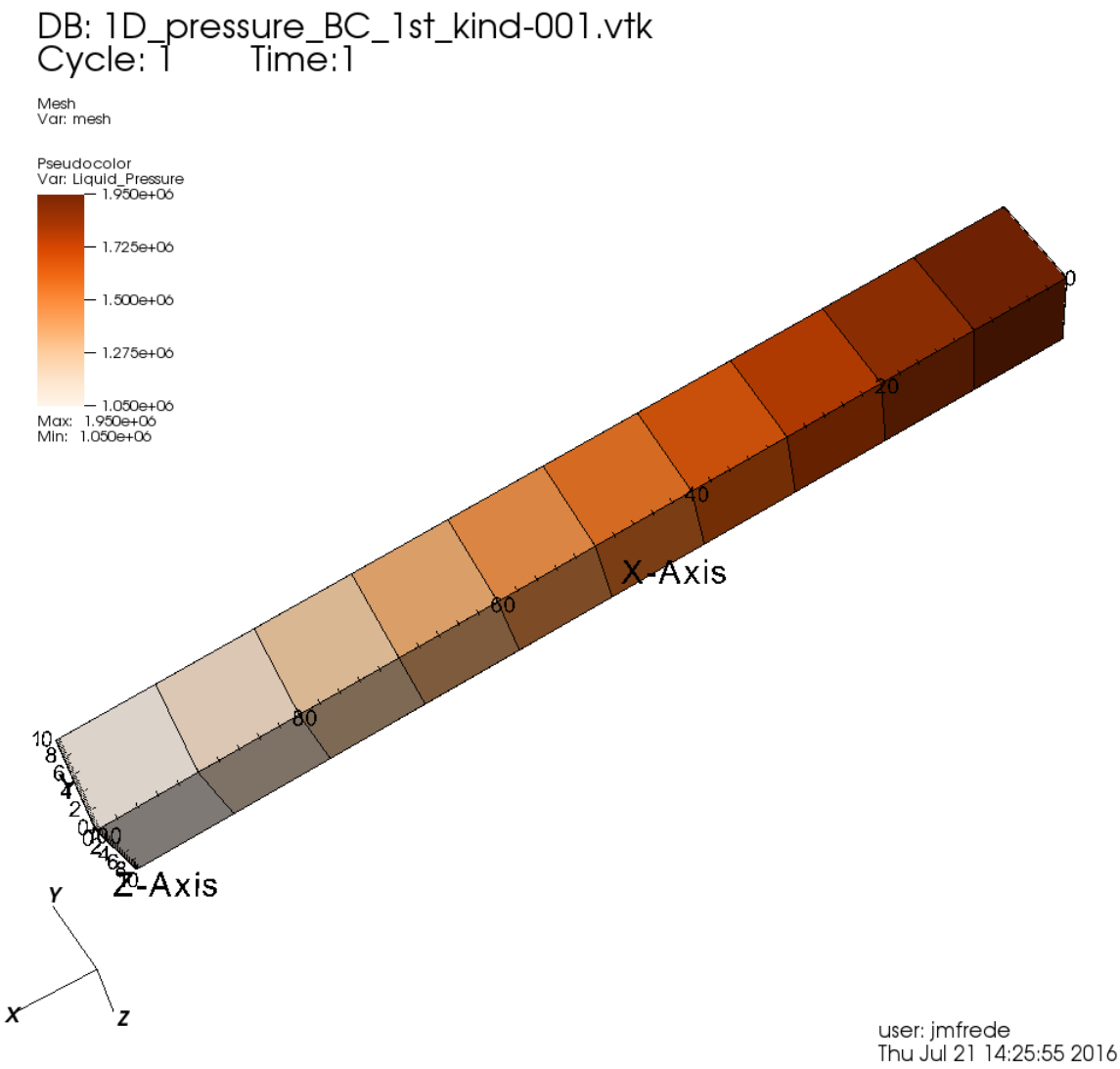

Figure 5-1. Model domain for simulation of 1-D steady flow with boundary conditions of the first kind (Frederick, 2018).

Table 5-1. Parameter values for simulation of 1-D steady flow with boundary conditions of the first kind.

Parameter	Value	Units
Permeability (k)	10^{-15}	m^2
Viscosity (μ)	10^{-3}	Pa-s
Density (ρ)	1000	kg/m^3
Pressure ($P_{x=0}$)	2×10^6	Pa
Pressure ($P_{x=100}$)	1×10^6	Pa

5.2.1.2 2-Dimensional (2-D) steady flow with boundary conditions of the first kind

The model domain is a 1 m × 1 m × 1 m slab extending in the positive x and y directions, discretized into 20 × 20 × 1 hexahedral grid cells, each 0.05 m × 0.05 m × 1 m. Constant pressure (Dirichlet) boundary conditions are held on the faces of the domain orthogonal to the x and y axes (Figure 5-2). Material and fluid properties and boundary conditions are given in Table 5-2. The steady-state pressure solution is provided in Kolditz et al. (2015), Section 2.2.3.

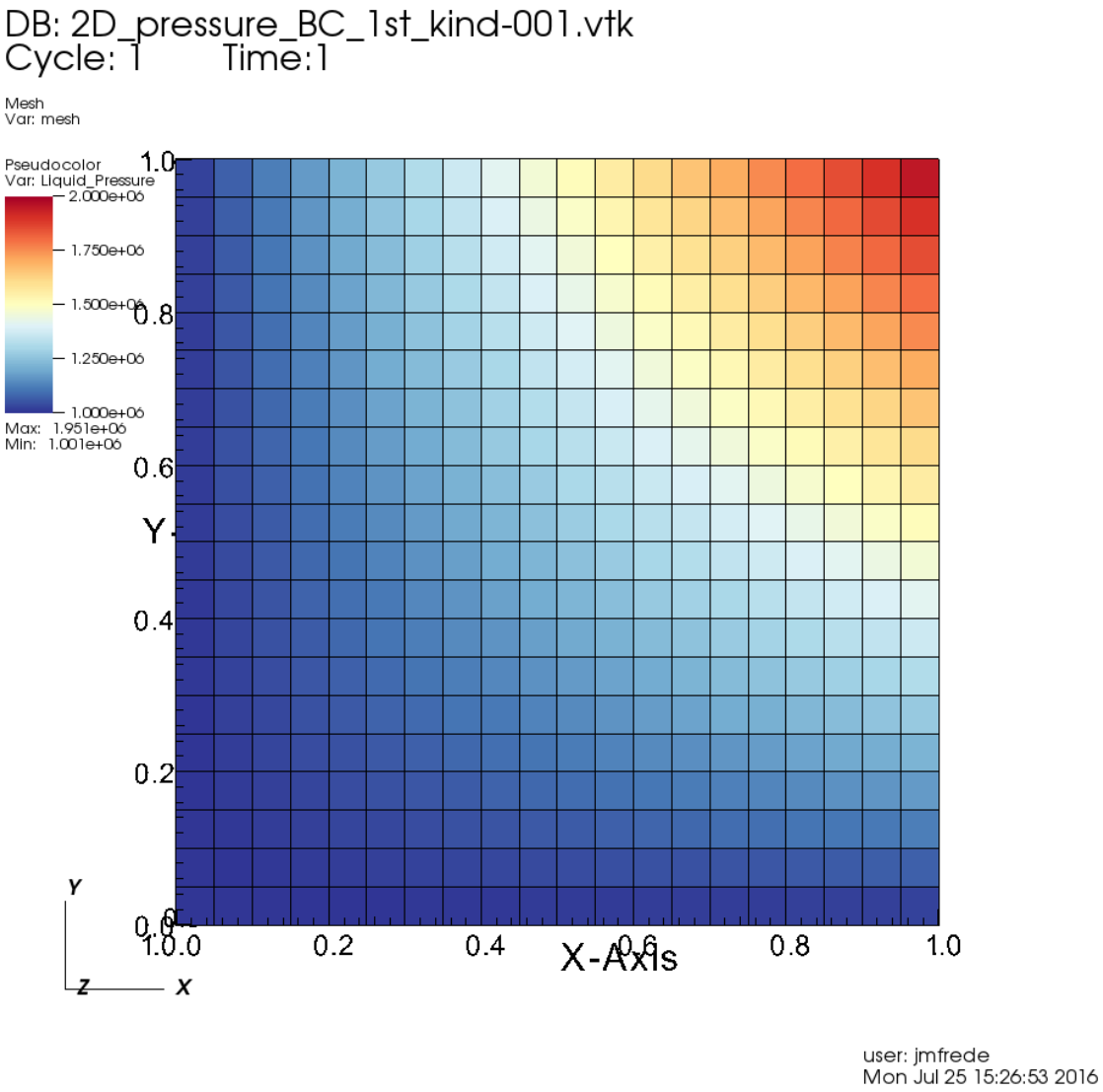

Figure 5-2. Model domain for simulation of 2-D steady flow with boundary conditions of the first kind (Frederick, 2018).

Table 5-2. Parameter values for simulation of 2-D steady flow with boundary conditions of the first kind.

Parameter	Value	Units
Permeability (k)	10^{-15}	m^2
Viscosity (μ)	10^{-3}	Pa-s
Density (ρ)	1000	kg/m^3
Pressure, $P(x = 0, y)$	1×10^6	Pa
Pressure, $P(x = L, y)$	$P_0 \frac{y}{L} + 1 \times 10^6$	Pa
Pressure, $P(x, y = 0)$	1×10^6	Pa
Pressure, $P(x, y = L)$	$P_0 \frac{x}{L} + 1 \times 10^6$	Pa
P_0	1×10^6	Pa
L	1	M

5.2.1.3 3-Dimensional (3-D) steady flow with boundary conditions of the first kind

The model domain is a 1 m × 1 m × 1 m cube extending in the positive *x*, *y* and *z* directions, discretized into cubic grid cells, each 0.1 m × 0.1 m × 0.1 m. Constant pressure (Dirichlet) boundary conditions are held on all six faces of the domain Figure 5-3). Material and fluid properties and boundary conditions are given in Table 5-3. The steady-state pressure solution is provided in Kolditz et al. (2015), Section 2.2.5.

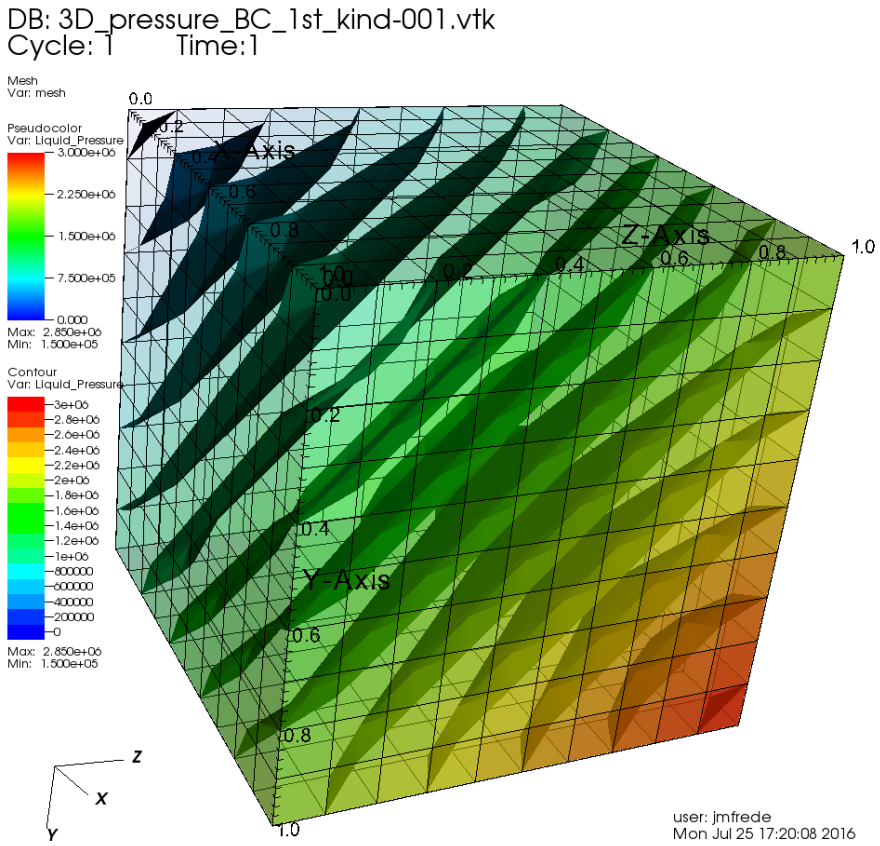

Figure 5-3. Model domain for simulation of 3-D steady flow with boundary conditions of the first kind (Frederick, 2018).

Table 5-3. Parameter values for simulation of 3-D steady flow with boundary conditions of the first kind.

Parameter	Value	Units
Permeability (k)	10^{-10}	m^2
Viscosity (μ)	10^{-3}	Pa-s
Density (ρ)	1000	kg/m^3
Pressure, $P(x=0,y,z)$	$P_0\left(0+\frac{y}{L}+\frac{z}{L}\right)$	Pa
Pressure, $P(x,y=0,z)$	$P_0\left(\frac{x}{L}+0+\frac{z}{L}\right)$	Pa
Pressure, $P(x,y,z=0)$	$P_0\left(\frac{x}{L}+\frac{y}{L}+0\right)$	Pa
Pressure, $P(x=L,y,z)$	$P_0\left(L+\frac{y}{L}+\frac{z}{L}\right)$	Pa
Pressure, $P(x,y=L,z)$	$P_0\left(\frac{x}{L}+L+\frac{z}{L}\right)$	Pa
Pressure, $P(x,y,z=L)$	$P_0\left(\frac{x}{L}+\frac{y}{L}+L\right)$	Pa
P_0	1×10^6	Pa
L	1	m

5.2.2 Transient Transport

1-D transient advection and dispersion of three tracers (conservative, decaying, and adsorbing) will be compared to analytical solutions. The proposed test problem is adapted from Kolditz et al. (2015), Section 2.5.2.

The model domain is a 10 m × 1 m × 1 m beam extending in the positive x direction, discretized into 200 hexahedral grid cells, each 0.05 m × 1 m × 1 m (Figure 5-4). A steady-state flow field (constant specific discharge) is applied. At the inflow face ($x = 0$), concentrations of all three tracers are held at 1 mol/L from 0 to 15000 s, and zero afterward. Concentrations in the model domain are compared to the analytical solution at 20000 s. Material and fluid properties and boundary conditions are given in Table 5-4. Solutions are provided in Kolditz et al. (2015), Section 2.5.2.

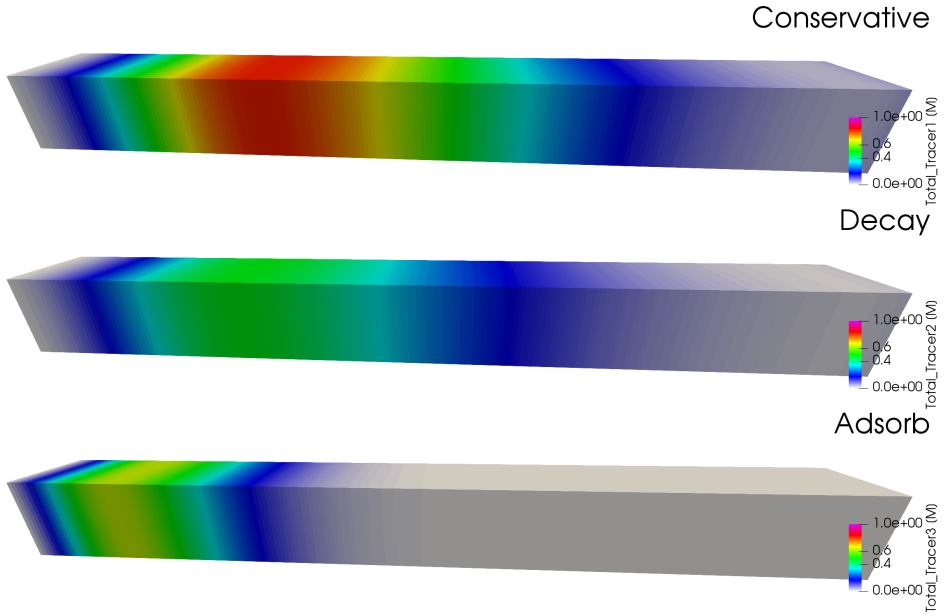

Figure 5-4. Model domain for simulation of transient advection and dispersion.

Table 5-4. Parameter values for simulation of transient advection and dispersion.

Parameter	Value	Units
Specific discharge (q)	10^{-4}	m/s
Dispersion coefficient (D)	10^{-4}	m^2/s
Porosity (ϕ)	0.4	–
Decay constant (λ)	5×10^{-5}	1/s
Linear distribution coefficient (K_d)	6.8×10^{-4}	m^3 H_2O / kg solid
Liquid density (ρ)	1000	kg/m^3
Solid grain density (ρ_s)	2000	kg/m^3

5.2.3 Fracture Transport with Matrix Diffusion

Matrix diffusion is the migration of dissolved solutes from flowing fractures into the pore space of the rock matrix (and vice versa). The proposed benchmark test is based on the analytical solution by Tang et al. (1981), for the problem of transport of a radionuclide in a single fracture, with diffusion into the rock

matrix. The fracture-rock matrix system is represented in Figure 5-5. The governing equations are derived from mass conservation of the radionuclide and the following assumptions are made:

1. The width of the fracture is much smaller than its length.
2. Transverse diffusion and dispersion within the fracture to assure complete mixing across the fracture width at all times.
3. The permeability of the porous matrix is very low and transport in the matrix will be mainly by molecular diffusion.
4. Transport along the fracture is much faster than transport within the matrix.

Concentration profiles along the fracture and the rock matrix ($x \geq b$) are compared to the analytical solution at 100, 1000 and 10000 days over 101 cells. The first set is compared with v_1 along a 6 m domain for the fracture and at z = 2 m with a domain of 2 m for the matrix. A second set is compared with v_2 along a 60 m domain for the fracture and at z = 20 m with a domain of 1 m for the matrix.

The governing equations are:

$$\frac{\partial c}{\partial t} + \frac{v}{R}\frac{\partial c}{\partial z} - \frac{D}{R}\frac{\partial^2 c}{\partial z^2} + \lambda c + \frac{J}{bR} = 0 \qquad \textbf{Eq. (5-1)}$$

$$\frac{\partial c'}{\partial t} - \frac{D'}{R'}\frac{\partial^2 c'}{\partial z^2} + \lambda c' = 0 \qquad \textbf{Eq. (5-2)}$$

Where c, c' are the concentration of solute in solution in the fracture and rock matrix respectively (M/L^3). With v as average linear groundwater velocity in the fracture (L/T) and D is the hydrodynamic dispersion coefficient in the fracture given by:

$$D = \alpha_L v + D^* \qquad \textbf{Eq. (5-3)}$$

The effective diffusion coefficient, D' is given by:

$$D' = \tau D^* \qquad \textbf{Eq. (5-4)}$$

And the diffusive mass flux J ($M/L^2/T$), from the fracture in the rock matrix is given by, at x = b:

$$J = -\phi D' \frac{\partial c'}{\partial x} \qquad \textbf{Eq. (5-5)}$$

The initial conditions are given by:

$$c(z, 0) = c'(x, z, 0) = 0$$

The boundary conditions are given by:

$$c(0, t) = c_0$$
$$c(\infty, t) = 0$$

$$c'(b, z, t) = c(z, t)$$
$$c'(\infty, z, t) = 0$$

Material and fluid properties are given in Table 5-5.

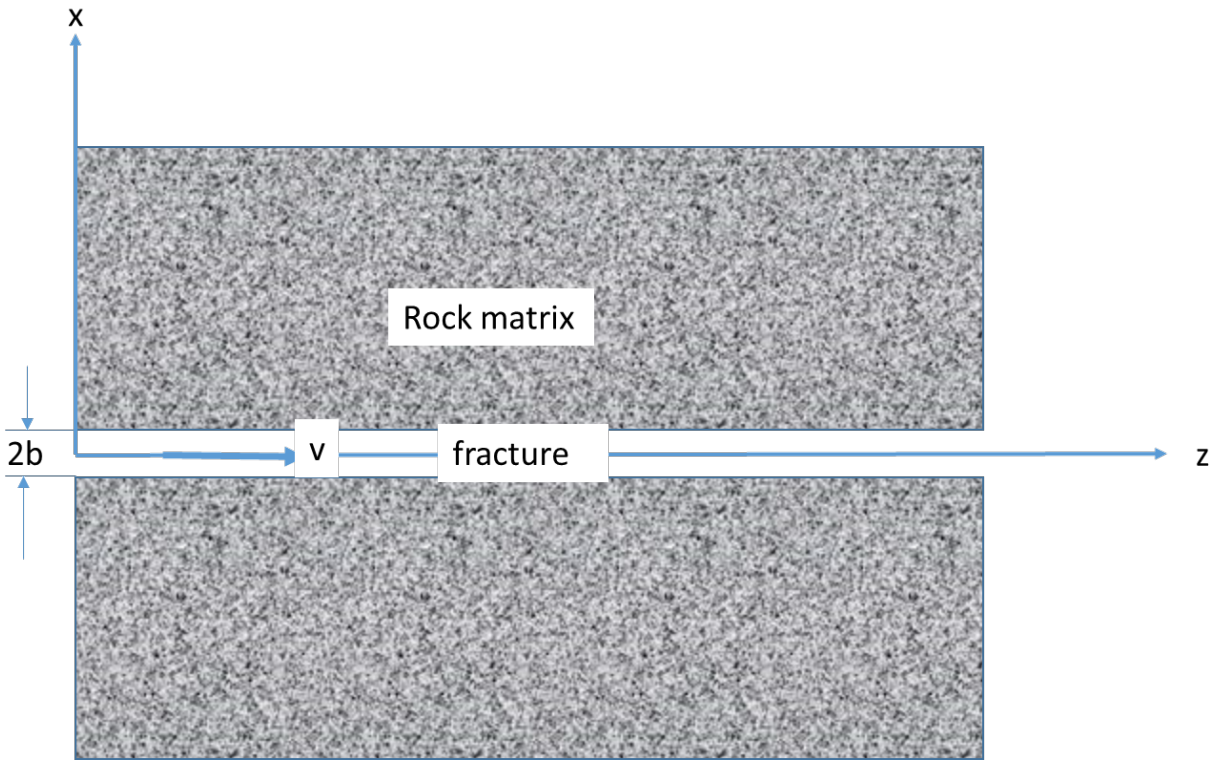

Figure 5-5. Fracture/rock matrix system

Table 5-5. Parameter values for simulation of fracture transport in matrix diffusion.

Parameter	Value	Units
Diffusion coefficient in water (D^*)	1.6×10^{-9}	m^2/s
Tortuosity (τ)	0.1	–
Fracture width ($2b$)	10^{-4}	m
Dispersivity (α_L)	0.5	m
Half-life ($t_{1/2}$), equivalent to Decay constant (λ)	12.35 1.779×10^{-9}	y s
Retardation factor in matrix (R')	1.0	–
Retardation factor in fracture (R)	1.0	–
Porosity (ϕ)	0.01	–
Concentration, c_0 (z=0)	1.0	mol/L
Average linear velocity (v_1)	0.01	m/d
Average linear velocity (v_2)	0.1	m/d

5.2.4 Transport in a 4-Fracture DFN

The four-fracture test problem will provide an opportunity for teams to practice generating deterministic fractures and to test methods for upscaling to ECPM or simulating particle tracking (if desired). The test problem (built based on an example provided with dfnWorks (Hyman et al., 2015)) models advection and

diffusion of a conservative tracer through four fractures within a cubic domain. It is assumed flow and transport only occur in the fractures; matrix diffusion is neglected. Groundwater flow is simulated by a steady state (saturated, single-phase) flow driven by a pressure gradient along the x-axis. Constant pressure (Dirichlet) boundary conditions are applied on the inflow and outflow faces. For simplicity, gravity is not included. No-flow boundary conditions are applied at all other faces of the domain.

An initial pulse of tracer, lasting one day, is inserted along the single fracture on the west face (x = -500) of the domain starting at time zero. The tracer exits the domain through the two fractures on the east face (x = 500). The tracer can be modeled using particle tracking (Lagrangian reference frame) or with the advection-dispersion equation (Eulerian reference frame). In particle tracking, the mass of each particle is equal and 1.0×10^4 particles are introduced on the inflow face. For comparison, normalized breakthrough curves (cumulative mass of tracer exiting the east face divided by the mass introduced at the west face) are generated at the outflow face and compared over 30 years. Since breakthrough curves are normalized to mass introduced, the concentration of the initial pulse is inconsequential. Teams will run these simulations with and without matrix diffusion as they are able.

The governing equation for advective-diffusive transport is,

$$\frac{\partial}{\partial t}(\phi\psi) + \nabla \cdot \Omega = 0 \qquad \textbf{Eq. (5-6)}$$

With ϕ as porosity and ψ denoting total concentration. The total flux Ω is given by,

$$\Omega = (q - D_e \cdot \nabla)\psi \qquad \textbf{Eq. (5-7)}$$

With D_e representing the effective diffusion coefficient, which is defined as,

$$D_e = \phi\tau D_m \qquad \textbf{Eq. (5-8)}$$

Where D_m is the molecular diffusion coefficient in free water [m^2/s] and τ is tortuosity. Tortuosity is defined as $(L/L_e)^2$, where L is the straight-line length and L_e is the average length of a tortuous path through a porous medium (Bear, 1972). Using this definition, tortuosity is a value less than or equal to one.

Pressure is modeled according to Darcy's law,

$$q = -\frac{k}{\mu}\nabla(P) \qquad \textbf{Eq. (5-9)}$$

Where k is permeability [m^2], μ is viscosity [Pa-s], and P is pressure [Pa].

Details can be found in Table 5-6 and vertex coordinates for the domain and fractures can be found in Table 5-7.

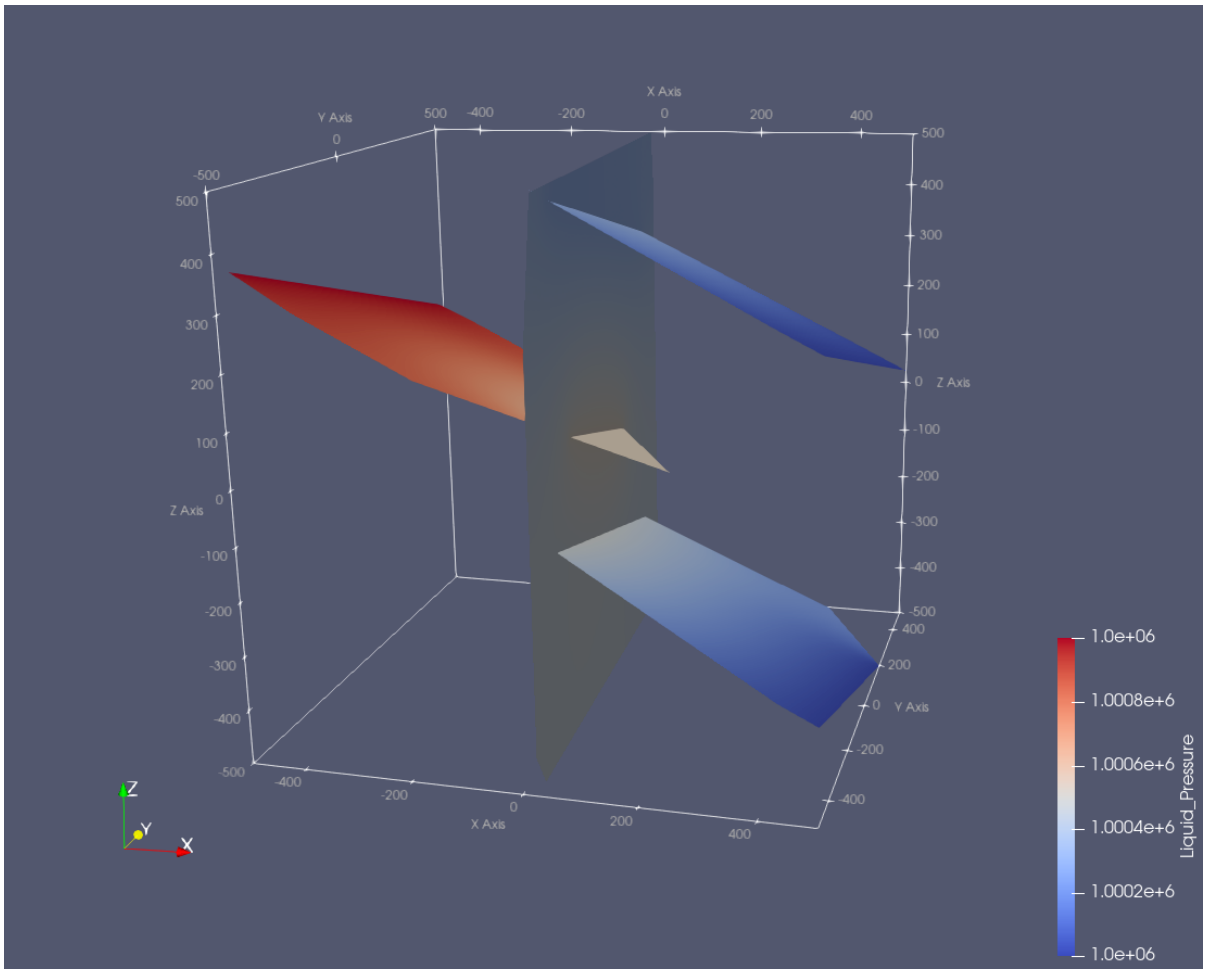

Figure 5-6. Four-fracture pressure simulation.

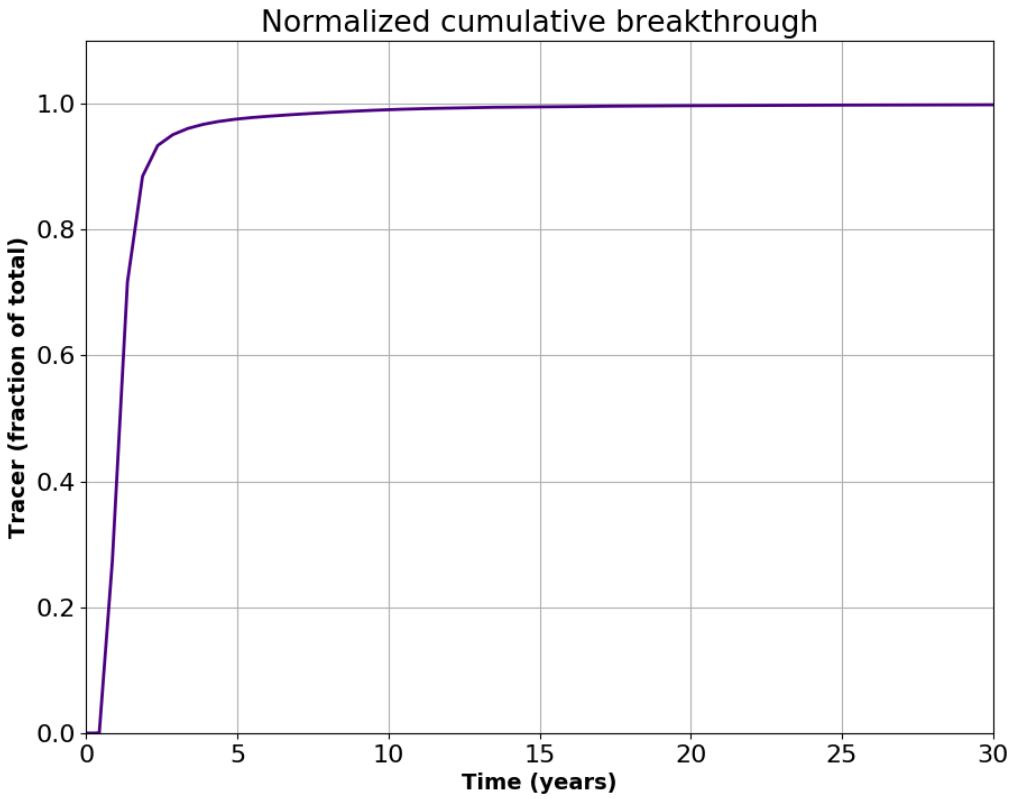

Figure 5-7. Example breakthrough curve

Table 5-6. Parameter values for four-fracture problem.

Parameter	Value	Units
Pressure (inlet, x = -500)	1.001×10^{6}	Pa
Pressure (outlet, x = 500)	1×10^{6}	Pa
Fracture 1 Aperture	1×10^{-3}	m
Fracture 2 Aperture	1×10^{-3}	m
Fracture 3 Aperture	1×10^{-3}	m
Fracture 4 Aperture	5×10^{-4}	m
Fracture 1 Permeability	8.333×10^{-8}	m^2
Fracture 2 Permeability	8.333×10^{-8}	m^2
Fracture 3 Permeability	8.333×10^{-8}	m^2
Fracture 4 Permeability	2.083×10^{-8}	m^2
Porosity in a fracture (ϕ)	1.0	–
Tortuosity in a fracture (τ)	1.0	–
Diffusion coefficient in water (D_m)	1.6×10^{-9}	m^2/s

Table 5-7. Coordinates for domain and fractures

Feature	Vertex
Domain	{-500, -500, -500} {-500, -500, 500} {-500, 500, 500} {-500, 500, -500} {500, -500, -500} {500, 500, -500} {500, 500, 500} {500, -500, 500}
Fracture 1	{-162.354, -500.000, 206.177} {138.978, -30.511, -61.861} {-229.987, 500.000, -10.007} {-417.374, 500.000, 83.687} {-500.000, 475.093, 131.227} {-500.00, -446.814, 361.704} {-367.607, -500.000, 308.800}
Fracture 2	{26.316, -500.000, -431.524} {23.472, -445.963, -500.000} {-21.371, 406.045, -500.000} {-26.316, 500.000, -397.831} {-26.316, 500.000, 392.163} {-25.312, 480.928, 500.000} {23.070, -438.334, 500.000} {26.316, -500.000, 261.673}
Fracture 3	{500.000, -500.000, 275.000} {500.000, 500.000, 25.000} {382.626, 500.000, 83.687} {-53.977, 368.388, 334.891} {-18.109, -319.021, 488.810} {432.393, -500.000, 308.804}
Fracture 4	{500.000, -500.000, -325.000} {500.000, 200.000, -500.000} {354.273, 491.453, -500.000} {-53.977, 368.388, -265.109} {-18.109, -319.021, -111.190} {432.393, -500.000, -291.196}

5.2.5 Transport in a 4-Fracture DFN with Stochastic Fractures

A note about Revision 4: This problem specification and associated files have been corrected in Revision 4. The DFN in “vertices.txt” provided with Revision 3 was generated with incorrect fracture orientations. When the fracture orientations were corrected, additional changes to model inputs were also

made. These include: (1) the pressure at the west face of the domain is increased to 1.1 MPa; the half-life of the decaying tracer is decreased to 100 y; the retardation coefficient in the fractures (see Eq. (5-12)) is increased to 5. Additionally, hydrologic properties of the matrix are added to the problem description, and the inputs necessary to generate the fracture network using dfnWorks (Hyman et al.,2015) and to upscale it using mapdfn.py (Stein et al., 2017) are provided separately.

The four-fracture benchmark case is extended by adding a realization of stochastically-generated fracture sets to the model domain. For this problem, teams use an identical fracture network. dfnWorks input files are provided to create the fracture network as well as input (mapdfn2pflotran.py) to upscale to an ECPM using mapdfn.py. Output files from dfnWorks and mapdfn.py are also provided for the DFN and ECPM. The ECPM consists of 125,000 cells, each of which is 20 m × 20 m × 20 m. Coordinates of the fracture vertices are provided in the text file polygons.dat. Fracture apertures and permeabilities are provided respectively in the text files aperture.dat and perm.dat. Coordinates of the fracture centers are provided in the text file translations.dat; fracture radii are provided in radii_Final.dat; and normal vectors for each fracture are provided in normal_vectors.dat. The parameters necessary for teams to generate their own stochastic fracture sets will be given in future problems.

The stochastic fractures for this problem are generated based on Central Hydraulic Unit West (CHUW) Case A distributions from Posiva WR 2012-42 (Hartley et al., 2013b) corresponding to Depth Zone 4, which applies at repository depth (Hartley et al., 2016). The problem models advection and diffusion of conservative, decaying, and adsorbing tracers according to Eq. (5-6) (Section 5.2.4), through the four fractures and stochastic fractures within a cubic domain. The problem uses the same assumptions for flow and transport as the four-fracture benchmark case and the domain coordinates remain the same.

Three fracture families, two subvertical and one subhorizontal, are defined. For each fracture family, fracture radius is sampled from a truncated power law distribution, and fracture orientation is sampled from a Fisher distribution. (Although a bivariate Bingham distribution is given for the subhorizontal fracture family, the option isn't yet implemented in dfnWorks, so for this initial test problem a Fisher distribution is used.) Fractures are assumed to be randomly distributed in space, with a fracture intensity for each fracture family expressed as fracture area per unit volume of rock (P_{32}).

Posiva employed truncated power law distributions with a minimum radius of 0.04 m and a maximum radius of 564 m in calibrating P_{32} and fracture transmissivity to borehole flow measurements (Hartley et al., 2013a) but employed larger minimum fracture radii (8.46 m in the far field and 0.5 m in the vicinity of the repository) in generating DFNs for flow and transport modeling (Hartley et al., 2013b). Similarly, to generate fractures for this test problem, the minimum fracture radius is increased to 30 m, and P_{32} is adjusted accordingly using the method in Hedin (2008).

In this test problem, fracture transmissivity (T [m^2/s]) is correlated with fracture radius (r [m]) according to:

$$T = ar^b \qquad \textbf{Eq. (5-10)}$$

In Eq. (5-10), a and b are dimensionless constants with values equal to 2.2e-9 and 0.8, respectively (Hartley et al., 2013b).

Fracture aperture is calculated from transmissivity using the cubic law (as in Bear, 1993):

$$T = \frac{\rho g}{\mu}\frac{B^3}{12} \qquad \textbf{Eq. (5-11)}$$

In Eq. (5-11), B is fracture aperture [m] (equal to $2b$ in Figure 5-5), ρ is the density of water [kg/m^3], g is acceleration due to gravity [m/s^2], and μ is the viscosity of water [Pa s].

An initial pulse of tracer, lasting one day, is inserted along the fractures on the west face (x = -500) of the domain starting at time zero. The tracer exits the domain through the fractures on the east face (x = 500). For comparison, normalized breakthrough curves (cumulative mass that has exited the east face divided by the mass introduced at the west face) are generated at the outflow face and compared over 1000000 years. Since breakthrough curves are normalized to introduced mass, the concentration of the initial pulse is inconsequential. The tracer can be modeled using particle tracking (Lagrangian reference frame) or with the advection-dispersion equation (Eulerian reference frame). Teams will run these simulations with and without matrix diffusion as they are able. The decaying tracer has a half-life of 100 years. The adsorbing tracer has a retardation coefficient in the fracture of 5. If a team's software requires a linear distribution coefficient instead of a retardation coefficient, Eq. (5-12) and Eq. (5-13) will assist in the conversion. The retardation coefficient (R [-]) is defined as (Tang et al., 1981):

$$R = 1 + \frac{K_f}{b} \qquad \textbf{Eq. (5-12)}$$

In Eq. (5-12), b is half the fracture aperture, and K_f is the linear distribution coefficient (K_d) in the fracture, defined as (Freeze and Cherry, 1979):

$$K_f = \frac{\text{mass sorbed} / \text{area fracture}}{\text{mass dissolved} / \text{volume water}}. \qquad \textbf{Eq. (5-13)}$$

Details for flow and transport parameters can be found in Table 5-8. The problem specification does not include fracture-matrix diffusion (such as might be simulated using a dual-porosity model). Hydrologic properties of the matrix are included for teams that choose to include the matrix in upscaling to an ECPM. These values correspond to the inputs given in mapdfn2pflotran.py associated with this problem; however, to minimize advection and diffusion in ECPM cells not intersected by fractures, teams may prefer to choose smaller values for matrix permeability and tortuosity or to deactivate matrix cells during simulations.

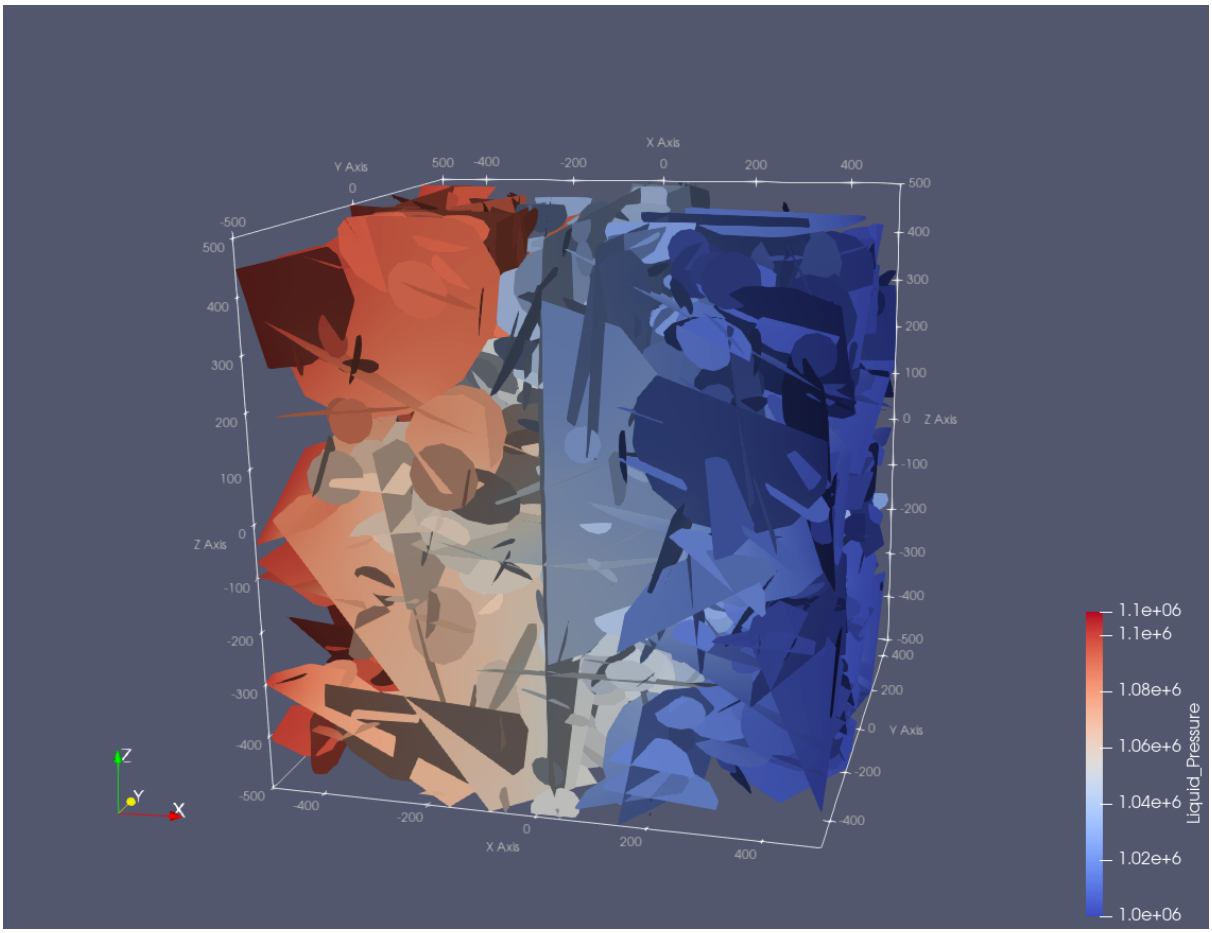

Figure 5-8 Four-fracture with stochastic fractures pressure simulation.

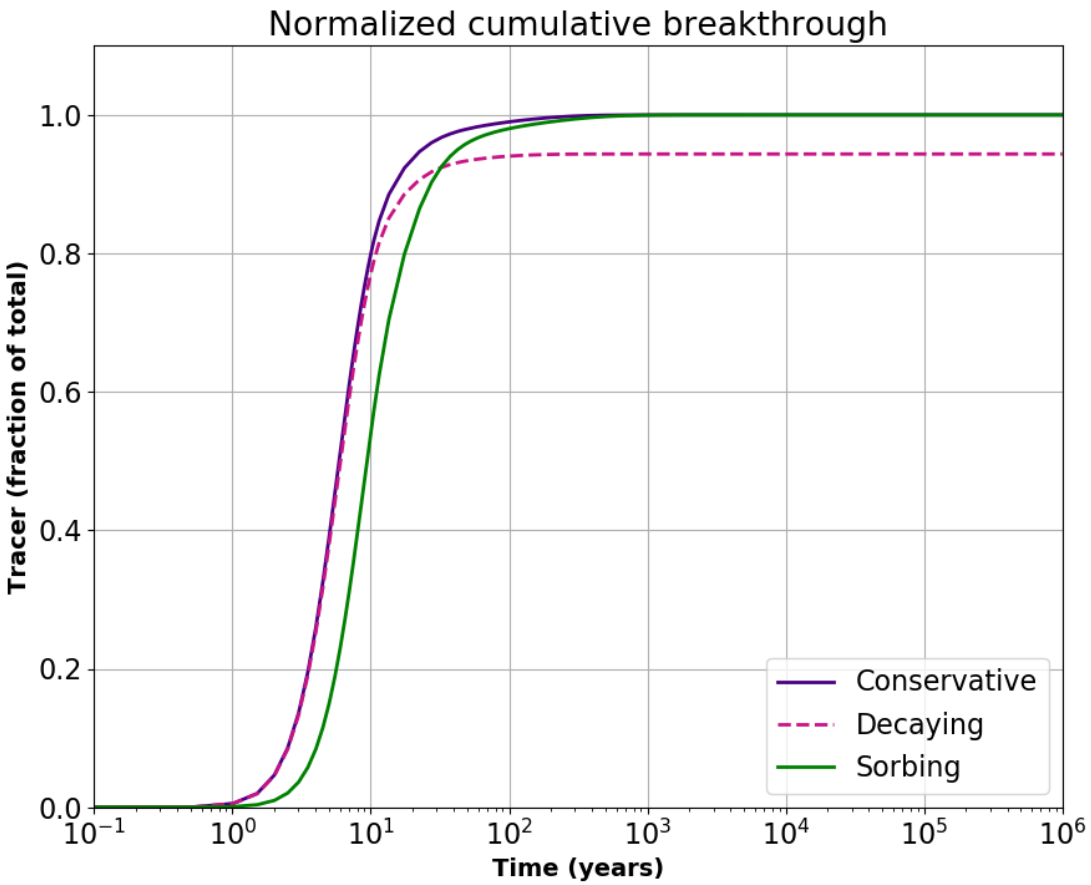

Figure 5-9. Example breakthrough curve

Table 5-8. Parameters for four fracture problem with stochastic fractures

Parameter	Value	Units
Pressure (inlet, x = -500)	1.1×10^6	Pa
Pressure (outlet, x = 500)	1×10^6	Pa
Porosity in a fracture	1.0	–
Tortuosity in a fracture	1.0	–
Matrix porosity	0.005	–
Matrix tortuosity[a]	0.2	–
Matrix permeability	10^{-18}	m^2
Diffusion coefficient in water (D_m)	1.6×10^{-9}	m^2/s
Half-life ($t_{1/2}$)	100	years
Retardation factor in fracture (R)	5	–

[a] The effective diffusion coefficient in the rock matrix is 1.6×10^{-12} m^2 (see Equation 8).

5.2.6 Revised Transport in a 4-Fracture DFN with Stochastic Fractures

The 4-Fracture DFN with stochastic fractures benchmark is revised in this section to be more consistent with the 4-Fracture DFN benchmark in Section 5.2.4. The apertures and permeabilities of the four deterministic fractures can now be found in Table 5-9. The four deterministic fractures represent the first four fractures listed in aperture.dat and perm.dat. The stochastic fracture sets are defined in Section 5.2.5. The inlet pressure boundary condition has also been revised to 1.001×10^6 Pa (Table 5-9).

Preliminary PFLOTRAN calculations of the ECPM indicate a steady state water inflow rate of 1.24×10^6 kg/yr for this revised benchmark. For a domain porosity of 4.52×10^{-6} and a water density of 997 kg/m^3, this corresponds to a mean Darcy velocity of 0.275 km/yr from the west side of the domain to the east side. Example breakthrough curves are shown in Figure 5-10. The stochastic fractures and all other parameters remain the same as section 5.2.5.

Table 5-9. Revised parameters for four fracture problem with stochastic fractures

Parameter	Value	Units
Pressure (inlet, x = -500)	1.001×10^6	Pa
Pressure (outlet, x = 500)	1×10^6	Pa
Deterministic Fracture 1 Aperture	1×10^{-3}	m
Deterministic Fracture 2 Aperture	1×10^{-3}	m
Deterministic Fracture 3 Aperture	1×10^{-3}	m
Deterministic Fracture 4 Aperture	5×10^{-4}	m
Deterministic Fracture 1 Permeability	8.333×10^{-8}	m^2
Deterministic Fracture 2 Permeability	8.333×10^{-8}	m^2
Deterministic Fracture 3 Permeability	8.333×10^{-8}	m^2
Deterministic Fracture 4 Permeability	2.083×10^{-8}	m^2

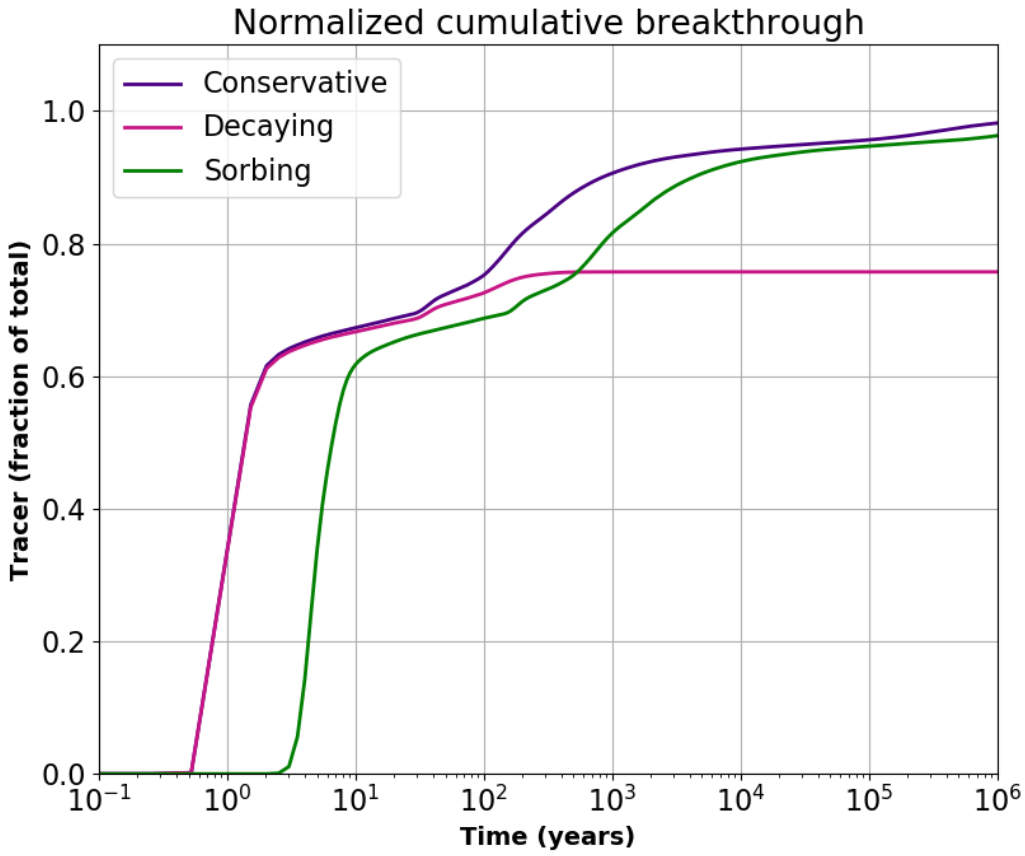

Figure 5-10. Example breakthrough curve

5.2.7 The 4-Fracture-Plus Benchmark with a Point Source

This benchmark simulates plume development in fractured rock from a continuous point source, as might happen for a slowly degrading waste form of a failed waste package. It uses the same domain, fractures, tracers, and flow conditions of the revised 4-fracture problem with stochastic fractures (Section 5.2.6). The only difference is how the tracers are introduced.

For this benchmark, the tracers are introduced continuously at a constant rate as a point source. The point source is assumed to have coordinates (-500,7.0, 248.25), as shown in Figure 5-11. The size of the point source is assumed to be the size of the cell that includes the point source location, which may vary depending on the resolution of the grid being used. No new grid refinement is requested for this benchmark. The method of tracer introduction into the point source cell must not significantly affect the flow field. Tracer is not allowed to diffuse out of the entire west boundary ("zero-gradient" boundary).

The magnitude of the constant mass flux of each tracer into the cell is not specified because breakthrough curves are normalized by the mass introduced. Breakthrough curves are calculated by dividing the tracer mass exiting the domain at each time step by the mass introduced at each time step. At steady state, this value is 1 for non-decaying tracers.

As teams are able, this benchmark is to be run with and without matrix diffusion (as discussed in Section 5.2.5). Running each of these cases will allow separate comparisons for fracture flow models and for the additional effects of different matrix diffusion models. In addition to the breakthrough curves, teams will report calculations of water inflow/outflow (kg/yr) assuming a water density of 997 kg/m^3, domain porosity, and mean Darcy flux (km/yr).

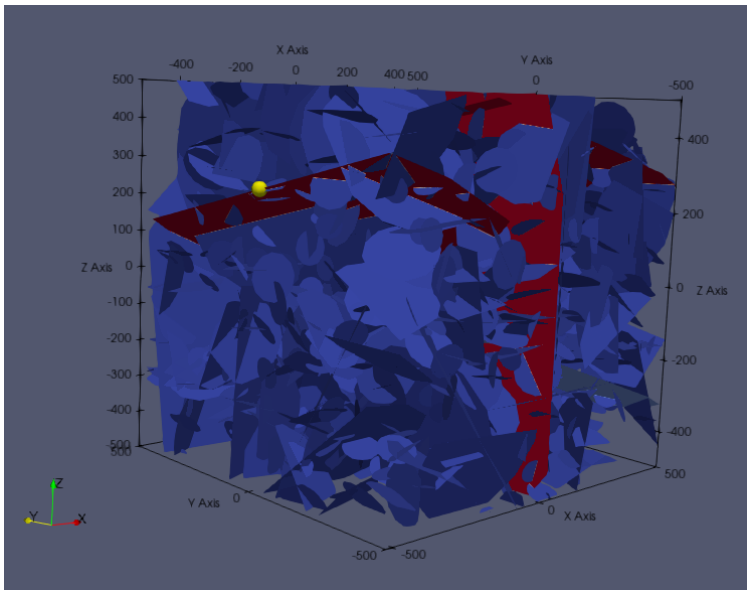

Figure 5-11. Location of point source (-500,7.0, 248.25) for point source benchmark.

5.3 Radionuclide Source Term Processes

The radionuclide source term depends on rates of radioactive decay and ingrowth, the timing of waste package breach, and degradation properties of SNF. Depending on implementation, limitations on radionuclide solubility within the waste canister may be accounted for in the source term model or considered separately. A test case for the source term is defined here to test the effects of the following on radionuclide release from the waste form:

1. Radioactive decay and ingrowth
2. Waste package breach time
3. Instant release fraction
4. Fuel matrix degradation rate
5. Solubility limitations

The fuel for this test case is BWR Atrium for a 10×10-9Q bundle, 4.2 wt% enrichment, 40% void history, and discharge burnup of 50 MWd/kgU, as defined in Anttila (2005). The initial activities and decay rates of selected radionuclides in the fuel are provided in Table 5-10. There is initially 1000 kg of fuel in the waste package. The fuel density is assumed to be 10970 kg/m^3.

Radioactive decay and ingrowth occur both in the fuel and in the water in contact with the fuel. In this problem, waste package breach occurs at 3000 years, cladding fails, and water contacts the fuel. Released radionuclides are assumed to be fully mixed in the water of the breached waste package. For simplicity for this test problem, the water, fuel, and released radionuclides remain in a closed system inside the waste package. The amount of water in the waste package is 10^4 kg.

Tc-99 is assumed to have an IRF of 3%, which is in the range reported in Johnson et al. (2005) for similar fuels and fuel histories. IRFs are assumed to be released to the water immediately upon waste package breach. The fuel matrix degrades at a fractional rate of 10^{-6} /yr starting at the time of waste package breach. Aqueous concentrations are potentially limited by the element solubility limits shown in Table 5-10.

Results of this test case are evaluated as follows:

1. Activities of the radionuclides in the ^{245}Cm to ^{229}Th decay chain are shown to match the activities calculated in Anttila (2005) at 5, 30, 10^2, 10^3, 10^4, 10^5, and 10^6 years.
2. Waste package breach is shown to occur at 3000 years.
3. An immediate transfer of 3% of the ^{99}Tc is shown to be released from the fuel when the waste package breaches, and the released ^{99}Tc is shown to be in the water plus possible precipitate if its concentration exceeds solubility limitations.
4. The fuel matrix is shown not to degrade before waste package breach and is shown to be 63.1% degraded at one million years. In addition, radionuclide release from fuel degradation is shown to be congruent.
5. Aqueous concentrations are shown to be limited by elemental solubility limits as appropriate. (A solubility-limited aqueous concentration of an isotope is reduced by the presence of other isotopes of the same element. However, for this test problem the concentrations of other isotopes are assumed negligible.)

Table 5-10. Properties and initial activities of selected radionuclides in BWR Atrium fuel in a 10×10^{-9} Q bundle, 4.2 wt% enrichment, 40% void history, and a discharge burnup of 50 MWd/kgU, as defined in Anttila (2005, Table 2.2.2.4, p. 152). Aqueous solubility limits for the test case are also defined.

Radionuclide	Element Solubility (M)[a]	Initial Activity (GBq/tU)[b]	Decay rate (1/s)	Daughter
^{245}Cm	6×10^{-6}	19.7	2.59×10^{-12}	^{241}Pu
^{241}Pu	2×10^{-7}	4.79×10^{6}	1.67×10^{-9}	^{241}Am
^{241}Am	6×10^{-6}	6.36×10^{3}	5.08×10^{-11}	^{237}Np
^{237}Np	1×10^{-9}	15.6	1.03×10^{-14}	^{233}Pa
^{233}Pa	1×10^{-9}	16.1	7.13×10^{-6}	^{233}U
^{233}U	4×10^{-10}	0	1.38×10^{-13}	^{229}Th
^{229}Th	4×10^{-7}	0	2.78×10^{-12}	^{209}Bi (stable)[c]
^{99}Tc	3×10^{-8}	732	1.04×10^{-13}	^{99}Ru (stable)

[a] Model calculations of element solubility for a brackish Na-Ca-Cl groundwater (Mariner et al. 2011, Table 2-5)

[b] 10^9 Bq per tonne initial uranium

[c] Daughters in decay chain between ^{229}Th and ^{209}Bi each have half-lives less than 15 days

5.4 Buffer and Canister Processes

A series of test problems related to buffer saturation and erosion and canister corrosion will be added here when such processes are included in the reference case.

6. STEP 1S – SALT REFERENCE CASE PROCESS MODEL COMPARISON

6.1 Objectives

The objective of Step 1S is to compare performance measures or other outputs resulting from simple test cases or subsystem process models. These will be addressed in an order that facilitates sequential development of the complete repository system model. Test cases provide an opportunity to understand how differences in model implementation and simulator capability affect how a problem can be specified and what results can be obtained. Test cases can also be used to assess the influence of modeling choices on calculated values of performance measures in relatively simple systems.

6.2 Flow and Transport

Two flow and transport benchmarks with analytical solutions are used as test cases for Task F2-salt:

- 1-D transient advection and dispersion of three tracers will be compared to analytical solutions.
- A 2-D transient advection and dispersion benchmark for a line source in a 2-D flow field.

6.2.1 1-D Transient Transport

The 1-D transport benchmarks of conservative, decaying, and adsorbing tracer advection and dispersion are the same as those completed for the crystalline case, shown in Section 5.2.1.1.

6.2.2 2-D Transient Transport

Transport of radionuclides to the overburden by shaft-seal failure is considered as the disruptive scenario for the DECOVALEX Task F2-salt case. Thus, the 2-D benchmark problem has been chosen to be a simplified model of transport of tracers through a 2-D semi-infinite domain with constant, unidirectional flow and tracer entering the domain from a line source. The 2-D domain represents idealized overburden sediment, while the line source represents the intersection of the shaft with the overburden. The analytical solution is one of the example models from Section 3.3.2.2 of Batu (2006).

6.2.2.1 Analytical model

The conceptual model for the benchmark is shown in Figure 6-1. The assumptions of the analytical model are (after Batu, 2006):

1. Unidirectional steady-state groundwater velocity field with flow in the x-direction.
2. Solute source is located at x = 0, planar and perpendicular to the velocity of the flow field.
3. Source concentration is a function of z-coordinate and time through an exponential function.
4. The medium is infinite in the x-direction and z is in the range (0,Z).

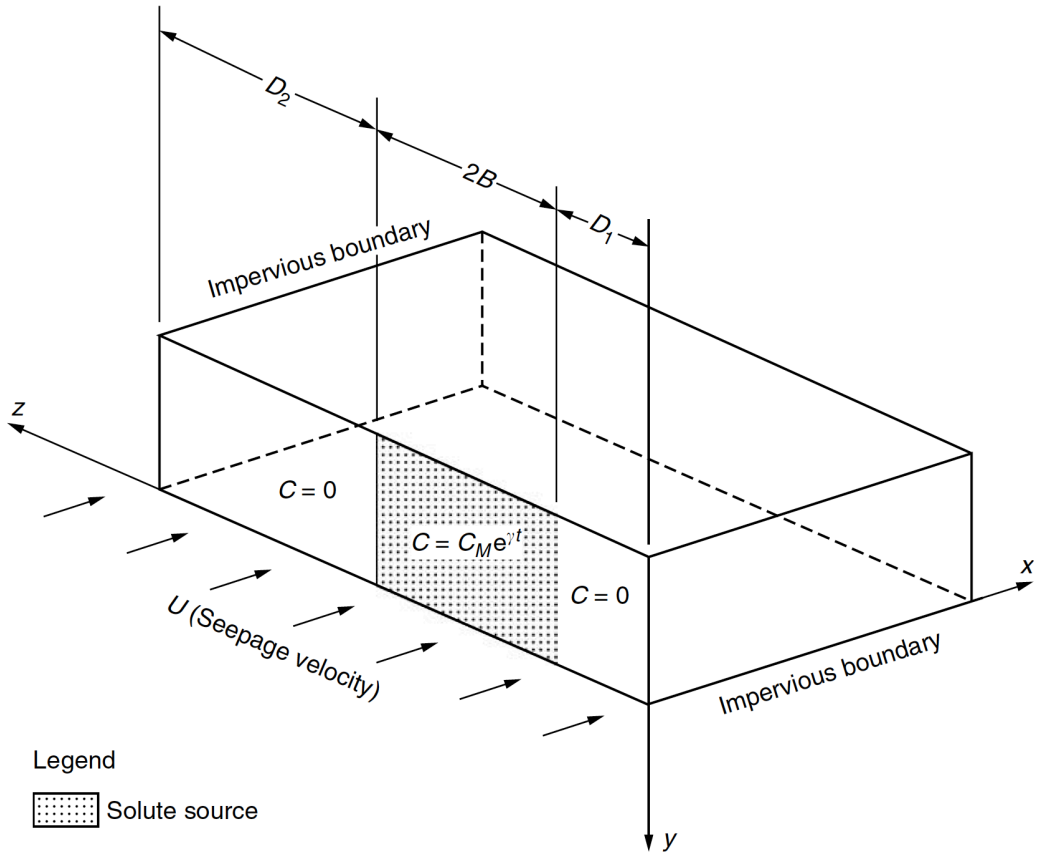

Figure 6-1. Schematic of chemical diffusion and transport from a planar source in a uniform flow field. Taken from Batu (2006).

The governing equation is:

$$\frac{\partial C}{\partial t} = \frac{D_x}{R_d}\frac{\partial^2 C}{\partial x^2} + \frac{D_z}{R_d}\frac{\partial^2 C}{\partial z^2} - \frac{U}{R_d}\frac{\partial C}{\partial x} - vC \qquad \textbf{Eq. (6-1)}$$

The initial condition is

$$C(x,z,0) = 0 \qquad \textbf{Eq. (6-2)}$$

and the boundary condition is

$$C(0,z,t) = \begin{cases} C_m \exp(\gamma t) & D_1 < z < D_1 + 2B \\ 0 & \text{otherwise} \end{cases} \qquad \textbf{Eq. (6-3)}$$

In this equation C_m is the initial tracer concentration at the source, U is the groundwater seepage velocity, v is the interstitial velocity, γ is the chemical decay rate of the source, R_d is the retardation factor. D_1 is the distance of the source from the z = 0 axis, D_2 is the distance from the z = Z outer boundary of the model, and B is the half-length of the planar source. $R_d = 1$ for flow without adsorption and $\gamma = 0$ for a constant rate tracer source.

The solution to this equation is:

$$C(x,z,t) = C_m P_1 \left[\exp(-P_2)\operatorname{erfc}(P_3 - P_4) + \exp(P_2)\operatorname{erfc}(P_3 + P_4)\right] + \frac{C_m}{\pi} P_5 P_6 \sum_{n=1}^{\infty} P_{7_n} \left[\exp(-P_{8_n})\operatorname{erfc}(P_3 - P_{9_n}) + \exp(P_{8_n})\operatorname{erfc}(P_3 + P_{9_n})\right] \quad \textbf{Eq. (6-4)}$$

where

$$P_1 = \frac{B}{D_1 + 2B + D_2}\exp\left(\gamma t + \frac{Ux}{2D_x}\right) \qquad P_2 = \left(\frac{vR_d}{D_x} + \frac{U^2}{4D_x^2} + \frac{\gamma R_d}{D_x}\right)^{\frac{1}{2}} x$$

$$P_3 = \frac{R_d x}{2(D_x R_d t)^{\frac{1}{2}}} \quad P_4 = \left[\left(v + \frac{U^2}{4D_x R_d} + \gamma\right) t\right]^{\frac{1}{2}} \quad P_5 = \exp\left(\frac{Ux}{2D_x}\right)$$

$$P_6 = \exp(\gamma t) \quad P_{7_n} = \frac{1}{n}\left\{\sin\left[\lambda_n (D_1 + 2B)\right] - \sin(\lambda_n D_1)\right\}\cos(\lambda_n z)$$

$$P_{8_n} = \left(\frac{vR_d}{D_x} + \frac{D_z}{D_x}\lambda_n^2 + \frac{U^2}{4D_x^2} + \frac{\gamma R_d}{D_x}\right)^{\frac{1}{2}} x \quad P_{9_n} = \left[\left(v + \frac{D_z}{R_d}\lambda_n^2 + \frac{U^2}{4D_x R_d} + \gamma\right) t\right]^{\frac{1}{2}}$$

$$\lambda_n = \frac{n\pi}{D_1 + 2B + D_2}, \quad n = 1, 2, \ldots$$

The analytical model is based on Example 3-9 of Batu (2006). Parameters for the benchmark are shown in Table 6-1. The domain for the analytical solution is infinite in the x-direction (flow direction), but concentrations will only be calculated up to X = 900 m downstream of the shafts. The model is Z= 2,010 m in the z-direction with $D_1 = D_2 = 1{,}000$ m and 2B = 10 m. The porous medium is 10 m thick and porosity $\phi = 0.25$. The background flux rate is U = 0.15 m/day and the domain is assumed to be water-saturated. Dispersion is anisotropic with longitudinal dispersivity $\alpha_l = 21.3$ m and transverse dispersivity $\alpha_t = 4.3$ m. Effective molecular diffusion is assumed to be negligible, so that $D^* = 0$ m^2/day, and directional dispersion is $D_x = D^* + U\alpha_l$ and $D_z = D^* + U\alpha_t$ All parameters are shown in Table 6-1.

The analytical solution is also calculated for a tracer with retardation factor greater than one and a decaying rate source. A reference partition coefficient, K_d, value representative of Cs(I) in the overburden at neutral conditions is chosen (see Table 4-13). $K_d = 0.433$ m^3/kg so that $R_d = 1 + K_d/\phi = 2.732$. The decay rate of the source assigned the value $\gamma = -0.001$ 1/day, as in Example 3-9 of Batu (2006).

Table 6-1. Hydraulic, thermal, and mechanical parameters for DECOVALEX Task F salt analytical benchmark. Height and permeability are only needed for simulations.

Parameter	Value
Distance to source, D_l [m]	1000
Half-width of source, B [m]	5
Width of the model in z-direction, Z [m]	2,010
Length of the model in x-direction, X [m]	9,000
Interstitial velocity [m/day]	0.15
Longitudinal dispersivity, a_l [m]	21.3
Transverse dispersivity, a_t [m]	4.3
Diffusion coefficient, D^* [m^2/day]	0.0
Concentration at source, C_m [kg/m^3]	1.0
Retardation factor for Case 2, R_d [m^3/kg]	2.732
Decay rate for Case 3, g [1/day]	-0.001
Porosity [-]	0.25
Permeability [m^2]	1×10^{-15}
Height [m]	10

6.2.2.2 Solution

The analytical solution is scripted in python3 for comparison with simulated results and has been provided to teams separately. The series solution shown in Eq. (6-4) is challenging to compute numerically. Many terms in the infinite series are required for convergence. All analytical solutions shown have n = 500 terms of the series. Furthermore, many of the exponential and error functions contain very large arguments, especially at late time. It is not always possible to use regular python float variables because of overflow, and the 'decimal.getcontext().prec' library is required.

The analytical solution near the source for Case 1 with no retardation or decay in the source after 20 years is shown in Figure 6-2, and is identical to the contours in Figure 3-24 of Batu (2006). The analytical solution near the source for Case 2 at 20 years is in Figure 6-3, and shows that the tracer stays much closer to the source with retardation in the model. Figure 6-4 shows the analytical solution for Case 3 after 10 years and is identical to Figure 3-27 in Batu (2006).

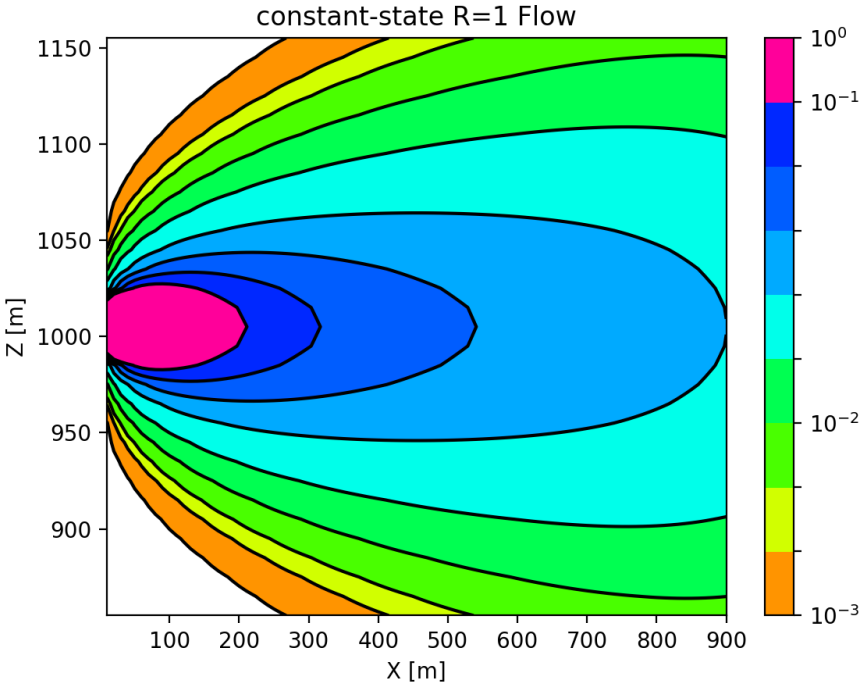

Figure 6-2. **Tracer distribution [kg/m^3] near the source for 2-D analytical benchmark problem with no retardation and constant-rate source after 20 years.**

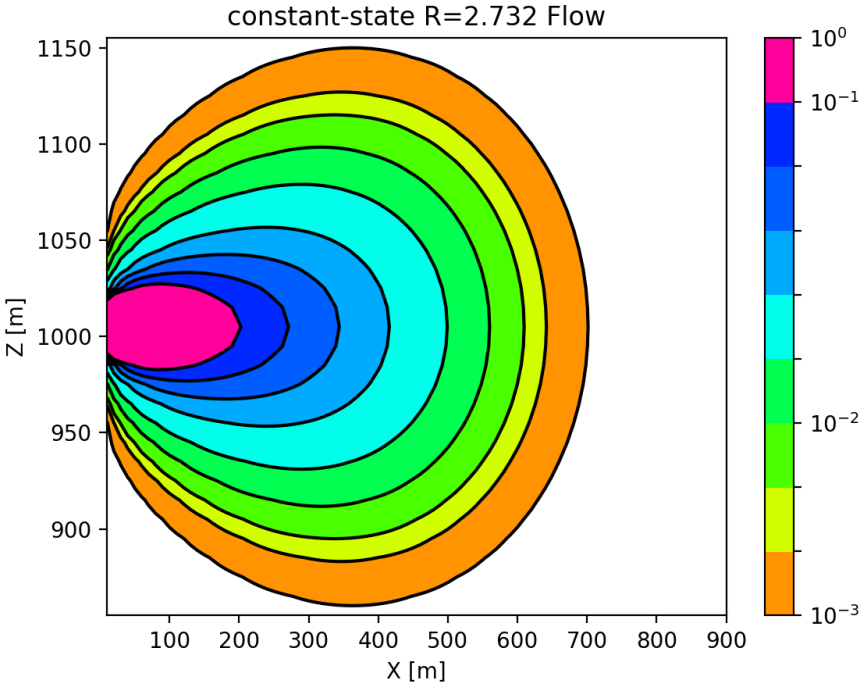

Figure 6-3. **Tracer distribution [kg/m^3] near the source for 2-D analytical benchmark problem with retardation factor R_d = 2.732 m^3/kg, representative of Cs(I) retardation and no decay in the tracer source after 20 years.**

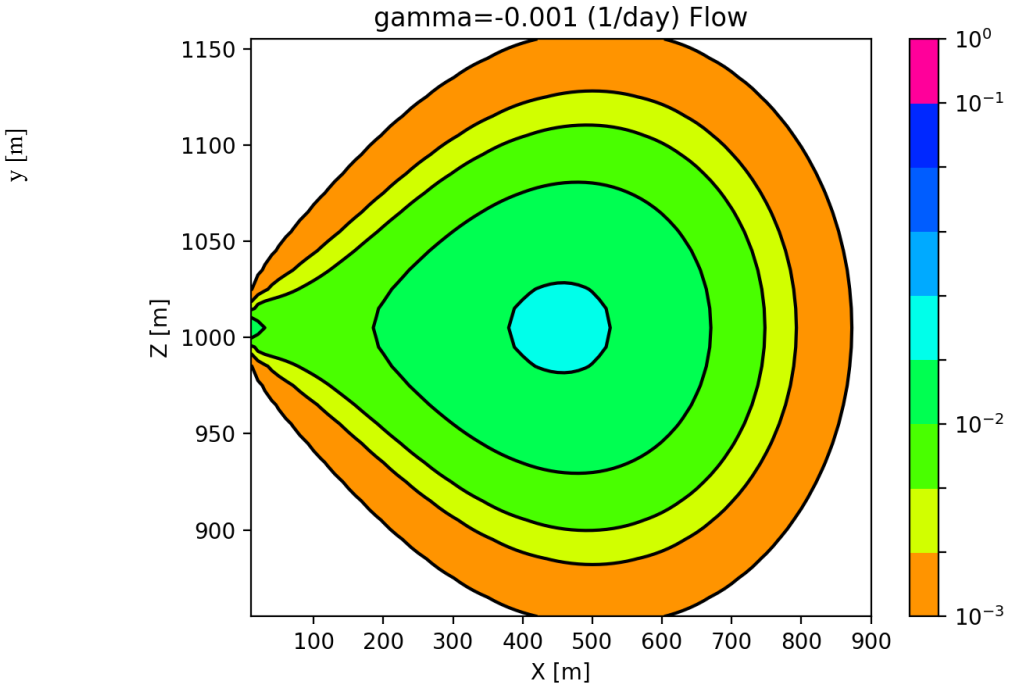

Figure 6-4. Tracer distribution [kg/m^3] near the source for 2-D analytical benchmark problem without retardation and with time-dependent tracer source γ = -0.001 (1/day) after 10 years.

6.2.2.3 Comparison quantities

In order to allow teams to choose different resolutions for their simulations, comparison of simulated solutions with the analytical model will be done at snapshots in time and discrete points in the domain. The proposed comparison quantities are:

Cross sections at 5 years and 10 years:

- X parallel section at the mid-point of the source in the Z-direction (Z=1005 m)
- X parallel section at Z=1055 m
- Z parallel sections at X=100, 200 and 500 m.

Analytical cross sections for each of the three benchmark cases are shown in Figure 6-5 to Figure 6-7.

Profiles at discrete points as a function of time from 0 to 20 years at the intersection of the cross sections:

- (X,Z) = (100,1005)
- (X,Z) = (200,1005)
- (X,Z) = (100,1055)
- (X,Z) = (200,1055)

Profiles in time for each of the three benchmark cases are shown in Figure 6-8 to Figure 6-10.

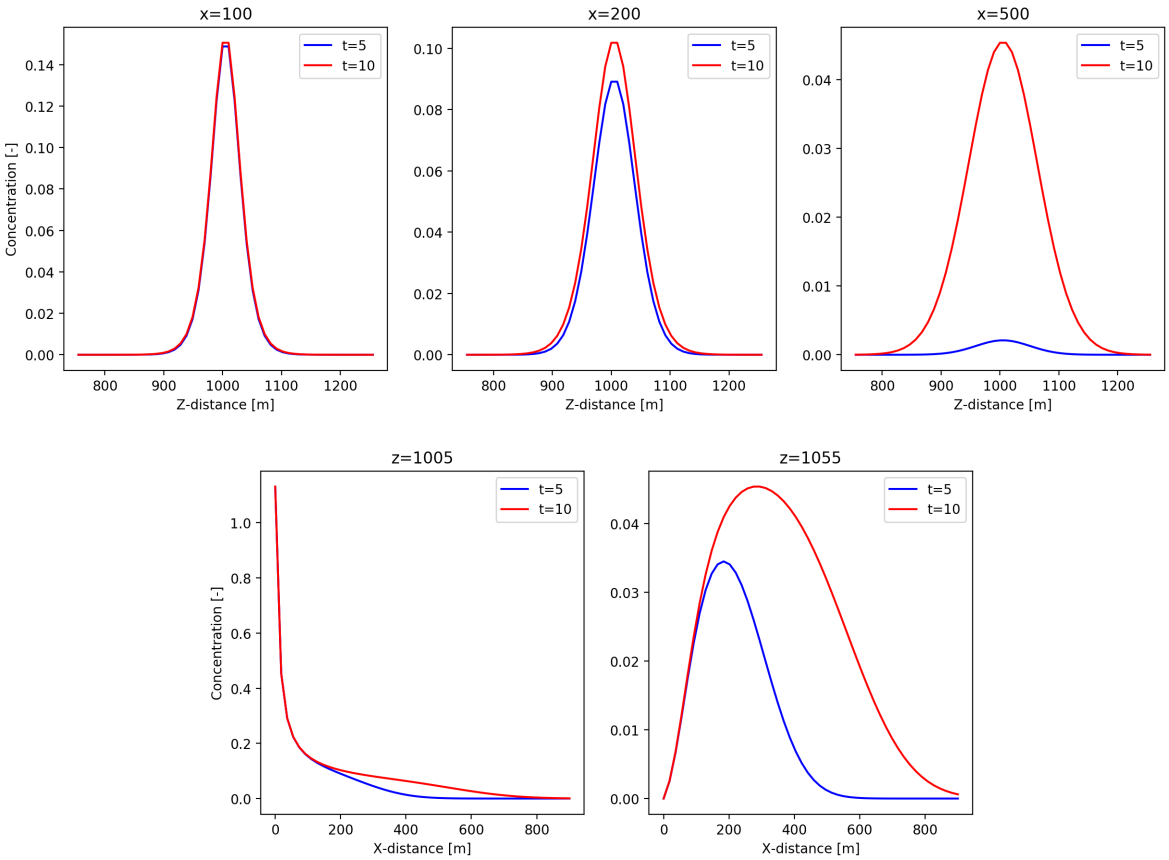

Figure 6-5. **Analytical cross-sections for benchmark model with R=1 and a constant tracer source at time t=5 years (blue) and t=10 years (red). Top row: Concentration as a function of the z-coordinate on the line x = 100 m (left), x= 200 m (middle), x = 500 m (right). Bottom row: Concentration as a function of the z-coordinate on the line z = 1005 m (left), z = 1055 m (right).**

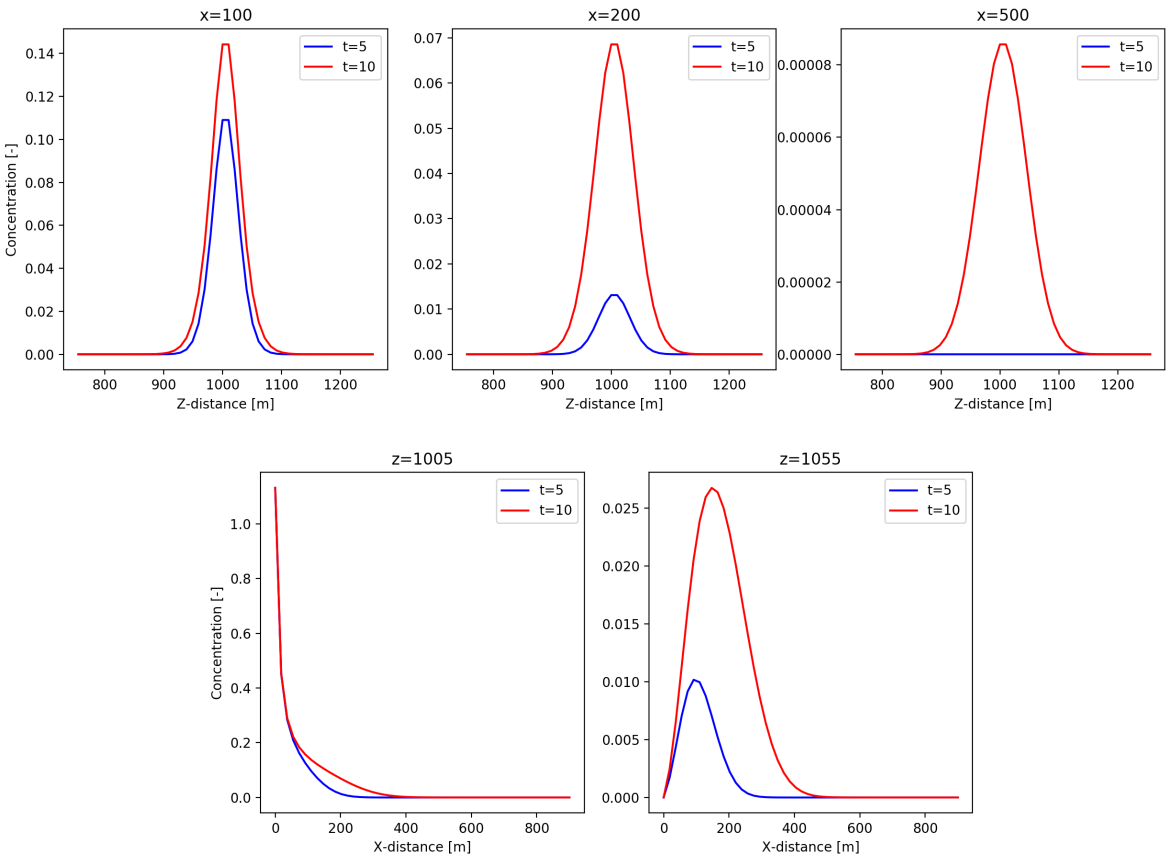

Figure 6-6. **Analytical cross-sections for benchmark model with R = 2.732 and a constant tracer source at time t=5 years (blue) and t=10 years (red). Top row: Concentration as a function of the z-coordinate on the line x = 100 m (left), x= 200 m (middle), x = 500 m (right). Bottom row: Concentration as a function of the z-coordinate on the line z = 1005 m (left), z = 1055 m (right).**

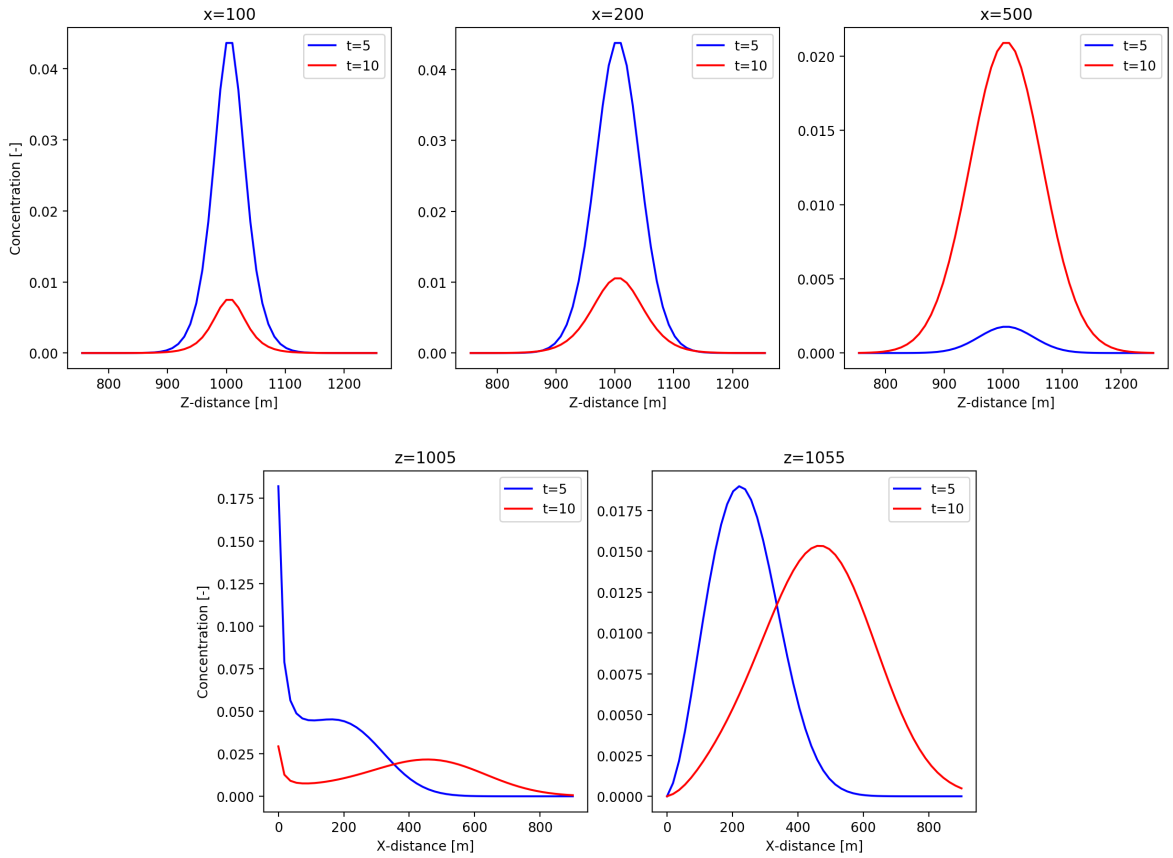

Figure 6-7. **Analytical cross-sections for analytical model with R = 1 and decaying tracer source with rate γ = -0.001 (1/yr) at time t=5 years (blue) and t=10 years (red). Top row: Concentration as a function of the z-coordinate on the line x = 100 m (left), x= 200 m (middle), x = 500 m (right). Bottom row: Concentration as a function of the z-coordinate on the line z = 1005 m (left), z = 1055 m (right).**

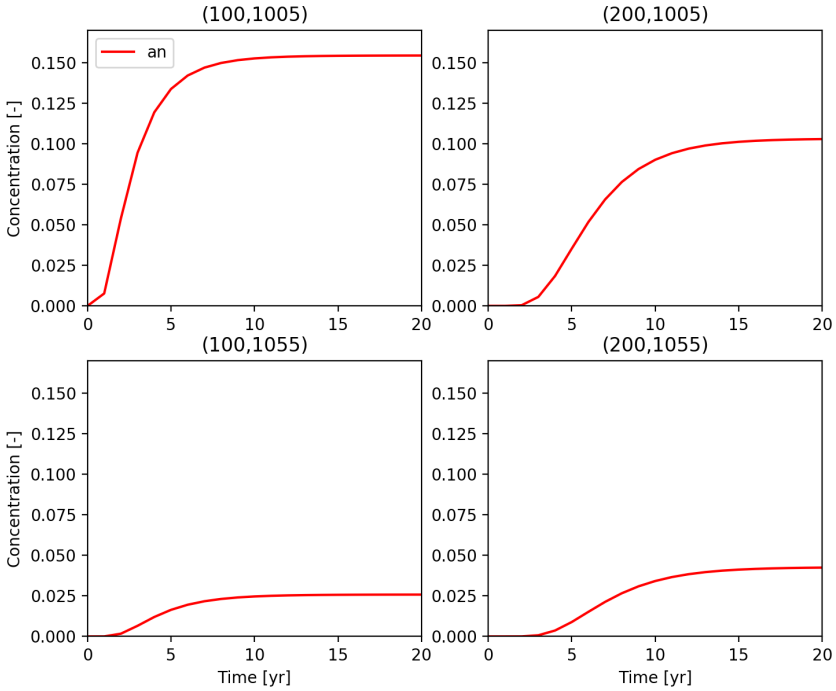

Figure 6-8. Analytical profile for benchmark model with R=1 and a constant tracer source as a function of time at four points in the domain. Top left: (100,1005) m. Top right: (200,1005) m. Bottom left: (100,1055) m. Bottom right: (200,1055) m.

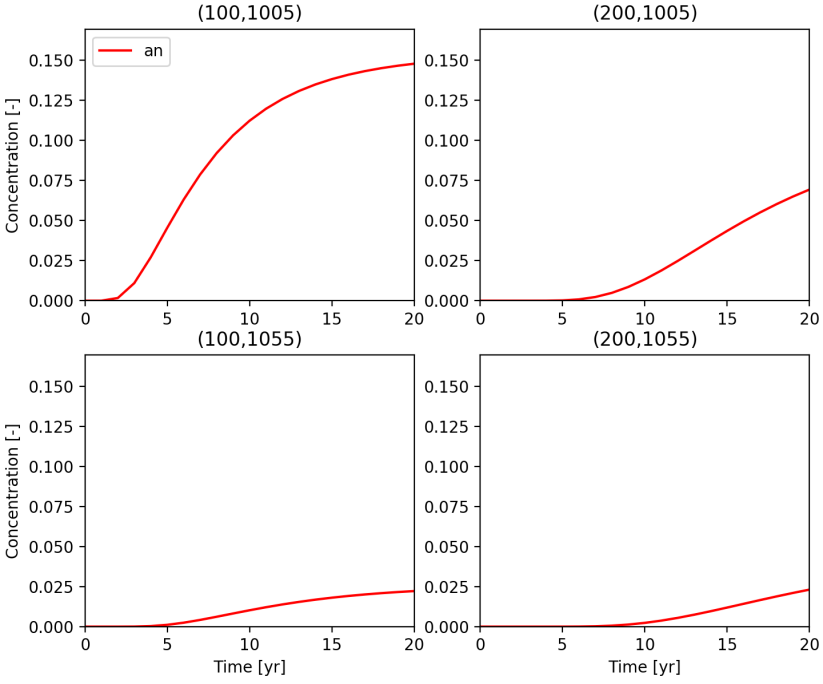

Figure 6-9. Analytical profile for benchmark model with R=2.732 and a constant tracer source as a function of time at four points in the domain. Top left: (100,1005) m. Top right: (200,1005) m. Bottom left: (100,1055) m. Bottom right: (200,1055) m.

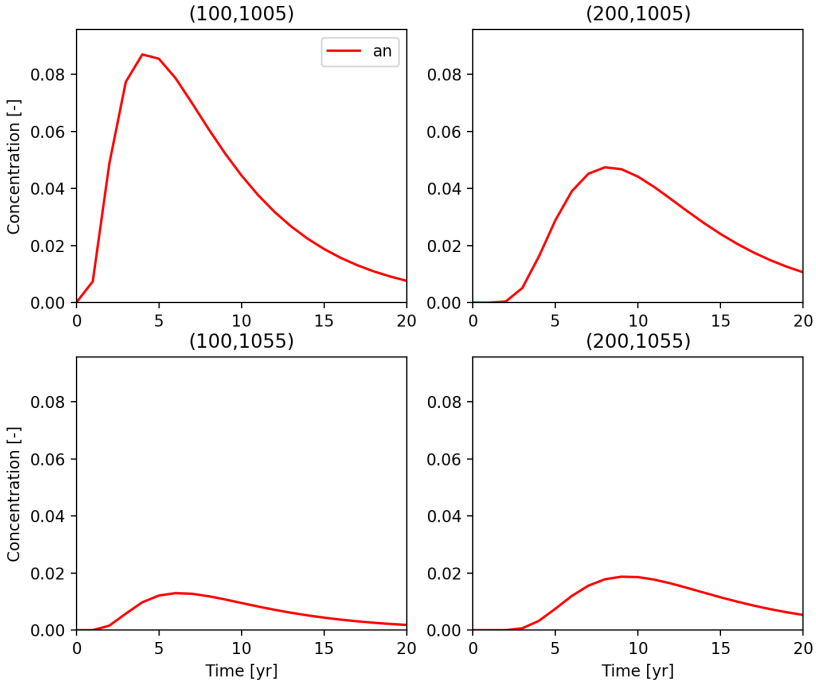

Figure 6-10. Analytical profile for model with R=1 and source decay rate γ=-0.001 (1/yr) as a function of time at four points in the domain. Top left: (100,1005) m. Top right: (200,1005) m. Bottom left: (100,1055) m. Bottom right: (200,1055) m.

This page is intentionally left blank.

7. APPENDIX - CRUSHED SALT COMPACTION

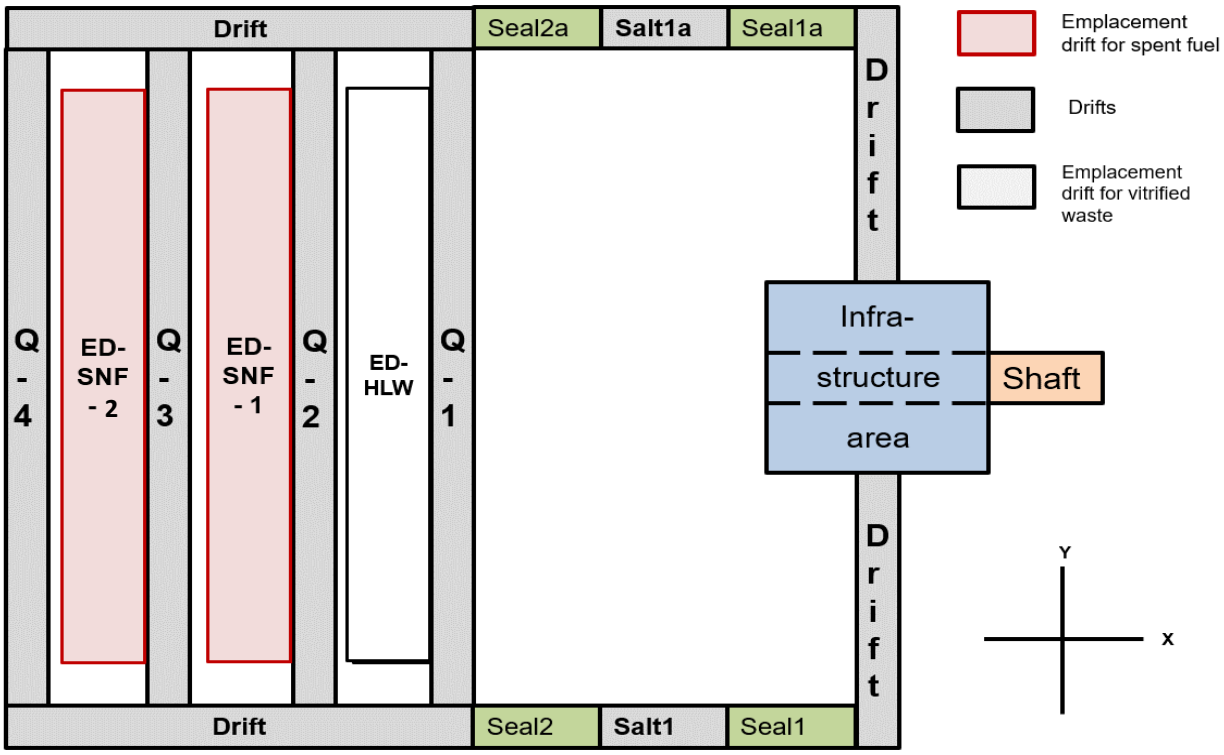

Figure 7-1. Legend showing repository areas for salt consolidation rate and porosity as a function of time in Table 7-1 to Table 7-3.

Table 7-1. Crushed salt reconsolidation rate and porosity as a function of time for high level waste (ED-HLW), spent nuclear fuel drifts region one (ED-SNF-1), and spent nuclear fuel drifts region one (ED-SNF-2). Repository regions are shown in Figure 7-1.

Time [y]	K(t) (ED-HLW) [1/y]	Φ (ED-HLW) [-]	K(t) (ED-SNF-1) [1/y]	Φ (ED-SNF-1) [-]	K(t) (ED-SNF-2) [1/y]	Φ (ED-SNF-2) [-]
1.00E-03	9.86E-02	1.40E-01	9.86E-02	9.99E-02	9.86E-02	9.99E-02
1.02E-02	9.78E-02	1.39E-01	9.72E-02	9.91E-02	9.72E-02	9.91E-02
2.02E-02	9.69E-02	1.38E-01	9.57E-02	9.82E-02	9.57E-02	9.82E-02
2.94E-02	9.60E-02	1.38E-01	9.43E-02	9.74E-02	9.43E-02	9.74E-02
4.00E-02	9.51E-02	1.37E-01	9.29E-02	9.66E-02	9.29E-02	9.66E-02
5.10E-02	9.41E-02	1.36E-01	9.13E-02	9.56E-02	9.13E-02	9.56E-02
6.14E-02	9.32E-02	1.35E-01	9.00E-02	9.48E-02	9.00E-02	9.48E-02
7.29E-02	9.22E-02	1.34E-01	8.83E-02	9.39E-02	8.83E-02	9.39E-02
8.37E-02	9.13E-02	1.33E-01	8.70E-02	9.30E-02	8.70E-02	9.30E-02
9.45E-02	9.04E-02	1.32E-01	8.56E-02	9.22E-02	8.56E-02	9.22E-02
1.00E-01	8.94E-02	1.32E-01	8.42E-02	9.17E-02	8.42E-02	9.17E-02
1.50E-01	8.58E-02	1.28E-01	7.89E-02	8.80E-02	7.89E-02	8.80E-02
1.94E-01	8.25E-02	1.25E-01	7.42E-02	8.50E-02	7.42E-02	8.50E-02
2.52E-01	7.78E-02	1.21E-01	6.80E-02	8.12E-02	6.80E-02	8.12E-02

2.98E-01	7.39E-02	1.18E-01	6.30E-02	7.85E-02	6.30E-02	7.85E-02
3.51E-01	7.01E-02	1.14E-01	5.84E-02	7.55E-02	5.84E-02	7.55E-02
4.02E-01	6.69E-02	1.11E-01	5.45E-02	7.28E-02	5.45E-02	7.28E-02
4.95E-01	6.19E-02	1.06E-01	4.89E-02	6.84E-02	4.89E-02	6.84E-02
6.01E-01	5.68E-02	1.00E-01	4.36E-02	6.39E-02	4.36E-02	6.39E-02
6.50E-01	5.39E-02	9.79E-02	4.06E-02	6.20E-02	4.06E-02	6.20E-02
6.99E-01	5.09E-02	9.56E-02	3.76E-02	6.02E-02	3.76E-02	6.02E-02
7.94E-01	4.74E-02	9.14E-02	3.43E-02	5.70E-02	3.43E-02	5.70E-02
9.17E-01	4.32E-02	8.64E-02	3.05E-02	5.33E-02	3.05E-02	5.33E-02
1.01E+00	3.93E-02	8.30E-02	2.71E-02	5.09E-02	2.71E-02	5.09E-02
1.22E+00	3.37E-02	7.60E-02	2.25E-02	4.59E-02	2.25E-02	4.59E-02
1.42E+00	2.86E-02	7.02E-02	1.85E-02	4.20E-02	1.85E-02	4.20E-02
1.61E+00	2.53E-02	6.56E-02	1.60E-02	3.90E-02	1.60E-02	3.90E-02
1.79E+00	2.26E-02	6.14E-02	1.42E-02	3.63E-02	1.42E-02	3.63E-02
2.00E+00	1.92E-02	5.75E-02	1.18E-02	3.38E-02	1.18E-02	3.38E-02
2.52E+00	1.43E-02	4.93E-02	8.55E-03	2.87E-02	8.55E-03	2.87E-02
3.03E+00	1.10E-02	4.33E-02	6.46E-03	2.51E-02	6.46E-03	2.51E-02
3.47E+00	9.17E-03	3.90E-02	5.37E-03	2.25E-02	5.37E-03	2.25E-02
4.07E+00	6.90E-03	3.44E-02	9.78E-04	2.13E-02	9.78E-04	2.13E-02
4.47E+00	5.95E-03	3.20E-02	9.21E-04	2.09E-02	9.21E-04	2.09E-02
5.01E+00	2.59E-03	3.02E-02	8.51E-04	2.04E-02	8.51E-04	2.04E-02
6.03E+00	2.02E-03	2.79E-02	7.42E-04	1.96E-02	7.42E-04	1.96E-02
7.08E+00	1.61E-03	2.60E-02	6.52E-04	1.89E-02	6.52E-04	1.89E-02
8.13E+00	1.33E-03	2.46E-02	5.79E-04	1.83E-02	5.79E-04	1.83E-02
9.12E+00	1.13E-03	2.34E-02	5.22E-04	1.77E-02	5.22E-04	1.77E-02
1.00E+01	9.87E-04	2.25E-02	4.79E-04	1.73E-02	4.79E-04	1.73E-02
1.51E+01	1.65E-04	2.04E-02	1.18E-04	1.56E-02	3.14E-04	1.54E-02
2.00E+01	1.16E-04	1.99E-02	6.06E-05	1.53E-02	7.94E-05	1.48E-02
3.02E+01	9.18E-05	1.88E-02	3.75E-05	1.48E-02	2.18E-05	1.43E-02
3.98E+01	8.71E-05	1.80E-02	3.59E-05	1.44E-02	2.12E-05	1.40E-02
6.03E+01	1.35E-06	1.74E-02	1.43E-06	1.42E-02	1.28E-06	1.39E-02
7.94E+01	1.17E-06	1.73E-02	1.25E-06	1.41E-02	1.13E-06	1.39E-02
1.00E+02	1.01E-06	1.73E-02	1.10E-06	1.41E-02	9.99E-07	1.38E-02
2.00E+02	5.83E-07	1.72E-02	6.52E-07	1.40E-02	6.04E-07	1.38E-02
3.02E+02	3.82E-07	1.72E-02	4.35E-07	1.40E-02	4.07E-07	1.37E-02
3.98E+02	2.78E-07	1.72E-02	3.20E-07	1.39E-02	3.01E-07	1.37E-02
5.01E+02	2.10E-07	1.71E-02	2.43E-07	1.39E-02	2.30E-07	1.37E-02
1.00E+03	8.22E-08	1.71E-02	9.66E-08	1.38E-02	9.23E-08	1.36E-02
2.51E+03	2.05E-08	1.70E-02	2.42E-08	1.38E-02	2.33E-08	1.35E-02
5.01E+03	6.79E-09	1.70E-02	8.05E-09	1.37E-02	7.76E-09	1.35E-02
7.25E+03	3.73E-09	1.70E-02	4.43E-09	1.37E-02	4.27E-09	1.35E-02
1.00E+04	2.20E-09	1.70E-02	2.61E-09	1.37E-02	2.52E-09	1.35E-02
2.51E+04	4.92E-10	1.70E-02	5.83E-10	1.37E-02	5.63E-10	1.34E-02
5.01E+04	1.63E-10	1.70E-02	1.93E-10	1.37E-02	1.86E-10	1.34E-02

7.25E+04	9.15E-11	1.70E-02	1.09E-10	1.37E-02	1.05E-10	1.34E-02
1.00E+05	5.59E-11	1.70E-02	6.63E-11	1.37E-02	6.40E-11	1.34E-02

Table 7-2. Crushed salt reconsolidation rate and porosity as a function of time for drift seal salt (Salt-1), drift seal salt (Salt-1a), drift connecting HLW (Q1) and drift connecting SNF-1 (Q2). Repository regions are shown in Figure 7-1.

Time [y]	K(t) (Salt) [1/y]	Φ (Salt) [-]	K(t) (Q1) [1/y]	Φ (Q1) [-]	K(t) (Q2) [1/y]	Φ (Q2) [-]
1.00E-03	2.00E-02	1.00E-01	6.14E-02	9.99E-02	6.15E-02	9.99E-02
1.02E-02	2.00E-02	9.98E-02	5.75E-02	9.94E-02	5.75E-02	9.94E-02
2.02E-02	1.99E-02	9.96E-02	5.35E-02	9.89E-02	5.35E-02	9.89E-02
2.94E-02	1.98E-02	9.95E-02	5.06E-02	9.85E-02	5.06E-02	9.85E-02
4.00E-02	1.98E-02	9.93E-02	4.79E-02	9.81E-02	4.79E-02	9.81E-02
5.10E-02	1.97E-02	9.91E-02	4.52E-02	9.76E-02	4.52E-02	9.76E-02
6.14E-02	1.96E-02	9.89E-02	4.32E-02	9.72E-02	4.32E-02	9.72E-02
7.29E-02	1.95E-02	9.87E-02	4.11E-02	9.67E-02	4.11E-02	9.67E-02
8.37E-02	1.94E-02	9.85E-02	3.95E-02	9.64E-02	3.95E-02	9.64E-02
9.45E-02	1.93E-02	9.83E-02	3.79E-02	9.60E-02	3.79E-02	9.60E-02
1.00E-01	1.92E-02	9.82E-02	3.65E-02	9.58E-02	3.65E-02	9.58E-02
1.50E-01	1.89E-02	9.74E-02	3.20E-02	9.43E-02	3.20E-02	9.43E-02
1.94E-01	1.86E-02	9.66E-02	2.88E-02	9.31E-02	2.88E-02	9.31E-02
2.52E-01	1.82E-02	9.57E-02	2.54E-02	9.17E-02	2.54E-02	9.17E-02
2.98E-01	1.79E-02	9.49E-02	2.31E-02	9.07E-02	2.31E-02	9.07E-02
3.51E-01	1.75E-02	9.41E-02	2.12E-02	8.96E-02	2.12E-02	8.96E-02
4.02E-01	1.72E-02	9.33E-02	1.98E-02	8.87E-02	1.98E-02	8.87E-02
4.95E-01	1.66E-02	9.18E-02	1.79E-02	8.71E-02	1.79E-02	8.71E-02
6.01E-01	1.61E-02	9.03E-02	1.62E-02	8.54E-02	1.62E-02	8.54E-02
6.50E-01	1.58E-02	8.96E-02	1.53E-02	8.47E-02	1.53E-02	8.47E-02
6.99E-01	1.54E-02	8.89E-02	1.45E-02	8.41E-02	1.45E-02	8.41E-02
7.94E-01	1.50E-02	8.75E-02	1.36E-02	8.29E-02	1.36E-02	8.29E-02
9.17E-01	1.44E-02	8.59E-02	1.25E-02	8.14E-02	1.25E-02	8.14E-02
1.01E+00	1.39E-02	8.47E-02	1.16E-02	8.04E-02	1.16E-02	8.04E-02
1.22E+00	1.31E-02	8.21E-02	1.04E-02	7.83E-02	1.04E-02	7.83E-02
1.42E+00	1.22E-02	7.98E-02	9.29E-03	7.64E-02	9.28E-03	7.65E-02
1.61E+00	1.16E-02	7.78E-02	8.59E-03	7.50E-02	8.59E-03	7.50E-02
1.79E+00	1.10E-02	7.58E-02	8.03E-03	7.35E-02	8.02E-03	7.35E-02
2.00E+00	1.03E-02	7.38E-02	7.30E-03	7.21E-02	7.29E-03	7.21E-02
2.52E+00	8.94E-03	6.92E-02	6.18E-03	6.88E-02	6.18E-03	6.88E-02
3.03E+00	7.85E-03	6.52E-02	5.36E-03	6.61E-02	5.36E-03	6.61E-02
3.47E+00	7.17E-03	6.21E-02	4.88E-03	6.40E-02	4.88E-03	6.40E-02
4.07E+00	6.16E-03	5.84E-02	4.21E-03	6.14E-02	4.22E-03	6.15E-02
4.47E+00	5.68E-03	5.62E-02	3.90E-03	5.99E-02	3.93E-03	6.00E-02
5.01E+00	5.10E-03	5.34E-02	3.58E-03	5.80E-02	3.58E-03	5.80E-02
6.03E+00	4.23E-03	4.90E-02	3.11E-03	5.48E-02	3.07E-03	5.49E-02

7.08E+00	3.55E-03	4.51E-02	2.74E-03	5.19E-02	2.67E-03	5.20E-02
8.13E+00	3.03E-03	4.18E-02	2.43E-03	4.94E-02	2.35E-03	4.95E-02
9.12E+00	2.63E-03	3.91E-02	2.19E-03	4.72E-02	2.12E-03	4.74E-02
1.00E+01	2.34E-03	3.70E-02	2.02E-03	4.54E-02	1.94E-03	4.57E-02
1.51E+01	1.34E-03	2.82E-02	3.76E-04	3.93E-02	4.82E-04	3.86E-02
2.00E+01	8.90E-04	2.31E-02	2.36E-04	3.81E-02	1.56E-04	3.76E-02
3.02E+01	1.64E-04	2.02E-02	1.81E-04	3.60E-02	7.88E-05	3.64E-02
3.98E+01	1.29E-04	1.88E-02	1.78E-04	3.44E-02	7.75E-05	3.57E-02
6.03E+01	3.71E-05	1.75E-02	1.52E-06	3.32E-02	1.60E-06	3.51E-02
7.94E+01	3.24E-05	1.68E-02	1.32E-06	3.31E-02	1.40E-06	3.51E-02
1.00E+02	2.83E-05	1.62E-02	1.14E-06	3.31E-02	1.22E-06	3.51E-02
2.00E+02	1.71E-05	1.41E-02	6.54E-07	3.30E-02	7.17E-07	3.50E-02
3.02E+02	1.16E-05	1.26E-02	4.27E-07	3.30E-02	4.75E-07	3.49E-02
3.98E+02	8.79E-06	1.17E-02	3.11E-07	3.29E-02	3.49E-07	3.49E-02
5.01E+02	6.84E-06	1.09E-02	2.34E-07	3.29E-02	2.64E-07	3.49E-02
1.00E+03	3.03E-06	8.67E-03	9.19E-08	3.29E-02	1.05E-07	3.48E-02
2.51E+03	9.25E-07	6.22E-03	2.29E-08	3.28E-02	2.62E-08	3.47E-02
5.01E+03	3.64E-07	4.79E-03	7.59E-09	3.28E-02	8.72E-09	3.47E-02
7.25E+03	2.19E-07	4.17E-03	4.17E-09	3.27E-02	4.80E-09	3.47E-02
1.00E+04	1.40E-07	3.69E-03	2.46E-09	3.27E-02	2.83E-09	3.47E-02
2.51E+04	3.90E-08	2.61E-03	5.50E-10	3.27E-02	6.32E-10	3.46E-02
5.01E+04	1.49E-08	2.02E-03	1.82E-10	3.27E-02	2.10E-10	3.46E-02
7.25E+04	8.90E-09	1.76E-03	1.02E-10	3.27E-02	1.18E-10	3.46E-02
1.00E+05	5.68E-09	1.57E-03	6.25E-11	3.27E-02	7.20E-11	3.46E-02

Table 7-3. Crushed salt reconsolidation rate and porosity as a function of time for drift connecting SNF-1 (Q3), drift along the left of the repository (Q4), and drift connecting SNF and HLW to the seals (DRIFTS). Repository regions are shown in Figure 7-1.

Time [y]	K(t) (Q3) [1/y]	Φ (Q3) [-]	K(t) (Q4) [1/y]	Φ (Q4) [-]	K(t) (Drifts) [1/y]	Φ (Drifts) [-]
1.00E-03	6.15E-02	9.99E-02	6.15E-02	9.99E-02	6.15E-02	9.99E-02
1.02E-02	5.75E-02	9.94E-02	5.75E-02	9.94E-02	5.75E-02	9.94E-02
2.02E-02	5.35E-02	9.89E-02	5.35E-02	9.89E-02	5.35E-02	9.89E-02
2.94E-02	5.06E-02	9.85E-02	5.06E-02	9.85E-02	5.06E-02	9.85E-02
4.00E-02	4.79E-02	9.81E-02	4.79E-02	9.81E-02	4.79E-02	9.81E-02
5.10E-02	4.52E-02	9.76E-02	4.52E-02	9.76E-02	4.52E-02	9.76E-02
6.14E-02	4.32E-02	9.72E-02	4.32E-02	9.72E-02	4.32E-02	9.72E-02
7.29E-02	4.11E-02	9.67E-02	4.11E-02	9.67E-02	4.11E-02	9.67E-02
8.37E-02	3.95E-02	9.64E-02	3.95E-02	9.64E-02	3.95E-02	9.64E-02
9.45E-02	3.79E-02	9.60E-02	3.79E-02	9.60E-02	3.79E-02	9.60E-02
1.00E-01	3.65E-02	9.58E-02	3.65E-02	9.58E-02	3.65E-02	9.58E-02
1.50E-01	3.20E-02	9.43E-02	3.20E-02	9.43E-02	3.20E-02	9.43E-02
1.94E-01	2.88E-02	9.31E-02	2.88E-02	9.31E-02	2.88E-02	9.31E-02
2.52E-01	2.54E-02	9.17E-02	2.54E-02	9.17E-02	2.54E-02	9.17E-02

2.98E-01	2.31E-02	9.07E-02	2.31E-02	9.07E-02	2.31E-02	9.07E-02
3.51E-01	2.12E-02	8.96E-02	2.12E-02	8.96E-02	2.12E-02	8.96E-02
4.02E-01	1.98E-02	8.87E-02	1.98E-02	8.87E-02	1.98E-02	8.87E-02
4.95E-01	1.79E-02	8.71E-02	1.79E-02	8.71E-02	1.79E-02	8.71E-02
6.01E-01	1.62E-02	8.54E-02	1.62E-02	8.54E-02	1.62E-02	8.54E-02
6.50E-01	1.53E-02	8.47E-02	1.53E-02	8.47E-02	1.53E-02	8.47E-02
6.99E-01	1.45E-02	8.41E-02	1.45E-02	8.41E-02	1.45E-02	8.41E-02
7.94E-01	1.36E-02	8.29E-02	1.36E-02	8.29E-02	1.36E-02	8.29E-02
9.17E-01	1.25E-02	8.14E-02	1.25E-02	8.14E-02	1.25E-02	8.14E-02
1.01E+00	1.16E-02	8.04E-02	1.16E-02	8.04E-02	1.16E-02	8.04E-02
1.22E+00	1.04E-02	7.83E-02	1.04E-02	7.83E-02	1.04E-02	7.83E-02
1.42E+00	9.28E-03	7.65E-02	9.28E-03	7.65E-02	9.28E-03	7.65E-02
1.61E+00	8.59E-03	7.50E-02	8.58E-03	7.50E-02	8.59E-03	7.50E-02
1.79E+00	8.02E-03	7.35E-02	8.02E-03	7.35E-02	8.02E-03	7.35E-02
2.00E+00	7.29E-03	7.21E-02	7.29E-03	7.21E-02	7.29E-03	7.21E-02
2.52E+00	6.18E-03	6.88E-02	6.18E-03	6.88E-02	6.18E-03	6.88E-02
3.03E+00	5.36E-03	6.61E-02	5.36E-03	6.61E-02	5.36E-03	6.61E-02
3.47E+00	4.88E-03	6.40E-02	4.88E-03	6.40E-02	4.88E-03	6.40E-02
4.07E+00	4.22E-03	6.15E-02	4.20E-03	6.15E-02	4.22E-03	6.15E-02
4.47E+00	3.93E-03	6.00E-02	3.90E-03	6.00E-02	3.93E-03	6.00E-02
5.01E+00	3.58E-03	5.80E-02	3.53E-03	5.81E-02	3.58E-03	5.80E-02
6.03E+00	3.07E-03	5.49E-02	3.01E-03	5.50E-02	3.07E-03	5.49E-02
7.08E+00	2.67E-03	5.20E-02	2.59E-03	5.22E-02	2.67E-03	5.20E-02
8.13E+00	2.35E-03	4.95E-02	2.28E-03	4.98E-02	2.35E-03	4.95E-02
9.12E+00	2.12E-03	4.74E-02	2.04E-03	4.77E-02	2.11E-03	4.74E-02
1.00E+01	1.94E-03	4.57E-02	1.86E-03	4.61E-02	1.94E-03	4.57E-02
1.51E+01	1.27E-03	3.80E-02	1.20E-03	3.88E-02	4.80E-04	3.85E-02
2.00E+01	2.58E-04	3.56E-02	8.98E-04	3.40E-02	1.56E-04	3.75E-02
3.02E+01	3.52E-05	3.41E-02	1.75E-05	2.86E-02	7.84E-05	3.63E-02
3.98E+01	3.49E-05	3.38E-02	1.74E-05	2.85E-02	7.71E-05	3.56E-02
6.03E+01	1.33E-06	3.36E-02	8.62E-07	2.83E-02	1.60E-06	3.51E-02
7.94E+01	1.17E-06	3.35E-02	7.59E-07	2.83E-02	1.39E-06	3.50E-02
1.00E+02	1.03E-06	3.35E-02	6.68E-07	2.83E-02	1.22E-06	3.50E-02
2.00E+02	6.16E-07	3.34E-02	4.04E-07	2.83E-02	7.14E-07	3.49E-02
3.02E+02	4.12E-07	3.34E-02	2.71E-07	2.82E-02	4.73E-07	3.49E-02
3.98E+02	3.04E-07	3.33E-02	2.01E-07	2.82E-02	3.47E-07	3.48E-02
5.01E+02	2.31E-07	3.33E-02	1.53E-07	2.82E-02	2.63E-07	3.48E-02
1.00E+03	9.27E-08	3.33E-02	6.16E-08	2.81E-02	1.04E-07	3.47E-02
2.51E+03	2.34E-08	3.32E-02	1.56E-08	2.81E-02	2.61E-08	3.46E-02
5.01E+03	7.79E-09	3.31E-02	5.20E-09	2.81E-02	8.68E-09	3.46E-02
7.25E+03	4.29E-09	3.31E-02	2.86E-09	2.81E-02	4.77E-09	3.46E-02
1.00E+04	2.53E-09	3.31E-02	1.69E-09	2.81E-02	2.82E-09	3.46E-02
2.51E+04	5.66E-10	3.31E-02	3.78E-10	2.80E-02	6.29E-10	3.46E-02
5.01E+04	1.88E-10	3.31E-02	1.25E-10	2.80E-02	2.08E-10	3.46E-02

7.25E+04	1.05E-10	3.31E-02	7.04E-11	2.80E-02	1.17E-10	3.45E-02
1.00E+05	6.44E-11	3.31E-02	4.31E-11	2.80E-02	7.16E-11	3.45E-02

This page is intentionally left blank.

8. REFERENCES

Anttila, M. (2005). *Radioactive Characteristics of the Spent Fuel of the Finnish Nuclear Power Plants*. Working Report 2005-71. Posiva Oy, Olkiluoto, Finland.

Baeyens, B., Thoenen, T., Bradbury M. H., and Fernandes, M. Marques. (2014). *Sorption Data Bases for Argillaceous Rocks and Bentonite for the Provisional Safety Analyses for SGT-E2*. NAGRA Technical Report. National Cooperative for the Disposal of Radioactive Waste (NAGRA), Wettingen, Switzerland.

Batu, V. (2006). *Applied Flow and Solute Transport Modelling in Aquifers*. CRC Taylor and Francis.

Bear, J. (1972). *Dynamics of Fluids in Porous Media*, American Elsevier Publishing, Inc., New York, NY.

Bear J. (1993). *Flow and Contaminent Transport in Fractured Rocks,* Academic Press: 1-37.

Bertrams, N., Bollingerfehr, W., Eickemeier, R., Fahland, S. Flügge, J., Frenzel, B., Hammer, J., Kindlein, J. Liu, W., Maßmann, J., Mayer, K.-M., Mönig, J., Mrugalla, S., Müller-Hoeppe, N., Reinhold, K., Rübel, A., Schubarth-Engel- schall, N., Simo, E., Thiedau, J., Thiemeyer, T., Weber, J.R., Wolf, J. (2020a). *Grundlagen zur Bewertung eines Endlagersystems in flach lagernden Salzformationen (S1) - Ergebnisse aus dem Vorhaben RESUS*. BGE TEC 2020.

Bertrams, N., Bollingerfehr, W., Eickemeier, R., Fahland, S. Flügge, J., Frenzel, B., Hammer, J., Kindlein, J. Liu, W., Maßmann, J., Mayer, K.-M., Mönig, J., Mrugalla, S., Müller-Hoeppe, N., Reinhold, K., Rübel, A., Schubarth-Engel- schall, N., Simo, E., Thiedau, J., Thiemeyer, T., Weber, J.R., Wolf, J. (2020b). *Grundlagen zur Bewertung eines Endlagersystems in steil lagernden Salzformationen (S2) - Ergebnisse aus dem Vorhaben RESUS*. BGE TEC 2020.

Beuth, T., Bracke, G., Buhmann, D., Dresbach, C., Keller, S., Krone, J., Lommerzheim, A., Mönig, A., Mrugalla, S., Rübel, A., and Wolf, J. (2012). *Szenarienentwicklunng: Methodic und Anwendung. Bericht zum Arbeitspaket 8. Vorläufige Sicherheitsanalyse für den Standort Gorleben*, Gesellschaft für Anlagen und Reaktorsicherheit (GRS) mbH, GRS-284, Köln, ISBN 978-3-939355-60-1.

Blanco-Martin, L., Rutqvist, J., Battistelli, A., and Birkholzer, J.T. (2018). Coupled processes modeling in rock salt and crushed salt including halite solubility constraints: Application to disposal of heat-generating nuclear waste. Transport in Porous Media 124: 159-182.

Bollingerfehr, W., Filbert, W., Pöhler, M., Tholen, M., and Wehrmann, J. (2008). *Konzeptionelle Endlagerplanung und Zusammen- stellung des endzulagernden Inventars (Design planning of a final repository and summary of the inventory to be stored) – Project ISIBEL*, Peine, April 2008.

Bollingerfehr, W., Bertrams, N., Buhmann, D., Eickemeier, R., Fahland, S., Filbert, W., Hammer, J., Kindlein, J., Knauth, M., and Wenting, L. (2018). *Concept developments for a generic repository for heat-generating waste in bedded salt formations in Germany*. Synthesis Report (No. BGE TEC 2018-13). BGE TECHNOLOGY GmbH.

Bollingerfehr, W., Buhmann, D. and Doerr, S. (2017). *Evaluation of methods and tools to develop safety concepts and to demonstrate safety for an HLW repository in salt*. Final Report (No. TEC-03-2017-AB). DBE Technology GmbH.

Carter, J., Luptak, A. J., Gastelum, J., Stockman, C. T., and Miller, A. (2013). *Fuel Cycle Potential Waste Inventory for Disposition*. FCR&D-USED-2010-000031 Rev 6. Savannah River National Laboratory, Aiken, SC.

Chang, C.-C., Chang H.-T., and Yu-Hsiang, S. (2021). *Specifications of the draft Taiwan's repository facility*. Presented to the Task F crystalline group, August 24, 2021.

Choi, H. J., Lee, J. Y., and Choi, J. (2013). "Development of Geological Disposal Systems for Spent Fuels and Hight-Level Radioactive Wastes in Korea". *Nuclear Engineering and Technology, 45*(1), 29-40. doi: 10.5516/net.06.2012.006

Cho, D.K., N.Y. Ko, Y.K. Koh, J.S. Kwon, I.Y. Kim, J.W. Kim, J.H. Ryu, K.W. Park, C.K. Park, T.J. Park, M.H. Baik, S. Yoon, M. Lee, S.Y. Lee, J.K. Lee, J.O. Lee, J. Lee, C. Lee, S. Jung, J. Jeong, and S.H Ji. (2016). *A Safety Case of the Conceptual Disposal System for Pyro-processing High-Level Waste Based on the KURT Site (AKRS-16): VI Models and Data, KAERI/TR-6732/2016.*

Clayton, D., G. Freeze, T. Hadgu, E. Hardin, J. Lee, J. Prouty, R. Rogers, W. M. Nutt, J. Birkholzer, H. H. Liu, L. Zheng, and S. Chu (2011). *Generic Disposal System Modeling - Fiscal Year 2011 Progress Report*. SAND 2011-5828P; FCRD-USED-2011-000184. Sandia National Laboratories, Albuquerque, NM.

Croff, A.G. (1983). "ORIGEN2: A Versatile Computer Code for Calculating the Nuclide Compositions and Characteristics of Nuclear Materials," *Nuclear Technology*, 62(3), 335-352. doi: dx.doi.org/10.13182/NT83-1.

Ecay, L., Grégoire, D., and Pijaudier-Cabot G. (2020). On the prediction of permeability and relative permeability from pore size distributions. *Cement and Concrete Research*, 133: 106074.

Follin, S., Hartley, L., Jackson, P., Joyce, S., Roberts, D., and Swift, B. (2007). *Hydrogeological characterization and modeling of deformation zones and fracture domains, Forsmark modelling stage 2.2*. SKB R-07-48. Svensk Kärnbränslehantering AB, Stockholm, Sweden.

Frederick, J. M. (2018). PFLOTRAN QA Test Suite. Retrieved April 25, 2020, from qa.pflotran.org

Freeze, R. A. and Cherry, J. A. (1979). *Groundwater*, Prentice-Hall, Englewood Cliffs, NJ.

Freeze, G., Voegele, M., Vaughn, P., Prouty, J., Nutt, W.M., Hardin, E., and Sevougian, S.D. (2013). Generic Deep Geologic Disposal Safety Case. FCRD-UFD-2012-000146 Rev. 1, SAND2013-0974P. Sandia National Laboratories, Albuquerque, NM.

GRS. (2012). Radionuclide Inventory of Vitrified Waste after Spent Nuclear Fuel Reprocessing at La Hague. Gesellschaft für Anlagen- und Reaktorischerhet, Germany. GRS-294.

Hartley, L., Appleyard, P., Baxter, S., Hoek, J., Roberts, D., and Swan, D. (2013a). *Development of a Hydrogeological Discrete Fracture Network Model for the Olkiluoto Site Descriptive Model 2011*. Working Report 2012-32. Posiva Oy, Eurajaki, Finland.

Hartley, L., Hoek, J., Swan, D., Appleyard, P., Baxter, S., Roberts, D., and Simpson, T. (2013b). *Hydrogeological Modelling for Assessment of Radionuclide Release Scenarios for the Repository System 2012*. Working Report 2012-42. Posiva Oy,

Hartley, L., P. Appleyard, S. Baxter, J. Hoek, S. Joyce, K. Mosley, T. Williams, A. Fox, M. Cottrell, P. La Pointe, S. Gehör, C. Darcel, R. Le Goc, I. Aaltonen, O. Vanhanarkaus, J. Löfman, and A. Poteri (2018). *Discrete Fracture Network Modelling (Version 3) in Support of Olkiluoto Site Description 2018*. Working Report 2017-32. Posiva Oy, Eurajoki, Finland.

Hartley, L., Baxter, S., and Williams, T. (2016). *Geomechanical Coupled Flow in Fractures during Temperate and Glacial Conditions*. Working Report 2016-08. Posiva Oy, Eurajoki, Finland.

Hedin, A. (2008). Semi-Analytic Stereological Analysis of Waste Package/Fracture Intersections in a Granitic Rock Nuclear Waste Repository. *Mathematical Geosciences*, *40*(6), 619–637. https://doi.org/10.1007/s11004-008-9175-3

Hirsekorn, Rolf-Peter, Brigitte Boese, Dieter Buhmann. (1999). *LOPOS: Programm zur Berechnung der Schadstofffreisetzung aus netzwerkartigen Grubengebäuden*. GRS Germany, GRS - 157

Hyman, J. D., Karra, S., Makedonska, N., Gable, C. W., Painter, S. L., and Viswanathan, H. S. (2015). "DFNWORKS: A discrete fracture network framework for modeling subsurface flow and transport". *Computers & Geosciences*, 84, 10-19. doi: 10.1016/j.cageo.2015.08.001

Johnson, L. R., Ferry, C., Poinssot C., and Lovera P. (2005). Spent fuel radionuclide source term model for assessing spent fuel performance in geological disposal. Part I: Assessment of the Instant Release Fraction. Journal of Nuclear Materials 346: 66-77.

Joyce, S., T. Simpson, L. Hartley, D. Applegate, J. Hoek, P. Jackson, D. Swan, N. Marsic, and S. Follin (2010). *Groundwater flow modelling of periods with temperate climate conditions - Forsmark*. SKB R-09-20. Svensk Kärnbränslehantering AB, Stockholm, Sweden.

Kienzler, B., M. Altmaier, C. Bube and V. Metz (2012). *Radionuclide Source Term for HLW Glass, Spent Nuclear Fuel, and Compacted Hulls and End Pieces (CSD-C Waste)*. KIT Scientific Reports 7624. Karlsruhe Institute of Technology, Baden-Württemberg, Germany.

Kolditz, O., Shao, H., Wang, W., and Bauer, S. (2015). *Thermo-Hydro-Mechanical-Chemical Processes in Fractured Porous Media: Modelling and Benchmarking Closed-Form Solutions* (O. Kolditz, H. Shao, W. Wang, & S. Bauer Eds.). Switzerland: Springer International Publishing.

LaForce, T., Chang, K.W., Perry, F.V., Lowry, T.S., Basurto, E., Jayne, R., Brooks, D., Jordan, S., Stein, E., Leone, R., and Nole, M. (2020). *GDSA Repository Systems Analysis Investigations in FY2020*. M2SF-20SN010304052, SAND2020-12028 R. Sandia National Laboratories, Albuquerque, NM.

Maak, P., Gierszewski, P., and Saiedfar, M. (2001). Early failure probability of used-fuel containers in a deep geologic repository. Ontario Power Generation, Nuclear Waste Management Division Report 06819-REP-01300-10022-R00. Toronto, Canada.

Mariner, P. E., J. H. Lee, E. L. Hardin, F. D. Hansen, G. A. Freeze, A. S. Lord, B. Goldstein and R. H. Price (2011). *Granite Disposal of U.S. High-Level Radioactive Waste*. SAND2011-6203. Sandia National Laboratories, Albuquerque, New Mexico.

Mariner, P. E., W. P. Gardner, G. Hammond, S. D. Sevougian, and E. R. Stein (2015). *Application of Generic Disposal System Models*. FCRD-UFD-2015-000126; SAND2015-10037R. Sandia National Laboratories, Albuquerque, NM.

Noseck, Ulrich, Wernt Brewitz, Dirk-Alexander Becker, Dieter Buhmann, Christine Fahrenholz, Eckhard Fein, Peter Hirsekorn, Sven Keesmann, Klaus-Peter Kröhn, Ingo Müller-Lyda, André Rübel, Anke Schneider, Richard Storck. (2005). *Wissenschaftliche Grundlagen zum Nachweis der Langzeitsicherheit von Endlagern*. GRS, Germany, GRS-204.

NWMO. (2012). *Used Fuel Repository Conceptual Design and Postclosure Safety Assessment in Crystalline Rock*. NWMO TR-2012-16. Nuclear Waste Management Organization, Toronto, Ontario.

OCRWM. (1990). *Performance Assessment Strategy Plan for the Geologic Repository Program*. DOE-RW-0266P. U.S. Department of Energy, Office of Civilian Radioactive Waste Management, Washington, DC.

Ollila, K. (2008). *Dissolution of unirradiated UO2 and UO2 doped with 233U in low- and high-ionic strength NaCl under anoxic and reducing conditions*. Working Report 2008-50. Posiva Oy, Eurajoki, Finland.

Osselin, F., Fabbri, A., Fen-Chong, T., Pereira, J., Lassin, A., and Dangla, P. (2015). Experimental Investigation of the Influence of Supercritical State on the Relative Permeability of Vosges Sandstone. *Comptes Rendus Mécanique*, 343: 495-502.

Pettersson, S. and Lönnerberg, B. (2008), 16-18 June 2008. *Final Repository for Spent Nuclear Fuel in Granite - The KBS-3V Concept in Sweden and Finland.* Paper presented at the International Conference Underground Disposal Unit Design & Emplacement Processes for a Deep Geological Repository, Prague.

Poley, A.D., (1999). Concept ontwerp terughaalbare opslag van radioactief afval in diepe boorgaten in steenzout (Torad-B) 1–54.

Rübel, A., Buhmann, D., Kindlein, J. and Lauke, T. (2016). *Performance assessment of sealing systems. Conceptual and integrated modelling of plugs and seals* (No. GRS-415). Gesellschaft fuer Anlagen-und Reaktorsicherheit (GRS) gGmbH.

Sassani, D., Jang, J.-H., Mariner, P. E., Price, L., Rechard, R., Rigali, M., Rogers, R., Stein, E. R., Walkow, W., and Weck, P. (2016). The On-line Waste Library (OWL): Usage and Inventory Status Report. FCRD-UFD_2016-000080 / SAND2016-9485R. Sandia National Laboratories, Albuquerque, NM

SKB (Svensk Kärnbränslehantering AB) (2010a). *Design, production and initial state of the canister*. SKB TR-10-14. Svensk Kärnbränslehantering AB, Stockholm, Sweden.

SKB (Svensk Kärnbränslehantering AB) (2010b). *Design, production and initial state of the backfill and plug in deposition tunnels*. SKB TR-10-16. Svensk Kärnbränslehantering AB, Stockholm, Sweden.

SKB (Svensk Kärnbränslehantering AB) (2011). *Long-term safety for the final repository for spent nuclear fuel at Forsmark*. SKB TR-11-01. Svensk Kärnbränslehantering AB, Stockholm, Sweden.

Stein, E. R., J. M. Frederick, G. E. Hammond, K. L. Kuhlmann, P. E. Mariner, and S. D. Sevougian (2017), April 9-13, 2017. *Modeling Coupled Reactive Flow Processes in Fractured Crystalline Rock*. Paper presented at the International High-Level Radioactive Waste Management Conference, Charlotte, NC.

Strachan, D. (2004). *Defense HLW Glass Degradation Model*. ANL-EBS-MD-000016 REV 02. Sandia National Laboratories, Albuquerque, New Mexico.

Storck, R., D. Buhmann, R.-P. Hirsekorn, T. Kühle, L. Lührmann. (1996). *Das Programmpaket EMOS zur Analyse der Langzeitsicherheit eines Endlagers für radioaktive Abfälle Version 5.* 1996. Germany, GRS-122.

Swiler, L. P., E. Basurto, D. M. Brooks, A.C. Eckert, P. E. Mariner, T. Portone, and E. R. Stein (2020). *Advances in Uncertainty Quantification and Sensitivity Analysis Methods and Applications in GDSA Framework*. SAND2020-10802 R. Sandia National Laboratories, Albuquerque, NM.

Tang, D.H., Frind, E.O .and Sudicky, E.A, (1981). "Contaminant transport in fracture porous media: analytical solution for a single fracture". *Water Resources Research,* 17(3), 555-564. doi: 10:1029/WR017i003p00555

TPC (Taiwan Power Company) (2017). *The Technical Feasibility Assessment Report on Spent Nuclear Fuel Final Disposal*. Main Report. Taiwan Power Company, Taipei, Taiwan.

Verhoef, E.V., Neeft, E.A., Deissmann, G., Filby, A., Wiegers, R.B., Kers, D.A. (2016). *Waste families in OPERA*. The Netherlands, OPERA-PG-COV023.

Vienna, J. D., Ryan, J. V., Gin, S., and Inagaki, Y. (2013). Current understanding and remaining challenges in modeling long-term degradation of borosilicate nuclear waste glasses. International Journal of Applied Glass Science 4(4): 283-294.

Von Mises-Fisher distribution (accessed 23 October 2021) https://en.wikipedia.org/wiki/Von_Mises%E2%80%93Fisher_distribution

Wang, Y., and J. Lee. Eds. (2010). *Generic Disposal System Environment Modeling--Fiscal Year 2010 Progress Report.* Prepared for U.S. Department of Energy, Office of Nuclear Energy, Fuel Cycle Research and Development Program. Sandia National Laboratories, Albuquerque, NM.

Weast, R. C. and M. J. Astle, Eds. (1981). CRC Handbook of Chemistry and Physics. Boca Raton, Florida, CRC Press, Inc.

Werme, L. O., L. H. Johnson, V. M. Oversby, F. King, K. Spahiu, B. Grambow, and D. W. Shoesmith (2004). *Spent fuel performance under repository conditions: A model for use in SR-Can*. SKB TR-04-19. Svensk Kärnbränslehantering AB, Stockholm, Sweden.